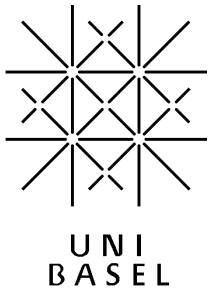

Trial Methods For Bernoulli's Free Boundary Problem

Inauguraldissertation
zur
Erlangung der Würde eines Doktors der Philosophie
vorgelegt der
Philosophisch-Naturwissenschaftlichen Fakultät
der Universität Basel

von

Giannoula Mitrou
aus Kerkyra, Griechenland

Basel, 2014

Genehmigt von der Philosophisch-Naturwissenschaftlichen Fakultät
auf Antrag von

Helmut Harbrecht Marc Dambrine

Basel, den 18. Februar 2014

Prof. Dr. Jörg Schibler,
Dekan

To my parents

Abstract

Free boundary problems deal with solving partial differential equations in a domain, a part of whose boundary is unknown – the so-called free boundary. Beside the standard boundary conditions that are needed in order to solve the partial differential equation, an additional boundary condition is imposed at the free boundary. One aims thus to determine both, the free boundary and the solution of the partial differential equation.

This thesis is dedicated to the solution of the generalized exterior Bernoulli free boundary problem which is an important model problem for developing algorithms in a broad band of applications such as optimal design, fluid dynamics, electromagnentic shaping etc. Due to its various advantages in the analysis and implementation, the trial method, which is a fixed-point type iteration method, has been chosen as numerical method.

The iterative scheme starts with an initial guess of the free boundary. Given one boundary condition at the free boundary, the boundary element method is applied to compute an approximation of the violated boundary data. The free boundary is then updated such that the violated boundary condition is satisfied at the new boundary. Taylor's expansion of the violated boundary data around the actual boundary yields the underlying equation, which is formulated as an optimization problem for the sought update function. When a target tolerance is achieved the iterative procedure stops and the approximate solution of the free boundary problem is detected.

How efficient or quick the trial method is converging depends significantly on the update rule for the free boundary, and thus on the violated boundary condition. Firstly, the trial method with violated Dirichlet data is examined and updates based on the first and the second order Taylor expansion are performed. A thorough analysis of the convergence of the trial method in combination with results from shape sensitivity analysis motivates the development of higher order convergent versions of the trial method. Finally, the gained experience is exploited to draw very important conclusions about the trial method with violated Neumann data, which is until now poorly explored and has never been numerically implemented.

Acknowledgements

It is a pleasure to thank the many people who made this thesis possible.

First and foremost I would like to thank my supervisor Prof. Dr. Helmut Harbrecht. It has been an honor to be his first PhD student and a member of his research group. I am very grateful to him for his helpful guidance and support to complete my dissertation and for the experience I obtained at the University of Bonn, at the University of Stuttgart and at the University of Basel.

I wish to thank Prof. Dr. Marc Dambrine from the University of Pau for his willingness to take over the role of the co-referee.

I have been very privileged to get to know and to collaborate with many great people in all time of research for this thesis. For the excellent working conditions and the exchange of ideas and knowledge I would like to thank all my colleagues. However, I owe a special acknowledgement to Dr. Loredana Gaudio and Michaela Mehlin for reading an early draft of my work and for their helpful suggestions.

Moreover, I would also like to sincerely thank the secretaries Mrs Karen Bingel (Bonn International Graduate School in Mathematics), Mrs Brit Steiner (Institute of Applied Analysis and Numerical Simulation at the University of Stuttgart) and Mrs Barbara Fridez (Department of Mathematics at the University of Basel) for their willingness and assistance but mainly for helping me to relocate and integrate.

I wish to express my love and gratitude to my parents, Apostolos and Kallitsa, for their understanding and support through the duration of my studies and for teaching me to strive and reach my goals. Finally, I am thankful and fortunate enough for getting constant encouragement and support from my brother and my friends, but especially for the love and patience of Arthur.

Table of Contents

Chapter 1

Introduction

In many cases, problems in areas such as physics, engineering, finance and biology are described by partial differential equations for the unknown functions. If there are additional geometrical unknowns in these problems we speak of free boundary problems. In practice, free boundary problems are problems, which consist of a partial differential equation in the domain and boundary conditions at the boundary of the domain. On the unknown part of the domain though, the so-called free boundary, there are given two boundary conditions which serve different purposes; the first one is to solve the differential equation and the second one is to find the location of the free boundary. The simultaneous solution of both the unknown function and its domain of definition requires a challenging numerical simulation of the problem. Within the last two decades, various new ideas, techniques and methods have been developed for the solution of free boundary problems, and hence many new free boundary problems have been studied.

1.1 Bernoulli's free boundary problem

The aim of this thesis is to address and analyze some aspects related to Bernoulli's free boundary problem, an important model problem for developing algorithms in shape optimization, fluid dynamics, optimal design, electrochemistry, electromagnetics and many further applications.

1.1.1 Problem formulation

We consider a generalized version of the exterior Bernoulli free boundary problem which involves the Poisson equation and non-constant boundary data. The related domain, displayed in Figure 1.1, can be described as follows: Let $T \subset \mathbb{R}^2$ denote a bounded domain with free boundary $\partial T = \Gamma$. Inside the domain T we assume the existence of a simply connected subdomain $S \subset T$ with fixed boundary $\partial S = \Sigma$. The resulting annular domain $T \setminus \overline{S}$ is denoted by Ω.

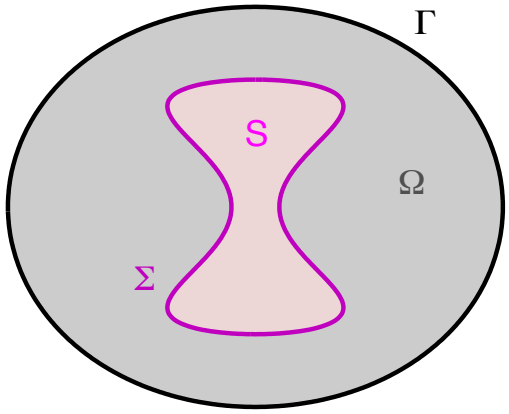

Figure 1.1: The domain Ω and its boundaries Γ and Σ.

For the given topological situation, the exterior Bernoulli free boundary problem reads as: Seek the domain Ω and the state u which satisfy the overdetermined boundary value problem

$$-\Delta u = f \quad \text{in} \quad \Omega \tag{1.1a}$$
$$u = g \quad \text{on} \quad \Sigma \tag{1.1b}$$
$$u = 0 \quad \text{on} \quad \Gamma \tag{1.1c}$$
$$\frac{\partial u}{\partial \mathbf{n}} = h \quad \text{on} \quad \Gamma \tag{1.1d}$$

for given data f, g and h. The problem is called exterior free boundary problem since the exterior boundary Γ is sought such that the overdetermined boundary value problem (1.1) becomes solvable.

Assumption 1.1. In order to ensure the well posedness of the problem under consideration the functions $f \geq 0$, $g > 0$ and $h < 0$ are assumed to be sufficiently smooth in $\mathbb{R}^2$. In particular, we assume that $u \in C^2(\overline{\Omega})$, such that second order derivatives of the solution exist.

The vector $\mathbf{n}$ stands for the unit normal vector at Γ and $\partial u/\partial \mathbf{n}$ denotes the derivative of u in the normal direction. We like to stress that the sign conditions on the data ensure that u is positive in Ω and thus it holds in fact $\partial u/\partial \mathbf{n} < 0$ on Γ.

Assumption 1.2. The domain Ω belongs to the class of simply connected, bounded domains with smooth boundaries which are starshaped with respect to the origin.

Under this assumption, the domain Ω can be uniquely identified by a periodic and positive function r which represents the free boundary Γ since the boundary Σ is fixed. The free boundary is parametrized via polar coordinates by

$$\boldsymbol{\gamma} = [0, 2\pi] \to \Gamma, \qquad s \to \boldsymbol{\gamma}(s) := r(s)\mathbf{e}_r(s),$$

where $\mathbf{e}_r(s) = \big(\cos(s), \sin(s)\big)^T$ denotes the unit vector in the outward radial direction.

The problem under consideration can be viewed as the prototype of a large class of stationary free boundary problems which are involved in many applications of various engineering fields. For example, the growth of anodes in electrochemical processes might be modeled like above with $f = 0$, $g = 1$, $h = const.$ and corresponds to the original Bernoulli free boundary problem [33].

Some early results about the existence and uniqueness of solutions to the Bernoulli free boundary problem are found in [8, 11, 72]. About the geometric form of the solutions we address the reader to [1, 4] and the references therein. For the qualitative theory and the numerical approximation to the related interior Bernoulli free boundary problem we refer to [36]. The interior Bernoulli free boundary problem differs from the exterior in two regards. Firstly, the unknown boundary is the inner one, and secondly, the Dirichlet data at the fixed boundary and at the free boundary are exchanged.

1.1.2 Solution strategies

In the following, we briefly review the existing strategies to solve free boundary problems and present some related publications. These strategies are primarily divided into two categories: the shape optimization methods and the fixed-point methods. In this thesis we confine ourselves to the examination of the trial method, which falls into the latter category.

Shape optimization methods

In classical shape optimization approach one formulates a cost function that attains its minimum at a solution of the free boundary problem and accordingly updates the free boundary. There are roughly two ways to formulate the free boundary problem (1.1) as a shape optimization problem. The first one is the shape variational formulation, where the free boundary problem is related to an energy functional E whose minimizer is the free boundary. The second one is a least-squares formulation. In this case, at first the boundary value problem is solved in the domain Ω with one of the two boundary conditions at the free boundary. Then the mismatch of the violated boundary condition is tracked at the free boundary in the least-squares sense. Shape optimization approaches for the solution of the Bernoulli free boundary problem by tracking either the Dirichlet or the Neumann data at the free boundary have been investigated, for instance, in [45, 50, 73, 76] and in [30, 31, 32, 42].

Fixed-point methods

In the fixed-point approach the free boundary problem is solved by constructing a sequence of trial solutions u_k and trial free boundaries Γ_k by using some update rule in each iteration. Among the fixed-point methods we distinguish the trial method. Here, the update rules do not necessarily require the knowledge of shape sensitivity analysis. However there are algorithms which are based on concepts from shape optimization, see for example [52, 75, 77, 78].

A single step of the trial method starts with a "trial" free boundary curve Γ_k. Then the boundary value problem is solved in the related domain Ω_k by considering either the Dirichlet or the Neumann boundary condition at Γ_k. The solution of this problem is used to construct a new boundary curve Γ_{k+1} which comes closer to the desired free boundary.

When available, trial methods have the advantage of being essentially independent of the state problem solver and easy to implement. The drawback however is that it is not always obvious how to construct appropriate update rules such that the method converges or a convergence rate of high order is attained. According to [21] the methods of moving the boundary are classified as local, integral or global. Convergence and further analytical results for the trial method are included in [2, 3, 5, 36]. In [39] a modification of the state problem in view of a higher convergence order is introduced and the Neumann boundary condition at the free boundary is substituted by a Robin boundary condition which involves

the mean curvature of the free boundary. The same is later proved in [75] and applied in [51, 52, 73, 74]. This modification is moreover exploited in [36], where not only numerical schemes based on a local parametrization are developed but also the convergence rate of the corresponding trial method is estimated.

Other methods and applications

Another shape derivative free method to solve free boundary problems is the level set method which is implemented for Bernoulli's problem in [13, 14, 56]. It enjoys the property of allowing changes of the domain's topology. Nevertheless, all authors considered only constant Dirichlet and Neumann data which corresponds to the original Bernoulli free boundary problem.

In [55, 63, 64] an iterative method based on the idea of the analytic continuation of the field has been used in case of an inverse scattering problem. Inverse problems possess a slightly different formulation from free boundary problems since the roles of Σ and Γ are interchanged, which amounts to severely ill-posed problems. The detection of voids or inclusions in electrical impedance tomography for the non-destructive testing of materials or for medical diagnostics fall into this type of problems. Results concerning numerical algorithms are found in [6, 17, 29]. Within the scope of electrical impedance tomography we refer also to [7, 38] for uniqueness results and [15, 16] for methods using the Dirichlet-to-Neumann map.

In addition to the previously mentioned applications we cite [24, 28, 59, 61] for electromagnetic shaping problems which in the two-dimensional case [18, 19, 20, 27] fit the generalized form of Bernoulli's free boundary problem; by considering the Poisson equation as the state equation. The problem of the maximization of the torsional stiffness of an elastic cylindrical bar under simultaneous constraints on its volume and bending rigidity can also be seen as a free boundary problem, see [26] for the details. Finally, some practical applications of interior and exterior free boundary problems are concerned with fluid flow in porous media, with heat flow phase or with chemical reactions [37].

1.2 Trial methods

As we have already mentioned, the subject of this thesis is the trial method for the solution of the exterior Bernoulli free boundary problem (1.1). The basic algorithm of the underlying iterative scheme is described in Algorithm 1.1.

Algorithm 1.1: The trial method

1. Choose an initial guess Γ_0 of the free boundary.
2. a) Solve the boundary value problem with one boundary condition at the free boundary.
   b) Update the free boundary according to the remaining boundary condition at the free boundary.
3. Iterate step 2 until the process becomes stationary up to a specified precision.

The main ingredient of trial methods is an appropriate update rule for the free boundary. In fact we look for a suitable update function δr_k such that the free boundary is updated in the radial direction according to

$$\boldsymbol{\gamma}_{k+1} = \boldsymbol{\gamma}_k + \delta r_k \mathbf{e}_r. \tag{1.2}$$

As step 2b of Algorithm 1.1 suggests, this update function should be chosen such that the remaining boundary condition will approximately be satisfied at the new boundary. Since there are given two different boundary conditions at the free boundary, there are also two different ways to update the free boundary. There appears to be no general rule for deciding which boundary condition should be used in solving the elliptic equation and which for moving the free boundary. The choice depends on the problem and sometimes one is clearly more convenient or efficient than the other.

In case we choose to update the free boundary according to the Dirichlet boundary condition we consider the mixed boundary value problem

$$-\Delta \mathrm{v}_k = f \text{ in } \Omega_k, \quad \mathrm{v}_k = g \text{ on } \Sigma, \quad \frac{\partial \mathrm{v}_k}{\partial \mathbf{n}} = h \text{ on } \Gamma_k. \tag{1.3}$$

When the movement strategy of the free boundary is based on the Neumann boundary condition, this delivers the Dirichlet boundary value problem

$$-\Delta \mathrm{w}_k = f \text{ in } \Omega_k, \quad \mathrm{w}_k = g \text{ on } \Sigma, \quad \mathrm{w}_k = 0 \text{ on } \Gamma_k. \tag{1.4}$$

For sake of notational clarity we denote by v_k or w_k the function which satisfies the mixed or the Dirichlet boundary value problem, respectively. In both cases the boundary element method is shown to be an efficient tool to approximate the missing boundary data. By discretizing the boundary value problem by parametrized analytic curves, we are able to achieve an exponential convergent approach for the determination of these boundary data.

For the update rules, the main idea for obtaining the update function is to use Taylor's expansion of the violated boundary data around the current boundary Γ_k. We investigate and compare the boundary update rules which are computed from either the first or the second order Taylor expansion of the Dirichlet data. The free boundary is then updated not only in certain points of the boundary but also in the continuous sense. This corresponds to the well known approaches from optimization: "discretize-then-optimize" and "optimize-then-discretize".

The trial method is in general a linearly convergent method, which we verify following the lines of [75]. Nevertheless, we achieve update rules for the free boundary which enforce the convergence or ensure even quadratic convergence, see [43]. The novelty in the suggested method is that the state equation (1.3) needs not to be changed, contrary to the approach in [75]. On the one hand, this gives the opportunity of applying always the same boundary element method. On the other hand, the trial method is also applicable for nonconvex boundaries.

For the trial method based on the Neumann boundary condition the situation is not quite so ideal as in case of Dirichlet boundary condition, and this is theoretically and numerically proven. However, taking into account the analysis procedure and the observations from the trial method with updates for the free boundary according to the Dirichlet data we succeed to develop an update rule for which the convergence of the trial method is enforced.

Notice that parts of this thesis have already been published in [43, 44].

1.3 Outline of the thesis

After this introductory chapter the rest of the thesis is structured in two parts. The first part includes three chapters which focus on the trial method based on the update of the free boundary according to the Dirichlet data. These chapters contain in detail results on the boundary element method, on the derivation of the update rules for the free boundary and on the converge analysis of the trial method. In particular:

Chapter 2 is dedicated to the determination of the Dirichlet data at the unknown boundary. By considering a Newton potential we obtain a mixed boundary value problem for the Laplace equation and are thus able to apply the boundary element method. For this aim, we first review the fundamentals of the theory of integral equations including Green's function and layer potentials. Then, we get the Neumann-to-Dirichlet map which is a system of integral equations. It is solved

by the collocation method based on trigonometric polynomials. This method converges exponentially under specific conditions. Numerical examples verify this statement.

In Chapter 3 we obtain the update rules via Taylor's expansion of first and second order of the Dirichlet data. After a brief introduction to differential calculus, the update function is found by solving a discrete or continuous least-squares problem. This suggests mainly two methods to solve the problems: the Gauss-Newton and the Newton method. Some first numerical tests for the trial method are performed and conclusions are drawn about the first and second order update rules as well as about the approaches "discretize-then-optimize" and "optimize-then-discretize".

The convergence analysis of the trial method is presented in Chapter 4. Here, results from shape calculus are essential. We recall the basic notations and concepts related to shape and material derivatives and we prove why for the standard update rule (1.2) only linear convergence of the trial method can be expected. Nevertheless, we manage to derive an improved update rule for the free boundary which enforces the convergence. A Newton-type update ensures even quadratic convergence. Numerical examples conclude this chapter and the thesis' first part.

The thesis' second part and Chapter 5 contains the analysis of the trial method in case of updating the free boundary according to the Neumann data. The analysis starts with the solution of the Dirichlet-to-Neumann map for the computation of the violated Neumann data. Then the update function is derived by linearization of the Neumann data around the current boundary. Numerical tests for the resulting boundary update rule are performed. These results and the investigation of the convergence rate reveal some weak points of the trial method, which we manage to eliminate by considering a modified update rule. In particular we succeeded in enforcing the convergence of the trial method. The feasibility of the derived update rules is demonstrated via additional numerical examples.

In the last chapter we make some final conclusions and observations on the proposed trial methods.

Part I

The trial method for prescribed Neumann data

Chapter 2

Boundary element method

The topic of this chapter is the boundary element method for solving elliptic partial differential equations which have been formulated as equivalent boundary integral equations. When the solution is desired only at the boundary of the domain, then the boundary element method is more efficient than other methods, see e.g. [41, 70]. Its additional advantages are the easy treatment of exterior problems and the reduction of an n-dimensional problem defined in the domain to an $(n-1)$-dimensional problem defined on the boundary, as only the boundary of the domain has to be discretized. Although in our problem we have to solve the mixed boundary value problem for the Poisson equation, we can still apply the boundary element method by using an ansatz which includes a Newton potential. Our approach to get the system of integral equations is the direct formulation based on Green's fundamental solution. It determines the solution's unknown boundary data from the given boundary data. Afterwards, having the complete Cauchy data of the state at hand, Green's representation formula can be used again to calculate the solution in the interior of the domain. As particular boundary element method we choose the fully discrete collocation method based on trigonometric polynomials which possesses the unique benefit of an exponential convergence rate [54, 62].

2.1 Theoretical background

An introduction to integral equations is necessary for the subsequent analysis. We start with the definition of the function spaces as the smoothness of the domain is characterized by the function space that is defined on it.

By $C^m(\Omega)$ we denote the linear space of real-valued functions defined on the domain Ω, which are $m \in \mathbb{N}$ times continuously differentiable. For more refined analysis, we introduce Hölder spaces. An appropriate framework for formulating refined regularity properties is provided by the spaces of Hölder continuous functions

$$C^{m,\alpha}(\Omega) := \big\{\phi \in C^m(\Omega) : \|\phi\|_{C^{m,\alpha}(\Omega)} < \infty\big\},$$

where the norm is defined by

$$\|\phi\|_{C^{m,\alpha}(\Omega)} := \sum_{|\beta|\le m} \sup_{\mathbf{x}\in\Omega} \|\partial^\beta \phi(\mathbf{x})\| + \sum_{|\beta|=m} \sup_{\substack{\mathbf{x},\mathbf{y}\in\Omega \\ \mathbf{x}\neq\mathbf{y}}} \frac{\|\partial^\beta \phi(\mathbf{x}) - \partial^\beta \phi(\mathbf{y})\|}{\|\mathbf{x}-\mathbf{y}\|^\alpha} \tag{2.1}$$

for $m \in \mathbb{N}$ and $0 < \alpha < 1$. Here, for the multi-index $\beta = (\beta_1, \ldots, \beta_n) \in \mathbb{N}_0^n$, $|\beta| = \beta_1 + \cdots + \beta_n$ and ∂^β denotes the multivariate derivative

$$\partial^\beta := \partial_1^{\beta_1} \cdots \partial_n^{\beta_n}.$$

The spaces of Hölder continuous functions are complete vector spaces, and hence Banach spaces, see for example [79]. The space $C^{0,\alpha}(\Omega)$ defines the linear space of all functions in Ω which are bounded and uniformly Hölder continuous with exponent α. Note that, in the case $\alpha = 1$, we talk of Lipschitz continuous functions. Finally, the usual function spaces $C(\Omega)$ and $C^m(\Omega)$ can be defined as

$$C(\Omega) := C^{0,0}(\Omega) \quad \text{and} \quad C^m(\Omega) := C^{m,0}(\Omega).$$

In this thesis, we confine our attention to surfaces that are boundaries of a smooth domain in $\mathbb{R}^n$. The next definition explains the notion "$\partial\Omega$ belongs to class C^k".

Definition 2.1. *A bounded open domain $\Omega \subset \mathbb{R}^n$ with boundary $\partial\Omega$ is said to be of class C^k, $k \in \mathbb{N}$, if the closure $\overline{\Omega}$ admits a finite open covering*

$$\overline{\Omega} \subset \bigcup_{q=1}^{p} V_q$$

such that, for each V_q that intersects with the boundary $\partial\Omega$, we have the properties:

- *the intersection $V_q \cap \overline{\Omega}$ can be mapped bijectively onto the half-ball $H := \{\mathbf{x} \in \mathbb{R}^n : \|\mathbf{x}\| < 1,\ x_n \ge 0\}$ in $\mathbb{R}^n$;*
- *this mapping and its inverse are k times continuously differentiable;*
- *the intersection $V_q \cap \partial\Omega$ is mapped onto the disk $H \cap \{\mathbf{x} \in \mathbb{R}^n : x_n = 0\}$.*

Remark 2.2. On occasion, we will express the property of a domain Ω to be of class C^k also by saying that its boundary is of class C^k.

We close this introductory section with the definition of integral operators.

Definition 2.3. *An integral operator $W : C(\Omega) \to C(\Omega)$ is defined by*

$$(W\rho)(\mathbf{x}) := \int_\Omega k(\mathbf{x},\mathbf{y})\rho(\mathbf{y})\mathrm{d}\mathbf{y}, \quad \mathbf{x} \in \Omega,$$

with kernel $k : \Omega \times \Omega \to \mathbb{R}$ and density function $\rho : \Omega \to \mathbb{R}$. A kernel k is called weakly singular if k is continuous for all $\mathbf{x}$, $\mathbf{y} \in \Omega$, with $\mathbf{x} \neq \mathbf{y}$, and if there exist positive constants M and $\alpha \in (0, n]$ such that

$$\|k(\mathbf{x},\mathbf{y})\| \leq M\|\mathbf{x}-\mathbf{y}\|^{\alpha-n} \quad \textit{for all } \mathbf{x},\mathbf{y} \in \Omega \textit{ with } \mathbf{x} \neq \mathbf{y}.$$

Within this analytical background at hand, we are able to present the method for computing the solution of the boundary value problem under consideration.

2.2 Boundary integral equations

The solution of the mixed boundary value problem

$$-\Delta \mathrm{v} = f \qquad \text{in} \quad \Omega \tag{2.2a}$$

$$\mathrm{v} = g \qquad \text{on} \quad \Sigma \tag{2.2b}$$

$$\frac{\partial \mathrm{v}}{\partial \mathbf{n}} = h \qquad \text{on} \quad \Gamma \tag{2.2c}$$

by the boundary element method can be performed by a reformulation as a boundary integral equation with the help of a Newton potential.

2.2.1 Newton potential

Our objective is to find the Dirichlet data of the solution v satisfying the boundary value problem (2.2). Despite Poisson's equation, the boundary element method can still be applied by making the ansatz

$$\mathrm{v} = v + N_f \tag{2.3}$$

for a suitable Newton potential N_f and an unknown harmonic function v.

The Newton potential satisfies the equation $-\Delta N_f = f$ and has to be given analytically or computed in a sufficiently large domain $\widehat{\Omega}$. Nevertheless, since

this domain can be chosen fairly simple, efficient solution techniques can easily be applied.

As a consequence, our sight is set to the determination of the Dirichlet data of the harmonic function v which satisfies the boundary value problem

$$\Delta v = 0 \qquad \text{in} \quad \Omega \tag{2.4a}$$

$$v = g - N_f \qquad \text{on} \quad \Sigma \tag{2.4b}$$

$$\frac{\partial v}{\partial \mathbf{n}} = h - \frac{\partial N_f}{\partial \mathbf{n}} \qquad \text{on} \quad \Gamma. \tag{2.4c}$$

The boundary element method for this particular boundary value problem for the Laplace equation (2.4a) will be the subject of the next sections.

2.2.2 Harmonic functions and Green's theorems

Potential theory is a valuable source of results concerning harmonic functions. Some related theorems are listed below and their corresponding proofs can be found in [54, Chapter 6].

Definition 2.4. *A twice continuously differentiable real-valued function v, defined on a domain $\Omega \subset \mathbb{R}^2$, is called harmonic if it satisfies Laplace's equation*

$$\Delta v = 0 \qquad \text{in} \quad \Omega.$$

Theorem 2.5. *Harmonic functions defined in smooth domains are analytic.*

Theorem 2.6. *The function*

$$G(\mathbf{x}, \mathbf{y}) := -\frac{1}{2\pi} \log \|\mathbf{x} - \mathbf{y}\| \tag{2.5}$$

is called the fundamental solution of Laplace's equation. For fixed $\mathbf{y} \in \mathbb{R}^2$ it is harmonic in $\mathbb{R}^2 \setminus \{\mathbf{y}\}$.

Green's theorem provides an important tool in the analysis of the Laplace equation. It results from divergence theorem which reads as follows:

Theorem 2.7 (Divergence or Gauss theorem). *Assume that $\mathbf{F} : \overline{\Omega} \to \mathbb{R}^2$ with each component of $\mathbf{F}$ being contained in $C^1(\overline{\Omega})$. Then, it holds*

$$\int_\Omega \nabla \cdot \mathbf{F} \mathrm{d}\mathbf{y} = \int_{\partial\Omega} \langle \mathbf{F}, \mathbf{n} \rangle \mathrm{d}\sigma_{\mathbf{y}},$$

where $\mathbf{n}$ is the unit outward normal vector at the boundary $\partial\Omega$.

Theorem 2.8 (**Green's theorem**). *Let Ω be a bounded domain of class C^1 and let $\mathbf{n}$ denote the unit normal vector at the boundary $\partial\Omega$ directed to the exterior of Ω. Then, for $u \in C^1(\overline{\Omega})$ and $v \in C^2(\overline{\Omega})$ we have Green's first theorem*

$$\int_\Omega \big\{u\Delta v + \langle \nabla u, \nabla v\rangle\big\}\mathrm{d}\mathbf{y} = \int_{\partial\Omega} u\frac{\partial v}{\partial \mathbf{n}}\mathrm{d}\sigma_{\mathbf{y}} \tag{2.6}$$

and for $u, v \in C^2(\overline{\Omega})$ we have Green's second theorem

$$\int_\Omega \big(u\Delta v - v\Delta u\big)\mathrm{d}\mathbf{y} = \int_{\partial\Omega} \Big(u\frac{\partial v}{\partial \mathbf{n}} - v\frac{\partial u}{\partial \mathbf{n}}\Big)\mathrm{d}\sigma_{\mathbf{y}}. \tag{2.7}$$

The assumption $\partial\Omega$ is of class C^1 ensures that the normal vector $\mathbf{n}$ is well defined everywhere at $\partial\Omega$.

Given the Cauchy data of the function v at the boundary $\partial\Omega$, i.e., the Dirichlet and the Neumann data of v at $\partial\Omega$, the solution of (2.4) can be represented everywhere inside the domain Ω in the following form:

Theorem 2.9 (**Green's representation formula**). *Let Ω be as in Theorem 2.8 and let $v \in C^2(\overline{\Omega})$ be harmonic in Ω. Then, it holds*

$$v(\mathbf{x}) = \int_{\partial\Omega} \left\{G(\mathbf{x},\mathbf{y})\frac{\partial v}{\partial \mathbf{n}}(\mathbf{y}) - \frac{\partial G(\mathbf{x},\mathbf{y})}{\partial \mathbf{n}_{\mathbf{y}}} v(\mathbf{y})\right\}\mathrm{d}\sigma_{\mathbf{y}}, \quad \mathbf{x} \in \Omega. \tag{2.8}$$

Having in mind the application of the integral operators in boundary value problems, we expand the theory from the domain Ω to the boundary $\partial\Omega$. This can be achieved by the layer potentials and the associated jump relations.

2.2.3 Boundary integral operators

The representation formula (2.8) contains two potentials, the single-layer potential

$$\tau(\mathbf{x}) := \int_{\partial\Omega} G(\mathbf{x},\mathbf{y})\rho(\mathbf{y})\mathrm{d}\sigma_{\mathbf{y}}, \quad \mathbf{x} \in \mathbb{R}^2 \setminus \partial\Omega$$

and the double-layer potential

$$\omega(\mathbf{x}) := \int_{\partial\Omega} \frac{\partial G(\mathbf{x},\mathbf{y})}{\partial \mathbf{n}_{\mathbf{y}}}\rho(\mathbf{y})\mathrm{d}\sigma_{\mathbf{y}}, \quad \mathbf{x} \in \mathbb{R}^2 \setminus \partial\Omega,$$

where the densities ρ are the Cauchy data of v at the boundary $\partial\Omega$. The Cauchy data coincide with the boundary conditions which are not both given for boundary value problems. In the two-dimensional case, the potentials τ and ω are

called logarithmic single-layer potential and logarithmic double-layer potential, respectively. Obviously, the potentials τ and ω are harmonic functions. If we assume the C^2-regularity of the boundary and an integrable density function ρ, then they are analytic too.

The above potentials are defined for $\mathbf{x} \in \mathbb{R}^2 \setminus \partial\Omega$ while the limit formulae describe the behavior of the potentials when approaching the boundary $\partial\Omega$.

Theorem 2.10. *Let $\partial\Omega$ be of class C^2 and $\rho \in C(\partial\Omega)$. Then, the single-layer potential τ with density ρ is continuous throughout $\mathbb{R}^2$. For $\mathbf{x} \in \partial\Omega$, we have*

$$\tau(\mathbf{x}) = \int_{\partial\Omega} G(\mathbf{x}, \mathbf{y})\rho(\mathbf{y})\mathrm{d}\sigma_{\mathbf{y}},$$

where the integral exists as an improper integral.

Theorem 2.11. *For $\partial\Omega$ of class C^2, the double-layer potential ω with density $\rho \in C(\Omega)$ can continuously be extended from Ω to $\overline{\Omega}$ and from $\mathbb{R}^2 \setminus \overline{\Omega}$ to $\mathbb{R}^2 \setminus \Omega$ with limiting value*

$$\omega_{\pm}(\mathbf{x}) = \int_{\partial\Omega} \frac{\partial G(\mathbf{x}, \mathbf{y})}{\partial \mathbf{n}_{\mathbf{y}}} \rho(\mathbf{y})\mathrm{d}\sigma_{\mathbf{y}} \pm \frac{1}{2}\rho(\mathbf{x}), \quad \mathbf{x} \in \partial\Omega,$$

where

$$\omega_{\pm}(\mathbf{x}) = \lim_{\varepsilon \to +0} \omega\big(\mathbf{x} \pm \varepsilon \mathbf{n}(\mathbf{x})\big).$$

The integral exists as an improper integral.

Taking the limit of the potentials for $\mathbf{x}$ approaching $\partial\Omega$ leads to the definition of the single-layer integral operator

$$\big(\mathcal{V}\rho\big)(\mathbf{x}) = \lim_{\partial\Omega \ni \mathbf{z} \to \mathbf{x}} \tau(\mathbf{z}), \quad \mathbf{x} \in \partial\Omega \tag{2.9}$$

and the definition of the double-layer operator

$$\big(\mathcal{K}\rho\big)(\mathbf{x}) = \lim_{\partial\Omega \ni \mathbf{z} \to \mathbf{x}} \omega(\mathbf{z}) + \frac{1}{2}\rho(\mathbf{x}), \quad \mathbf{x} \in \partial\Omega. \tag{2.10}$$

Let us now introduce the boundary integral operators with respect to the boundaries $A, B \in \{\Gamma, \Sigma\}$. The single-layer operator is given by

$$\begin{aligned} \big(\mathcal{V}_{AB}\rho\big)(\mathbf{x}) &:= \int_A G(\mathbf{x}, \mathbf{y})\rho(\mathbf{y})\mathrm{d}\sigma_{\mathbf{y}} \\ &= -\frac{1}{4\pi} \int_A \log \|\mathbf{x} - \mathbf{y}\|^2 \rho(\mathbf{y})\mathrm{d}\sigma_{\mathbf{y}}, \quad \mathbf{x} \in B. \end{aligned} \tag{2.11}$$

The double-layer operator reads as

$$\begin{aligned}\big(\mathcal{K}_{AB}\rho\big)(\mathbf{x}) &:= \int_A \frac{\partial G(\mathbf{x},\mathbf{y})}{\partial \mathbf{n}_\mathbf{y}}\rho(\mathbf{y})\mathrm{d}\sigma_\mathbf{y} \\ &= \frac{1}{2\pi}\int_A \frac{\langle \mathbf{n}_\mathbf{y}, \mathbf{x}-\mathbf{y}\rangle}{\|\mathbf{x}-\mathbf{y}\|^2}\rho(\mathbf{y})\mathrm{d}\sigma_\mathbf{y}, \quad \mathbf{x}\in B. \end{aligned} \tag{2.12}$$

Considering that $\partial\Omega = \Gamma \cup \Sigma$, the jump relations from Theorems 2.10 and 2.11 can be written in terms of these operators. The mapping properties of the integral operators (2.11) and (2.12), included in (2.8), are specified by the following theorem.

Theorem 2.12. *Let $\partial\Omega$ be of class C^2 and $A, B \in \{\Gamma, \Sigma\}$. Then, the operators $\mathcal{V}_{AB}$ and $\mathcal{K}_{AB}$ are bounded as mappings from $C^{1,\alpha}(A)$ into $C^{1,\alpha}(B)$.*

We formulate now the result that establishes the desired unique relation between the Dirichlet and the Neumann data of v at the boundary $\partial\Omega$.

2.2.4 Dirichlet-to-Neumann map

By considering the limiting values of the potentials of the boundary, Green's representation formula (2.8) provides the direct boundary integral formulation of the problem (2.4), namely

$$\int_{\Gamma\cup\Sigma} G(\mathbf{x},\mathbf{y})\frac{\partial v}{\partial \mathbf{n}}(\mathbf{y})\mathrm{d}\sigma_\mathbf{y} = \frac{1}{2}v(\mathbf{x}) + \int_{\Gamma\cup\Sigma}\frac{\partial G(\mathbf{x},\mathbf{y})}{\partial \mathbf{n}_\mathbf{y}}v(\mathbf{y})\mathrm{d}\sigma_\mathbf{y}, \quad \mathbf{x}\in\partial\Omega. \tag{2.13}$$

Inserting the boundary integral operators (2.11) and (2.12) into (2.13) yields thus

$$\sum_{A\in\{\Gamma,\Sigma\}}\Big(\mathcal{V}_{AB}\frac{\partial v}{\partial \mathbf{n}}\Big) = \sum_{A\in\{\Gamma,\Sigma\}}\Big(\frac{1}{2}I + \mathcal{K}_{AB}\Big)v \quad \text{on } B\in\{\Gamma,\Sigma\}. \tag{2.14}$$

The equation (2.14) represents the relation between the Cauchy data of the function v at the domain's boundary $\partial\Omega = \Gamma\cup\Sigma$. This relation is known as the Dirichlet-to-Neumann map. In matrix form it can be written as

$$\begin{bmatrix} \mathcal{V}_{\Gamma\Gamma} & \mathcal{V}_{\Sigma\Gamma} \\ \mathcal{V}_{\Gamma\Sigma} & \mathcal{V}_{\Sigma\Sigma} \end{bmatrix}\begin{bmatrix} \frac{\partial v}{\partial \mathbf{n}}\big|_\Gamma \\ \frac{\partial v}{\partial \mathbf{n}}\big|_\Sigma \end{bmatrix} = \begin{bmatrix} \frac{1}{2}I + \mathcal{K}_{\Gamma\Gamma} & \mathcal{K}_{\Sigma\Gamma} \\ \mathcal{K}_{\Gamma\Sigma} & \frac{1}{2}I + \mathcal{K}_{\Sigma\Sigma} \end{bmatrix}\begin{bmatrix} v|_\Gamma \\ v|_\Sigma \end{bmatrix}. \tag{2.15}$$

2.2.5 Existence and uniqueness of the solution

For the mixed boundary value problem (2.4) the issue of existence and uniqueness of the solution is settled in [70, Theorem 4.11]. The existence and uniqueness of the solution to the boundary integral equations (2.15) are seen as follows.

Remark 2.13. We consider the case of a first kind integral equation for the single-layer operator with the logarithmic singularity of the form

$$-\frac{1}{4\pi}\int_A \log\|\mathbf{x}-\mathbf{y}\|^2\rho(\mathbf{y})\mathrm{d}\sigma_{\mathbf{y}} = q(\mathbf{x}).$$

We notice that the homogeneous equation

$$-\frac{1}{4\pi}\int_A \log\|\mathbf{x}-\mathbf{y}\|^2\rho(\mathbf{y})\mathrm{d}\sigma_{\mathbf{y}} = 0$$

does not always have the trivial solution. For example, in case of a circular boundary A of radius 1 and density $\rho = 1$, one can verify by direct integration that $\int_A \log\|\mathbf{x}-\mathbf{y}\|^2\mathrm{d}\sigma_{\mathbf{y}} = 0$. In order to avoid the non-uniqueness of the solution of the boundary integral equation (2.15) we shall assume that

$$\mathrm{diam}(\Omega) < 1,$$

see [48, 80]. This can always be guaranteed by an appropriate scaling of the domain Ω.

Remark 2.14. In general, the existence and the uniqueness of the solution to operator equations can equivalently be expressed by the existence of the inverse operator. In [70] it was proven that $\mathcal{V}$ is continuous and bijective provided that the logarithmic capacity of $\partial\Omega$ is strictly less than one, for which a sufficient criteria is $\mathrm{diam}(\Omega) < 1$. More details about the first kind integral equation with logarithmic kernel can be found in [40, 49, 66, 67]. In case of the second kind integral equation with compact operator the existence and uniqueness of its solution is established by the first and second Fredholm theorem, see [54].

For the boundary value problem (2.4), the Dirichlet-to-Neumann map (2.15) induces the following system of integral equations

$$\begin{bmatrix} \frac{1}{2}I + \mathcal{K}_{\Gamma\Gamma} & -\mathcal{V}_{\Sigma\Gamma} \\ \mathcal{K}_{\Gamma\Sigma} & -\mathcal{V}_{\Sigma\Sigma} \end{bmatrix} \begin{bmatrix} v|_\Gamma \\ \frac{\partial v}{\partial \mathbf{n}}\big|_\Sigma \end{bmatrix} = \begin{bmatrix} \mathcal{V}_{\Gamma\Gamma} & -\mathcal{K}_{\Sigma\Gamma} \\ \mathcal{V}_{\Gamma\Sigma} & -\frac{1}{2}I - \mathcal{K}_{\Sigma\Sigma} \end{bmatrix} \begin{bmatrix} \left(h - \frac{\partial N_f}{\partial \mathbf{n}}\right)\big|_\Gamma \\ (g - N_f)|_\Sigma \end{bmatrix}. \tag{2.16}$$

As we are interested in finding the Dirichlet data of v by giving its Neumann data at the free boundary, from now on we will refer to system (2.16) as Neumann-to-Dirichlet map. Due to Remark 2.14 about the existence and the uniqueness of the solution of the first and the second kind integral equation when compact operators are included, we can deduce that the above system of integral equations is solvable.

At last, we comment on the well-posedness of the boundary integral equations (2.15). The well-posedness of a problem in the sense of Hadamard is defined as the existence and uniqueness of the solution besides a continuous dependence of the solution on the given data. We have seen that the existence and the uniqueness of the solution of an operator equation are fulfilled whenever the operators are bijective. Moreover, for a bounded linear operator which maps a Banach space bijectively onto another Banach space, the inverse operator is bounded and therefore continuous by the inverse mapping theorem. These observations indicate the well-posedness of problem (2.15), which can thus be numerically solved, as we will see later, without any difficulty.

2.3 Solution of the boundary integral equation

The first step to solve the system of the boundary integral equations (2.15) is the parametrization of the boundaries and, as a consequence, the parametrization of the integral operators. Afterwards, we apply the collocation method.

2.3.1 Parametrization of the boundaries

For our purposes, we have assumed that $\partial\Omega = \Gamma \cup \Sigma$ is of class C^2. In particular, we assume that the fixed boundary Σ is sufficiently smooth and parametrized by

$$\boldsymbol{\gamma}_\Sigma : [0, 2\pi] \mapsto \Sigma.$$

If the domain T is starlike, then the free boundary Γ is parametrizable via polar coordinates according to

$$\boldsymbol{\gamma}_\Gamma : [0, 2\pi] \mapsto \Gamma, \quad \boldsymbol{\gamma}_\Gamma = r(s)\mathbf{e}_r(s),$$

where $\mathbf{e}_r(s) = \big(\cos(s), \sin(s)\big)^T$ denotes the unit vector in the radial direction. The radial function $r \in C^2_{\text{per}}\big([0, 2\pi]\big)$ with

$$C^2_{\text{per}}\big([0, 2\pi]\big) := \Big\{ r \in C^2\big([0, 2\pi]\big) : r^{(i)}(0) = r^{(i)}(2\pi),\ i = 0, 1, 2 \Big\} \tag{2.17}$$

is a positive function. Moreover, taking into account that the unit normal vector should point in the outward direction of Ω, the boundary curve $\boldsymbol{\gamma}_\Gamma$ should be counter-clockwise oriented while the boundary curve $\boldsymbol{\gamma}_\Sigma$ should be clockwise oriented.

2.3.2 Parametrized integral operators

Having established the solvability of the integral equations included in (2.15), we are now concerned with their parametrization.

The single-layer operator $\mathcal{V}_{AB}$ reads in parametrized form as

$$\Big(\mathcal{V}_{AB}\widetilde{\frac{\partial v}{\partial \mathbf{n}}}\Big)\big(\boldsymbol{\gamma}_B(s)\big) := -\frac{1}{4\pi}\int_0^{2\pi} k^{\mathcal{V}}_{A,B}(s,t)\widetilde{\frac{\partial v}{\partial \mathbf{n}}}\big(\boldsymbol{\gamma}_A(t)\big)\mathrm{d}t, \qquad s\in[0,2\pi] \tag{2.18}$$

with kernel

$$k^{\mathcal{V}}_{A,B}(s,t) = \log\|\boldsymbol{\gamma}_B(s)-\boldsymbol{\gamma}_A(t)\|^2 \tag{2.19}$$

for $A\neq B$ and density function

$$\widetilde{\frac{\partial v}{\partial \mathbf{n}}}\big(\boldsymbol{\gamma}_A(t)\big) = \frac{\partial v}{\partial \mathbf{n}}\big(\boldsymbol{\gamma}_A(t)\big)\|\boldsymbol{\gamma}'_A(t)\|.$$

For the double-layer operator $\mathcal{K}_{AB}$ we obtain

$$\big(\mathcal{K}_{AB}v\big)\big(\boldsymbol{\gamma}_B(s)\big) := \frac{1}{2\pi}\int_0^{2\pi} k^{\mathcal{K}}_{A,B}(s,t)v\big(\boldsymbol{\gamma}_A(t)\big)\mathrm{d}t, \quad s\in[0,2\pi] \tag{2.20}$$

with kernel

$$k^{\mathcal{K}}_{A,B}(s,t) = \frac{\langle \mathbf{n}_A(t), \boldsymbol{\gamma}_B(s)-\boldsymbol{\gamma}_A(t)\rangle}{\|\boldsymbol{\gamma}_B(s)-\boldsymbol{\gamma}_A(t)\|^2}\|\boldsymbol{\gamma}'_A(t)\| \tag{2.21}$$

for $A\neq B$.

The parametrized form of the equation (2.14) is given by

$$\begin{aligned}-\frac{1}{4\pi}\sum_{A\in\{\Gamma,\Sigma\}}\int_0^{2\pi} k^{\mathcal{V}}_{A,B}(s,t)\widetilde{\frac{\partial v}{\partial \mathbf{n}}}\big(\boldsymbol{\gamma}_A(t)\big)\mathrm{d}t \\ = \frac{1}{2}v\big(\boldsymbol{\gamma}_B(s)\big) + \frac{1}{2\pi}\sum_{A\in\{\Gamma,\Sigma\}}\int_0^{2\pi} k^{\mathcal{K}}_{A,B}(s,t)v\big(\boldsymbol{\gamma}_A(t)\big)\mathrm{d}t.\end{aligned} \tag{2.22}$$

In the special case of the integral operators being defined on the same boundary, the kernels are singular for $s=t$. The limit value of the kernel of the double-layer integral operator is given by the following lemma.

Lemma 2.15. *Assume that $\partial\Omega$ is of class C^2, represented by a twice continuously differentiable parametrization $\boldsymbol{\gamma}_A$. Then, the kernel of the double-layer operator*

$$\big(\mathcal{K}_{AA}v\big)\big(\boldsymbol{\gamma}_A(s)\big) = \frac{1}{2\pi}\int_0^{2\pi} k^{\mathcal{K}}_{A,A}(s,t)v\big(\boldsymbol{\gamma}_A(t)\big)\mathrm{d}t \tag{2.23}$$

is continuous and given by

$$k^{\mathcal{K}}_{A,A}(s,t) = \begin{cases} \dfrac{\langle \mathbf{n}_A(t), \boldsymbol{\gamma}_A(s) - \boldsymbol{\gamma}_A(t)\rangle}{\|\boldsymbol{\gamma}_A(s) - \boldsymbol{\gamma}_A(t)\|^2}\|\boldsymbol{\gamma}'_A(t)\|, & s \neq t \\ \dfrac{1}{2}\dfrac{\langle \mathbf{n}_A(t), \boldsymbol{\gamma}''_A(t)\rangle}{\|\boldsymbol{\gamma}'_A(t)\|}, & s = t. \end{cases} \tag{2.24}$$

Proof. The main tool for the approximation of the kernel in case of $s = t$ is the Taylor expansion of the parametrization $\boldsymbol{\gamma}_A(s)$ around t:

$$\boldsymbol{\gamma}_A(s) = \boldsymbol{\gamma}_A(t) + \boldsymbol{\gamma}'_A(t)(s-t) + \frac{1}{2}\boldsymbol{\gamma}''_A(t)(s-t)^2 + o(|s-t|^3). \tag{2.25}$$

Then the limiting value of the kernel $k^{\mathcal{K}}_{A,A}$ when $s \to t$ is written as

$$\begin{aligned}\lim_{s\to t} k^{\mathcal{K}}_{A,A}(s,t) &= \lim_{s\to t} \frac{\langle \mathbf{n}_A(t), \boldsymbol{\gamma}_A(s) - \boldsymbol{\gamma}_A(t)\rangle}{\|\boldsymbol{\gamma}_A(s) - \boldsymbol{\gamma}_A(t)\|^2}\|\boldsymbol{\gamma}'_A(t)\| \\ &= \frac{\langle \mathbf{n}_A(t), \boldsymbol{\gamma}'_A(t)(s-t) + \frac{1}{2}\boldsymbol{\gamma}''_A(t)(s-t)^2\rangle}{\|\boldsymbol{\gamma}'_A(t)(s-t)\|^2}\|\boldsymbol{\gamma}'_A(t)\|.\end{aligned}$$

As $\langle \mathbf{n}_A(t), \boldsymbol{\gamma}'_A(t)\rangle = 0$, it is an immediate result that the kernel $k^{\mathcal{K}}_{A,A}$ is continuously extendable by the value

$$\lim_{s\to t} k^{\mathcal{K}}_{A,A}(s,t) = \frac{1}{2}\frac{\langle \mathbf{n}_A(t), \boldsymbol{\gamma}''_A(t)\rangle}{\|\boldsymbol{\gamma}'_A(t)\|^2}\|\boldsymbol{\gamma}'_A(t)\| = \frac{1}{2}\kappa(t)\|\boldsymbol{\gamma}'_A(t)\|,$$

where κ denotes the curvature of the boundary A. □

The fundamental solution of the Laplace equation in two spatial dimensions contains a logarithmic singularity. Therefore, for the weakly singular single-layer operator $\mathcal{V}_{AA}$, the treatment is more involved and follows the approach in [9, 54].

For the proper numerical approximation of the single-layer operator $\mathcal{V}_{AA}$

$$\Big(\mathcal{V}_{AA}\widetilde{\frac{\partial v}{\partial \mathbf{n}}}\Big)\big(\boldsymbol{\gamma}_A(s)\big) = -\frac{1}{4\pi}\int_0^{2\pi} \log\|\boldsymbol{\gamma}_A(s) - \boldsymbol{\gamma}_A(t)\|^2 \widetilde{\frac{\partial v}{\partial \mathbf{n}}}\big(\boldsymbol{\gamma}_A(t)\big)\mathrm{d}t,$$

we split the kernel into two terms

$$\Big(\mathcal{V}_{AA}\widetilde{\frac{\partial v}{\partial \mathbf{n}}}\Big)\big(\boldsymbol{\gamma}_A(s)\big) := \Big(\mathcal{V}_1\widetilde{\frac{\partial v}{\partial \mathbf{n}}}\Big)\big(\boldsymbol{\gamma}_A(s)\big) - \Big(\mathcal{V}_2\widetilde{\frac{\partial v}{\partial \mathbf{n}}}\Big)\big(\boldsymbol{\gamma}_A(s)\big). \tag{2.26}$$

The first term on the right hand side of (2.26) corresponds to the single-layer operator in case of a circular boundary

$$\Big(\mathcal{V}_1\widetilde{\frac{\partial v}{\partial \mathbf{n}}}\Big)\big(\boldsymbol{\gamma}_A(s)\big) := -\frac{1}{4\pi}\int_0^{2\pi} \log\left(4\sin^2\left(\frac{s-t}{2}\right)\right)\widetilde{\frac{\partial v}{\partial \mathbf{n}}}\big(\boldsymbol{\gamma}_A(t)\big)\mathrm{d}t,\ \ s\in[0,2\pi]. \tag{2.27}$$

The second term on the right hand side of (2.26) with kernel $k^{\mathcal{V}}_{A,A}$ represents the perturbation from the unit circle to the given boundary curve, i.e.,

$$\Big(\mathcal{V}_2\widetilde{\frac{\partial v}{\partial \mathbf{n}}}\Big)\big(\boldsymbol{\gamma}_A(s)\big) := \frac{1}{4\pi}\int_0^{2\pi} k^{\mathcal{V}}_{A,A}(s,t)\widetilde{\frac{\partial v}{\partial \mathbf{n}}}\big(\boldsymbol{\gamma}_A(t)\big)\mathrm{d}t, \quad s\in[0,2\pi]. \tag{2.28}$$

In particular, the kernel of the operator $\mathcal{V}_2$ is smooth, provided that the boundary is smooth. We continue with the derivation of the exact form of the kernel $k^{\mathcal{V}}_{A,A}$.

Lemma 2.16. *The kernel $k^{\mathcal{V}}_{A,A}$ of the operator $\mathcal{V}_2$ is given by*

$$k^{\mathcal{V}}_{A,A}(s,t) = \begin{cases} \log\dfrac{\|\boldsymbol{\gamma}_A(s)-\boldsymbol{\gamma}_A(t)\|^2}{4\sin^2\left(\frac{s-t}{2}\right)}, & s\neq t \\ \log\|\boldsymbol{\gamma}_A'(t)\|^2, & s=t. \end{cases} \tag{2.29}$$

Proof. Using the same procedure and tools as in the proof of Lemma 2.15 and in view of the trigonometric term $\sin^2(s)$ and its approximation by the Taylor expansion $\sin^2(s-t) = (s-t)^2 + o\big(|s-t|^4\big)$, straightforward calculation shows

$$\lim_{s\to t} k^{\mathcal{V}}_{A,A}(s,t) = \lim_{s\to t}\log\frac{\|\boldsymbol{\gamma}_A(s)-\boldsymbol{\gamma}_A(t)\|^2}{4\sin^2\left(\frac{s-t}{2}\right)} = \log\frac{\|\boldsymbol{\gamma}_A'(t)(s-t)\|^2}{(s-t)^2} = \log\|\boldsymbol{\gamma}_A'(t)\|^2.$$

□

Having finally derived the parametrized form of the integral equations in (2.22) as well as the contained kernels, we move on to the approximation of the boundary integrals operators.

2.3.3 Operator approximation

A fundamental concept for approximately solving the system of operator equations

$$\sum_{A\in\{\Gamma,\Sigma\}} \Big(\mathcal{V}_{AB}\widetilde{\frac{\partial v}{\partial \mathbf{n}}}\Big)\big(\boldsymbol{\gamma}_B(s)\big) = \sum_{A\in\{\Gamma,\Sigma\}} \Big(\frac{1}{2}I + \mathcal{K}_{AB}\Big)v\big(\boldsymbol{\gamma}_B(s)\big), \quad B \in \{\Gamma,\Sigma\}$$

is to replace it by

$$\sum_{A\in\{\Gamma,\Sigma\}} \Big(\mathcal{V}^n_{AB}\widetilde{\frac{\partial v}{\partial \mathbf{n}}}^{\,n}\Big)\big(\boldsymbol{\gamma}_B(s)\big) = \sum_{A\in\{\Gamma,\Sigma\}} \Big(\frac{1}{2}I + \mathcal{K}^n_{AB}\Big)v^n\big(\boldsymbol{\gamma}_B(s)\big), \quad B \in \{\Gamma,\Sigma\}, \tag{2.30}$$

which includes an approximating sequence $\mathcal{V}^n_{AB},\ \mathcal{K}^n_{AB} : C^{1,\alpha}(\partial\Omega) \to C^{1,\alpha}(\partial\Omega),\ n \to \infty$, for each of the bounded linear operators $\mathcal{V}_{AB},\ \mathcal{K}_{AB} : C^{1,\alpha}(\partial\Omega) \to C^{1,\alpha}(\partial\Omega)$. For practical reasons, we aim here at the reduction of our system of integral equations to a finite dimensional linear system of equations. This is succeeded by an appropriate choice of the approximating sequence of bounded linear operators. In the two-dimensional case, the parametrized form (2.22) of the boundary integral equations contains periodic functions. This suggests the use of a global approximation in the form of trigonometric polynomials. There are several benefits in using trigonometric methods. In the first place, they provide schemes which converge of high order and under proper conditions even of exponential order. Additionally, in connection with the Fast Fourier Transform (FTT), see [34, 60], which provides a simple and fast tool to efficiently handle the Fourier representation of trigonometric functions, the trigonometric methods are also computationally cheap.

By $\rho^{(i)},\ i = 1, 2$, we denote the density functions in equation (2.22), namely

$$\rho^{(1)}(t) = \widetilde{\frac{\partial v}{\partial \mathbf{n}}}(t) \qquad \text{and} \qquad \rho^{(2)}(t) = v(t).$$

We assume that the densities are trigonometric functions with Fourier representations of the form

$$\rho^{(i,n)}(t_k) = \sum_{m=0}^{n} a_m^{(i)} \cos(mt_k) + \sum_{m=1}^{n-1} b_m^{(i)} \sin(mt_k), \quad i = 1, 2. \tag{2.31}$$

The Fourier coefficients $a_m^{(i)}$ and $b_m^{(i)}$ are given by point evaluation in the equidis-

tantly distributed points $t_k = \pi k/n,\ k = 0, \dots, 2n-1$:

$$a_m^{(i)} = \frac{1}{n} \sum_{k=0}^{2n-1} \rho^{(i)}(t_k) \cos(mt_k), \quad m = 0, \dots, n,$$
$$b_m^{(i)} = \frac{1}{n} \sum_{k=0}^{2n-1} \rho^{(i)}(t_k) \sin(mt_k), \quad m = 1, \dots, n-1.$$

In order to simplify the notation, in what follows we omit the superscript n for the numerical approximation of the quantities contained in (2.30).

2.3.4 Collocation method

The collocation method to approximately solve the boundary integral equations in (2.22) consists of seeking a solution from a finite dimensional subspace $X_n = \operatorname{span}\{s_0, \dots, s_{2n-1}\} \subset C\big([0, 2\pi]\big)$ so that the integral equations are satisfied at the collocation points. Let $s_j = \pi j/n,\ j = 0, \dots, 2n-1$, be an even number of equidistantly distributed points on the interval $[0, 2\pi]$, the so-called collocation points. We require that the integral equations (2.22) are satisfied in these points, that is,

$$-\frac{1}{4\pi} \sum_{A \in \{\Gamma, \Sigma\}} \int_0^{2\pi} k_{A,B}^{\mathcal{V}}(s_j, t) \widetilde{\frac{\partial v}{\partial \mathbf{n}}}\big(\boldsymbol{\gamma}_A(t)\big) \mathrm{d}t = \frac{1}{2} v\big(\boldsymbol{\gamma}_B(s_j)\big) + \frac{1}{2\pi} \sum_{A \in \{\Gamma, \Sigma\}} \int_0^{2\pi} k_{A,B}^{\mathcal{K}}(s_j, t) v\big(\boldsymbol{\gamma}_A(t)\big) \mathrm{d}t \quad (2.32)$$

for all $j = 0, \dots, 2n-1$. Inserting the ansatz (2.31) into (2.32), we obtain a linear system of equations for the unknown coefficients $a_m^{(i)}$ and $b_m^{(i)}$ of the approximating trigonometric polynomial. Nonetheless, it is more efficient to replace the representation (2.31) by using the trigonometric Lagrange basis defined by the interpolation property $L_k(s_j) = \delta_{jk},\ j, k = 0, \dots, 2n-1$. The Lagrange basis for the trigonometric polynomials is explicitly given by

$$L_k(s) = \frac{1}{n} \Big\{ 1 + \sum_{m=1}^{n-1} \cos m(s - t_k) + \cos n(s - t_k) \Big\}, \quad s \in [0, 2\pi]. \quad (2.33)$$

Replacing the continuous periodic functions v and $\widetilde{\partial v/\partial \mathbf{n}}$ by their trigonometric approximations, i.e.

$$v(s) = \sum_{k=0}^{2n-1} v(t_k) L_k(s) \quad \text{and} \quad \widetilde{\frac{\partial v}{\partial \mathbf{n}}}(s) = \sum_{k=0}^{2n-1} \widetilde{\frac{\partial v}{\partial \mathbf{n}}}(t_k) L_k(s),$$

the system (2.32) becomes

$$-\frac{1}{4\pi}\sum_{A\in\{\Gamma,\Sigma\}}\sum_{k=0}^{2n-1}\widetilde{\frac{\partial v}{\partial \mathbf{n}}}(t_k)\int_0^{2\pi}k^{\mathcal{V}}_{A,B}(s_j,t)L_k(t)\mathrm{d}t$$
$$=\frac{1}{2}v(s_j)+\frac{1}{2\pi}\sum_{A\in\{\Gamma,\Sigma\}}\sum_{k=0}^{2n-1}v(t_k)\int_0^{2\pi}k^{\mathcal{K}}_{A,B}(s_j,t)L_k(t)\mathrm{d}t. \quad (2.34)$$

The collocation method is a semi-discrete method. In order to make the method fully discrete we have to use a quadrature formula. The system of integral equations (2.34) involves operators with either continuous or weakly singular kernels. Therefore we proceed with the approximation of each boundary integral operator. Replacing the continuous periodic function $\widetilde{\partial v/\partial \mathbf{n}}$ by its trigonometric interpolation polynomial (2.31), the singular part (2.27) is written as

$$\Big(\mathcal{V}_1\widetilde{\frac{\partial v}{\partial \mathbf{n}}}\Big)(s_j)=-\frac{1}{4\pi}\sum_{k=0}^{2n-1}\widetilde{\frac{\partial v}{\partial \mathbf{n}}}(t_k)\int_0^{2\pi}\log\left(4\sin^2\Big(\frac{s_j-t}{2}\Big)\right)L_k(t)\mathrm{d}t. \quad (2.35)$$

Let R_k denote the quadrature weight in (2.35), namely,

$$R_k(s_j)=\frac{1}{2\pi}\int_0^{2\pi}\log\left(4\sin^2\Big(\frac{s_j-t}{2}\Big)\right)L_k(t)\mathrm{d}t.$$

Then, making use of the relation

$$\frac{1}{2\pi}\int_0^{2\pi}\log\Big(4\sin^2\frac{t}{2}\Big)e^{imt}\mathrm{d}t=\begin{cases}0, & m=0\\ -\dfrac{1}{|m|}, & m=\pm1,\pm2,\ldots,\end{cases} \quad (2.36)$$

(see [54, Lemma 8.21] for more details) and substituting the Lagrange basis according to (2.33), we can evaluate the quadrature weight R_k. This yields

$$R_k(s_j)=-\frac{1}{n}\Big\{\sum_{m=1}^{n-1}\frac{1}{m}\cos m(s_j-t_k)+\frac{1}{n}\cos n(s_j-t_k)\Big\}.$$

Hence, the singular part of the operator $\mathcal{V}_{AA}$ is computed by

$$\Big(\mathcal{V}_1\widetilde{\frac{\partial v}{\partial \mathbf{n}}}\Big)(s_j)=-\frac{1}{2}\sum_{k=0}^{2n-1}R_k(s_j)\widetilde{\frac{\partial v}{\partial \mathbf{n}}}(t_k). \quad (2.37)$$

We formulate next the fully discrete collocation method for the smooth part $\mathcal{V}_2$ defined in (2.28) of the operator $\mathcal{V}_{AA}$ in (2.26). As the kernel of the integral operator (2.28) is continuous, we get from the interpolation of the density

$$\Big(\mathcal{V}_2\widetilde{\frac{\partial v}{\partial \mathbf{n}}}\Big)(s_j)=\sum_{k=0}^{2n-1}\widetilde{\frac{\partial v}{\partial \mathbf{n}}}(t_k)\int_0^{2\pi}k^{\mathcal{V}}_{A,A}(s_j,t)L_k(t)\mathrm{d}t. \quad (2.38)$$

The approximation of the integral in (2.38) by the composite trapezoidal rule in the quadrature points $t_k = \pi k/n$, $k = 0, \ldots, 2n-1$, yields

$$\Big(\mathcal{V}_2 \widetilde{\frac{\partial v}{\partial \mathbf{n}}}\Big)(s_j) = -\frac{1}{4n} \sum_{k=0}^{2n-1} k^{\mathcal{V}}_{A,A}(s_j, t_k) \widetilde{\frac{\partial v}{\partial \mathbf{n}}}(t_k). \tag{2.39}$$

To summarize, the single-layer operator $\mathcal{V}_{AA}$ from equation (2.26) in the collocation points is given by

$$\big(\mathcal{V}_{AA} \widetilde{\frac{\partial v}{\partial \mathbf{n}}}\big)(s_j) = -\frac{1}{2} \sum_{k=0}^{2n-1} \Big\{ R_k(s_j) + \frac{1}{2n} k^{\mathcal{V}}_{A,A}(s_j, t_k) \Big\} \widetilde{\frac{\partial v}{\partial \mathbf{n}}}(t_k), \quad 0 \le j \le 2n-1.$$

The boundary integral operators $\mathcal{V}_{AB}$ from (2.18) for $A \neq B$ and $\mathcal{K}_{AB}$ from (2.20), which have smooth and continuous kernels, are directly computed by the composite trapezoidal rule. This means that

$$\Big(\mathcal{V}_{AB} \widetilde{\frac{\partial v}{\partial \mathbf{n}}}\Big)(s) = -\frac{1}{4\pi} \int_0^{2\pi} k^{\mathcal{V}}_{A,B}(s,t) \widetilde{\frac{\partial v}{\partial \mathbf{n}}}(t) \mathrm{d}t, \quad s \in [0, 2\pi],$$

for $A \neq B$ is approximated by the quadrature

$$\Big(\mathcal{V}_{AB} \widetilde{\frac{\partial v}{\partial \mathbf{n}}}\Big)(s_j) = -\frac{1}{4n} \sum_{k=0}^{2n-1} k^{\mathcal{V}}_{A,B}(s_j, t_k) \widetilde{\frac{\partial v}{\partial \mathbf{n}}}(t_k), \quad 0 \le j \le 2n-1.$$

Likewise, the double-layer operator

$$\big(\mathcal{K}_{AB} v\big)(s) = \frac{1}{2\pi} \int_0^{2\pi} k^{\mathcal{K}}_{A,B}(s,t) v(t) \mathrm{d}t, \quad s \in [0, 2\pi]$$

is fully discretized in the form

$$\big(\mathcal{K}_{AB} v\big)(s_j) = \frac{1}{2n} \sum_{k=0}^{2n-1} k^{\mathcal{K}}_{A,B}(s_j, t_k) v(t_k), \quad 0 \le j \le 2n-1,$$

where the kernel is given either by (2.21) in case of $A \neq B$ or by (2.24) in case of $A = B$.

Plugging all together, we obtain the linear system of equations

$$\mathbf{C} \begin{bmatrix} \widetilde{\dfrac{\partial v}{\partial \mathbf{n}}}\big(\boldsymbol{\gamma}_\Gamma(t_k)\big) \\ \widetilde{\dfrac{\partial v}{\partial \mathbf{n}}}\big(\boldsymbol{\gamma}_\Sigma(t_k)\big) \end{bmatrix} = \mathbf{D} \begin{bmatrix} v\big(\boldsymbol{\gamma}_\Gamma(t_k)\big) \\ v\big(\boldsymbol{\gamma}_\Sigma(t_k)\big) \end{bmatrix} \tag{2.40}$$

with

$$\mathbf{C} = \begin{bmatrix} -\frac{1}{2}\Big\{R_k(s_j) + \frac{1}{2n}k^{\mathcal{V}}_{\Gamma,\Gamma}(s_j,t_k)\Big\} & -\frac{1}{2n}\log\|\boldsymbol{\gamma}_\Gamma(s_j) - \boldsymbol{\gamma}_\Sigma(t_k)\| \\ -\frac{1}{2n}\log\|\boldsymbol{\gamma}_\Sigma(s_j) - \boldsymbol{\gamma}_\Gamma(t_k)\| & -\frac{1}{2}\Big\{R_k(s_j) + \frac{1}{2n}k^{\mathcal{V}}_{\Sigma,\Sigma}(s_j,t_k)\Big\} \end{bmatrix}$$

and

$$\mathbf{D} = \begin{bmatrix} \frac{1}{2}I + \frac{1}{2n}k^{\mathcal{K}}_{\Gamma,\Gamma}(s_j,t_k) & \frac{1}{2n}\dfrac{\big\langle \mathbf{n}_\Sigma(t_k), \boldsymbol{\gamma}_\Gamma(s_j) - \boldsymbol{\gamma}_\Sigma(t_k)\big\rangle}{\dfrac{\|\boldsymbol{\gamma}_\Gamma(s_j) - \boldsymbol{\gamma}_\Sigma(t_k)\|^2}{\|\boldsymbol{\gamma}'_\Sigma(t_k)\|}} \\ \frac{1}{2n}\dfrac{\big\langle \mathbf{n}_\Gamma(t_k), \boldsymbol{\gamma}_\Sigma(s_j) - \boldsymbol{\gamma}_\Gamma(t_k)\big\rangle}{\dfrac{\|\boldsymbol{\gamma}_\Sigma(s_j) - \boldsymbol{\gamma}_\Gamma(t_k)\|^2}{\|\boldsymbol{\gamma}'_\Gamma(t_k)\|}} & \frac{1}{2}I + \frac{1}{2n}k^{\mathcal{K}}_{\Sigma,\Sigma}(s_j,t_k) \end{bmatrix}.$$

Here, the kernels that show up in (2.40) are given by the relations (2.24) and (2.29).

2.4 Exponential convergence

In this section, the convergence analysis of the collocation method is presented. The collocation method can be considered as a special case of a projection method with a projection operator being generated by interpolation. As a result, the general error and convergence analysis for projection methods are applicable. Provided that the integral equations in (2.22) are uniquely solvable and that the kernels $k^{\mathcal{V}}_{A,B}$ and $k^{\mathcal{K}}_{A,B}$ are twice differentiable, the approximated system of integral equations (2.30) is also uniquely solvable for sufficiently large n. For $n \to \infty$, the approximate solutions ρ^n converge uniformly to the solution ρ of the integral equations. Results about the convergence of the collocation method [54, Chapter 13] show that the error $\|\rho^n - \rho\|$ between the exact solution ρ and the approximate solution ρ^n is uniformly bounded by the error $\|\rho^n_{\text{int}} - \rho\|$ of the trigonometric interpolation polynomial ρ^n_{int} to the exact solution ρ. This means that, for a smooth parametrization and analytic exact solution ρ, the approximation error decreases exponentially [53, 54].

In our case, we moreover have to consider that we approximate the solution of the system of equations (2.40) whose right hand side contains integral equations which are not exactly but approximately computed by the trapezoidal rule. Thereby additional approximation errors are imposed to the system. However, since the matrix $\mathbf{E} = \mathbf{C}^{-1}\mathbf{D}$ is well conditioned, the convergence order of the error remains

exponential. Therefore, our next objective is to examine if the requirements for an exponential convergence hold. Namely, we want to prove that the kernels $k^{\mathcal{V}}_{A,B}$ and $k^{\mathcal{K}}_{A,B}$ are analytic.

Due to Theorem 2.5 we know that harmonic functions are analytic. Then, in the case of the integral operators $\mathcal{V}_{AB}$ (2.18) and $\mathcal{K}_{AB}$ (2.20) with $A \neq B$, the corresponding kernels are analytic as they include the Green function and its normal derivative, respectively. In case $A = B$, it remains to prove that the kernels $k^{\mathcal{V}}_{A,A}$ and $k^{\mathcal{K}}_{A,A}$ are also analytic functions. For sake of simplicity in the underlying proofs of the subsequent theorems, we use s for the collocation points instead of $s_j = \pi j/n,\ j = 0, \dots, 2n-1$ and t for the quadrature points instead of $t_k = \pi k/n,\ k = 0, \dots, 2n-1$.

Lemma 2.17. *The kernel $k^{\mathcal{V}}_{A,A}$ which is given by* (2.29) *is an analytic function.*

Proof. For $2n$ grid points in $[0, 2\pi]$ and $n \geq 1$ there occur three cases.

1. If $|s-t| \leq 2\pi$, due to the assumption of smoothness of $\boldsymbol{\gamma}_A$, the kernel $k^{\mathcal{V}}_{A,A}(s,t)$ is analytic in the domain

$$Q := \{(s,t) \in [0,2\pi] \times [0,2\pi] : |s-t| < 2\pi\}.$$

Indeed, for $s \neq t$, we rewrite the kernel in the form

$$k^{\mathcal{V}}_{A,A}(s,t) = \log \frac{\|\boldsymbol{\gamma}_A(s) - \boldsymbol{\gamma}_A(t)\|^2}{(s-t)^2} \frac{\left(\frac{s-t}{2}\right)^2}{\sin^2\left(\frac{s-t}{2}\right)}. \tag{2.41}$$

Inserting, the Taylor expansion of the parametrization $\boldsymbol{\gamma}_A$, the first factor in (2.41) can be written as:

$$\begin{aligned}
\frac{\|\boldsymbol{\gamma}_A(s) - \boldsymbol{\gamma}_A(t)\|^2}{(s-t)^2} &= \frac{\left\| \sum_{i=1}^{\infty} \frac{\boldsymbol{\gamma}_A^{(i)}(t)}{i!} (s-t)^i \right\|^2}{(s-t)^2} \\
&= \frac{(s-t)^2}{(s-t)^2} \left\| \sum_{i=1}^{\infty} \frac{\boldsymbol{\gamma}_A^{(i)}(t)}{i!} (s-t)^{i-1} \right\|^2 \\
&= \left\| \sum_{i=1}^{\infty} \frac{\boldsymbol{\gamma}_A^{(i)}(t)}{i!} (s-t)^{i-1} \right\|^2 .
\end{aligned} \tag{2.42}$$

For sake of simplicity, we assume that the convergence radius of the Taylor series is bigger than 2π. Therefore, we can conclude that (2.42) is a convergent power

series. For the second part, denoting $\sigma = \dfrac{s-t}{2}$, we obtain

$$\frac{\sin\sigma}{\sigma} = \frac{1}{\sigma}\sum_{i=0}^{\infty}\frac{(-1)^i\sigma^{2i+1}}{(2i+1)!} = \sum_{i=0}^{\infty}\frac{(-1)^i\sigma^{2i}}{(2i+1)!} = 1 - \frac{\sigma^2}{3!} + \frac{\sigma^4}{5!} - \frac{\sigma^6}{7!} + \cdots .$$

Using the ratio test on $\theta_i = \displaystyle\sum_{i=0}^{\infty}\frac{(-1)^i\sigma^{2i}}{(2i+1)!}$, we conclude that the limit of successive ratios is less than 1 for any σ, i.e.,

$$\begin{aligned}\lim_{i\to\infty}\left|\frac{\theta_{i+1}}{\theta_i}\right| &= \lim_{i\to\infty}\left|\frac{(-1)^{i+1}\sigma^{2i+1}}{(2i+3)!}\frac{(2i+1)!}{(-1)^i\sigma^{2i}}\right| \\ &= \lim_{i\to\infty}\left|\frac{\sigma^2}{(2i+2)(2i+3)}\right| = 0.\end{aligned}$$

Therefore the series converges for all σ. From the property of analytic functions that the reciprocal of an analytic function that is nowhere zero is analytic, we conclude that the kernel of the singular layer potential is an analytic function since $|\sigma| = \left|\dfrac{s-t}{2}\right| \leq \pi$.

2. If $2\pi + s - t \leq 0$, then it follows

$$k^{\mathcal{V}}_{A,A}(s,t) = \begin{cases} \log\dfrac{\|\boldsymbol{\gamma}_A(s) - \boldsymbol{\gamma}_A(t)\|^2}{4\sin^2\left(\dfrac{2\pi+s-t}{2}\right)}, & (s,t) \neq (0,2\pi) \\ \log\|\boldsymbol{\gamma}'_A(t)\|^2, & (s,t) = (0,2\pi). \end{cases}$$

Due to the 2π-periodicity the kernel $k^{\mathcal{V}}_{A,A}(s,t)$ is analytic (see equations (2.41) and (2.42)) in the domain $Q := \{(s,t) \in [0,2\pi] \times [0,2\pi] \backslash (0,2\pi)\}$.

3. If $2\pi + t - s \leq 0$, then it holds

$$k^{\mathcal{V}}_{A,A}(s,t) = \begin{cases} \log\dfrac{\|\boldsymbol{\gamma}_A(s) - \boldsymbol{\gamma}_A(t)\|^2}{4\sin^2\left(\dfrac{2\pi+t-s}{2}\right)}, & (s,t) \neq (2\pi,0) \\ \log\|\boldsymbol{\gamma}'_A(t)\|^2, & (s,t) = (2\pi,0). \end{cases}$$

Using the same argument as before, the kernel is analytic in the domain $Q := \{(s,t) \in [0,2\pi] \times [0,2\pi] \backslash (2\pi,0)\}$. □

Likewise, we prove the analyticity of the kernel $k^{\mathcal{K}}_{A,A}$.

Lemma 2.18. *The kernel $k^{\mathcal{K}}_{A,A}$ given by* (2.24) *is an analytic function.*

Proof. For $s \neq t$, the kernel can be rewritten in the form

$$\frac{\langle \mathbf{n}_A(t), \boldsymbol{\gamma}_A(s) - \boldsymbol{\gamma}_A(t) \rangle}{(s-t)^2} \frac{(s-t)^2}{\|\boldsymbol{\gamma}_A(s) - \boldsymbol{\gamma}_A(t)\|^2} \|\boldsymbol{\gamma}_A'(t)\|. \tag{2.43}$$

Insering the Taylor expansion of the smooth parametrization $\boldsymbol{\gamma}_A$ yields for the first factor of (2.43)

$$\frac{\Big\langle \mathbf{n}_A(t), \sum_{i=1}^{\infty} \frac{\boldsymbol{\gamma}_A^{(i)}(t)}{i!}(s-t)^i \Big\rangle}{(s-t)^2} = \Big\langle \mathbf{n}_A(t), \sum_{i=2}^{\infty} \frac{\boldsymbol{\gamma}_A^{(i)}(t)}{i!}(s-t)^{i-2} \Big\rangle.$$

This is obviously an analytic function. By Lemma 2.17 and equation (2.42), the second factor of (2.43) is also analytic. Finally, for (2.43) the assumption of analyticity holds, as the product of analytic functions is an analytic function. All arguments hold also in case $s = t$, the kernel thereby is proven to be analytic. □

Having proved all the necessary requirements for an exponential convergence, we point to [54] and present the following theorem.

Theorem 2.19. *The fully discrete collocation method is converging exponentially provided that the parametrization and the solution v are analytic functions.*

The validity of Theorem 2.19 will be shown by numerical examples not only in the next section but also in the upcoming chapters.

Example 2.20. In this example we are looking for the Dirichlet data of the function v at the boundary Γ by applying collocation method, as it is presented in Section 2.3.4. We consider the domain Ω being described by a peanut shaped boundary Σ and a perturbed ellipse Γ as seen in Figure 2.1. The corresponding parametrizations read as

$$\boldsymbol{\gamma}_\Sigma : [0, 2\pi] \to \Sigma, \quad s \mapsto \boldsymbol{\gamma}_\Sigma(s) = \begin{bmatrix} 0.03 \sin(s)\big(1.25 + \cos(2s)\big) \\ 0.045 \cos(s) \end{bmatrix}$$

and

$$\boldsymbol{\gamma}_\Gamma : [0, 2\pi] \to \Gamma, \quad s \mapsto \boldsymbol{\gamma}_\Gamma(s) = \sqrt{0.006 \cos^2(3s) + 0.004 \sin^2(3s)} \begin{bmatrix} \cos(s) \\ \sin(s) \end{bmatrix}.$$

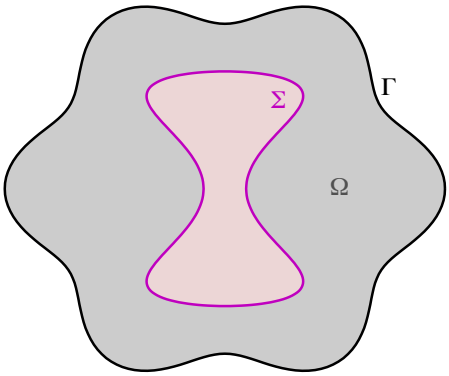

Figure 2.1: The domain Ω under consideration.

The harmonic function

$$v(x,y) = \log\left(\sqrt{(x-x_0)^2+(y-y_0)^2}\right)$$

with $(x_0, y_0) \notin \Omega$ satisfies the homogeneous partial differential equation (2.4a), i.e., $f = 0$ and thus also $N_f = 0$. We are interested in approximating the value of the unknown Dirichlet data of v at the boundary Γ by the boundary element method and compare it with the analytically given result. In Figure 2.2, the relative L^2-error between the analytical and the approximate Dirichlet data of v is illustrated with respect to the number of boundary elements (# of BE) per boundary. The table at the right hand side of the figure contains the values of these errors. Figure 2.2 verifies the predicted exponential convergence.

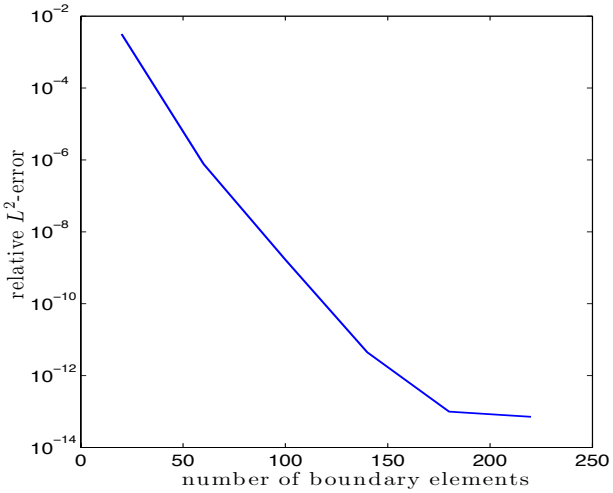

# of BE	error
20	0.003176
60	$7.716{\cdot}10^{-7}$
100	$1.682{\cdot}10^{-9}$
140	$4.446{\cdot}10^{-12}$
180	$9.948{\cdot}10^{-14}$
220	$7.129{\cdot}10^{-14}$

Figure 2.2: Relative L^2-error versus the number of boundary elements.

Moreover, by looking at the numerical results one can deduce that, for an appropriate number of boundary elements, the collocation method can compute the desired Dirichlet data at the boundary Γ sufficiently accurate. $\triangle$

Chapter 3

Update equations and numerical solution

The trial method for the solution of the free boundary problem requires an update rule for the free boundary. In combination with the iterative scheme of the trial method (see Algorithm 1.1), this update rule leads to the determination of the unknown free boundary Γ. This will be the subject of this chapter. At the beginning we review the theory behind optimization problems, including results in differential calculus as they appear in [58]. Then, we derive the update equations via Taylor's expansion of the first and second order of the Dirichlet data of the state at the current boundary Γ_k. We aim to elaborate the convergence of the trial method based on the resulting first order and second order update equation. The first order update rule for boundary updates in the normal direction has already been used in the context of the trial methods, e.g., in [36, 75], and in the context of the level set methods, e.g., in [56]. In order to derive the update rules we need to determine the update function which appropriately updates the current free boundary in the radial direction. Therefore, the derived update equations are formulated as minimization problems which are solved by optimization methods. There are two different approaches to numerically tackle minimization problems: "discretize-then-optimize" [35, 47, 58] and "optimize-then-discretize" [34, 47]. We discuss and implement in this chapter both approaches, since our goal is to compare them in order to conclude which is the more efficient approach. Finally, we present some numerical examples of the trial method so far to validate that the trial method based on the second order update rule has a more robust performance.

3.1 Introduction to continuous optimization

In this section we address the theory which deals with the optimization of a linear or a nonlinear function, cf. [12, 58, 60]. The basic formulation of an unconstrained optimization problem of a smooth function $f : \mathbb{R}^d \to \mathbb{R}$ is

$$\min f(\mathbf{x}),$$

where $\mathbf{x} = (x_1, x_2, \ldots, x_d) \in \mathbb{R}^d$ is a real vector. A local minimizer for f is an argument vector which gives the smallest function value inside its ε-neighborhood. More precisely:

Definition 3.1. *The point $\mathbf{x}^\star$ is called a local minimizer for f if there exists an $\varepsilon > 0$ such that*

$$f(\mathbf{x}^\star) \leq f(\mathbf{x}) \quad \textit{for all} \quad \|\mathbf{x}^\star - \mathbf{x}\| \leq \varepsilon.$$

The point $\mathbf{x}^\star$ is called a strict local minimizer for f if there exists an $\varepsilon > 0$ such that

$$f(\mathbf{x}^\star) < f(\mathbf{x}) \quad \textit{for all} \quad \|\mathbf{x}^\star - \mathbf{x}\| \leq \varepsilon \quad \textit{with} \quad \mathbf{x}^\star \neq \mathbf{x}.$$

If f is twice continuously differentiable, we may be able to tell that $\mathbf{x}^\star$ is a local minimizer by examining the gradient $\nabla f(\mathbf{x}^\star)$ and the Hessian $\nabla^2 f(\mathbf{x}^\star)$. First, we assume that $f \in C^1(\mathbb{R}^d)$ and the gradient of f is denoted by

$$\nabla f(\mathbf{x}) = \left(\frac{\partial f(\mathbf{x})}{\partial x_1}, \frac{\partial f(\mathbf{x})}{\partial x_2}, \ldots, \frac{\partial f(\mathbf{x})}{\partial x_d} \right)^T = \big(Df(\mathbf{x}) \big)^T.$$

Definition 3.2. *Let $\mathbf{V} \neq \mathbf{0}$ be a vector in $\mathbb{R}^d$. The derivative of f in the direction $\mathbf{V}$ is the function defined by the limit*

$$\frac{\partial f}{\partial \mathbf{V}}(\mathbf{x}) := \frac{\mathrm{d}}{\mathrm{d}\varepsilon} f(\mathbf{x} + \varepsilon \mathbf{V}) \Big|_{\varepsilon = 0} = \lim_{\varepsilon \to 0} \frac{f(\mathbf{x} + \varepsilon \mathbf{V}) - f(\mathbf{x})}{\varepsilon}.$$

If the function f is differentiable at $\mathbf{x}$, then the directional derivative exists along any vector $\mathbf{V}$, and one has $\partial f / \partial \mathbf{V} = \mathbf{V}^T \nabla f = \langle \nabla f, \mathbf{V} \rangle$. Provided that $f \in C^2(\mathbb{R}^d)$, the Hessian $\nabla^2 f$ of f is given by

$$\nabla^2 f(\mathbf{x}) = \begin{bmatrix} \dfrac{\partial^2 f(\mathbf{x})}{\partial x_1^2} & \cdots & \dfrac{\partial^2 f(\mathbf{x})}{\partial x_1 \partial x_d} \\ \vdots & \ddots & \vdots \\ \dfrac{\partial^2 f(\mathbf{x})}{\partial x_d \partial x_1} & \cdots & \dfrac{\partial^2 f(\mathbf{x})}{\partial x_d^2} \end{bmatrix}.$$

For given directions $\mathbf{V}, \mathbf{W} \neq \mathbf{0}$, the second order directional derivatives exist and it holds

$$\frac{\partial^2 f}{\partial \mathbf{W} \partial \mathbf{V}} = \mathbf{V}^T \nabla^2 f \mathbf{W} = \langle \nabla^2 f \cdot \mathbf{W}, \mathbf{V} \rangle.$$

In particular, they are symmetric, i.e.,

$$\frac{\partial^2 f}{\partial \mathbf{V} \partial \mathbf{W}} = \frac{\partial^2 f}{\partial \mathbf{W} \partial \mathbf{V}}.$$

The mathematical tool used to study minimizers of smooth functions is Taylor's expansion.

Theorem 3.3 (**Taylor's expansion**). *Suppose that $f : \mathbb{R}^d \to \mathbb{R}$ is continuously differentiable and that $\mathbf{V} \in \mathbb{R}^d$. Then it holds*

$$f(\mathbf{x} + \mathbf{V}) = f(\mathbf{x}) + \frac{\partial f}{\partial \mathbf{V}}(\mathbf{x}) + o(\|\mathbf{V}\|^2). \tag{3.1}$$

Moreover, if f is twice continuously differentiable, we find

$$f(\mathbf{x} + \mathbf{V}) = f(\mathbf{x}) + \frac{\partial f}{\partial \mathbf{V}}(\mathbf{x}) + \frac{1}{2} \frac{\partial^2 f}{\partial \mathbf{V}^2}(\mathbf{x}) + o(\|\mathbf{V}\|^3). \tag{3.2}$$

Note that we will only consider a vector field $\mathbf{V}$ with $\|\mathbf{V}\|$ so small that the last term is negligible compared to the others. Assuming that $\mathbf{x}^\star$ is a local minimizer, necessary and sufficient optimality conditions which use the gradient and the Hessian of f at $\mathbf{x}^\star$ are presented in the following theorems. Their proofs can be found in [58].

Theorem 3.4 (**First order necessary condition**). *If $\mathbf{x}^\star$ is a local minimizer and f is continuously differentiable in an open neighborhood of $\mathbf{x}^\star$, then $\nabla f(\mathbf{x}^\star) = \mathbf{0}$.*

The local minimizers are among the points $\mathbf{x}_s$ with $\nabla f(\mathbf{x}_s) = \mathbf{0}$, which are called stationary points. The stationary points are the local maximizers, the local minimizers and the saddle points. To distinguish between them, we refer to the following theorem. To that end, we first recall that a matrix $\mathbf{A}$ is positive semidefinite if $\mathbf{V}^T \mathbf{A} \mathbf{V} \geq 0$ and positive definite if $\mathbf{V}^T \mathbf{A} \mathbf{V} > 0$ for all $\mathbf{V} \neq \mathbf{0}$.

Theorem 3.5 (**Second order necessary condition**). *If $\mathbf{x}^\star$ is a local minimizer of f and $\nabla^2 f$ exists and is continuous in an open neighborhood of $\mathbf{x}^\star$, then $\nabla f(\mathbf{x}^\star) = \mathbf{0}$ and $\nabla^2 f(\mathbf{x}^\star)$ is positive semidefinite.*

Now we describe sufficient conditions, which are applied on the derivatives of f at a stationary point $\mathbf{x}^\star$ so as to guarantee that $\mathbf{x}^\star$ is a local minimizer.

Theorem 3.6 (**Second order sufficient condition**). *Suppose that $\nabla^2 f$ is continuous in an open neighborhood of $\mathbf{x}^\star$ and that $\nabla f(\mathbf{x}^\star) = \mathbf{0}$ and $\nabla^2 f(\mathbf{x}^\star)$ is positive definite. Then $\mathbf{x}^\star$ is a strict local minimizer of f.*

In case of a convex objective function the necessary condition from Theorem 3.4 becomes also a sufficient condition and the following theorem holds.

Theorem 3.7. *Let f be convex and differentiable. Then any stationary point $\mathbf{x}^\star$ is a global minimizer of f.*

Having introduced the necessary theoretical background, we proceed to the derivation of the update rules of the free boundary via Taylor's expansion.

Note 3.8. The results we obtain in the sequel refer only to the free boundary Γ. Due to this we find it more notationally proper and clear to use $\boldsymbol{\gamma}$ for its parametrization instead of $\boldsymbol{\gamma}_\Gamma$.

3.2 Update equations via Taylor's expansion

The trial method is an iterative procedure, where in each step we obtain a new approximation of the free boundary, denoted by Γ_k and with parametrization $\boldsymbol{\gamma}_k$. The current exterior boundary Γ_k identifies also the domain Ω_k, in which the solution v_k of the boundary value problem (2.2) is sought, i.e.,

$$\begin{aligned} -\Delta \mathrm{v}_k &= f \qquad \text{in} \quad \Omega_k \\ \mathrm{v}_k &= g \qquad \text{on} \quad \Sigma \\ \frac{\partial \mathrm{v}_k}{\partial \mathbf{n}} &= h \qquad \text{on} \quad \Gamma_k\,. \end{aligned} \tag{3.3}$$

In Chapter 2, we have seen that we can apply the boundary element method by means of the ansatz

$$\mathrm{v}_k = v_k + N_f \tag{3.4}$$

to the boundary value problem

$$\begin{aligned} \Delta v_k &= 0 \qquad\qquad\quad \text{in} \quad \Omega_k \\ v_k &= g - N_f \qquad \text{on} \quad \Sigma \\ \frac{\partial v_k}{\partial \mathbf{n}} &= h - \frac{\partial N_f}{\partial \mathbf{n}} \qquad \text{on} \quad \Gamma_k\,. \end{aligned} \tag{3.5}$$

The Dirichlet data of v_k at the boundary Γ_k are found by the Neumann-to-Dirichlet map (2.16). Then, we obtain the Dirichlet data of v_k at the boundary via the ansatz (3.4).

We remind that, as introduced in Section 1.1.1, the domain Ω_k is assumed to be simply connected and starshaped with respect to $\mathbf{0}$. The main advantage of this assumption is that the boundary Γ_k of such domains can uniquely be described by a continuous radial function r_k of the polar angle s. Moreover, vice versa, each radial function $r_k \in C^2_{\mathrm{per}}\big([0,2\pi]\big)$ can identify the boundary Γ_k via the parametrization

$$\boldsymbol{\gamma}_k : [0,2\pi] \to \Gamma_k, \quad s \mapsto \boldsymbol{\gamma}_k(s) = r_k(s)\mathbf{e}_r(s),$$

where $\mathbf{e}_r(s) = \big(\cos(s), \sin(s)\big)^T$ is the unit vector in the outward radial direction. Note that the unit normal vector is given by

$$\mathbf{n} = \frac{\boldsymbol{\gamma}_k'^{\perp}}{\|\boldsymbol{\gamma}_k'\|} = \frac{r_k' \begin{bmatrix} \sin(s) \\ -\cos(s) \end{bmatrix} + r_k \begin{bmatrix} \cos(s) \\ \sin(s) \end{bmatrix}}{\sqrt{r_k^2 + r_k'^2}}$$

and that similarly the unit tangential vector is written as

$$\mathbf{t} = \frac{\boldsymbol{\gamma}_k'}{\|\boldsymbol{\gamma}_k'\|} = \frac{r_k' \begin{bmatrix} \cos(s) \\ \sin(s) \end{bmatrix} + r_k \begin{bmatrix} -\sin(s) \\ \cos(s) \end{bmatrix}}{\sqrt{r_k^2 + r_k'^2}}.$$

We get an update of the old free boundary Γ_k by moving it in the radial direction such that the omitted boundary condition of the overdetermined boundary value problem (1.1) is fulfilled. In terms of the parametrization of the free boundary the update rule reads

$$\boldsymbol{\gamma}_{k+1} = \boldsymbol{\gamma}_k + \mathbf{V}, \tag{3.6}$$

where $\mathbf{V} := \delta\mathsf{r}_k \mathbf{e}_r$ is a vector field in the radial direction. Even if the direction of the update is fixed, the magnitude of the perturbation is described by the update function $\delta\mathsf{r}_k := \delta\mathsf{r}(r_k)$, which has to be sought in an appropriate space, namely $\delta\mathsf{r}_k \in C^2_{\mathrm{per}}\big([0,2\pi]\big)$. In the present setting, the new boundary Γ_{k+1} is determined by the requirement, that the violated Dirichlet condition should be satisfied on it:

$$\mathrm{v}_k \circ \boldsymbol{\gamma}_{k+1} \overset{!}{=} 0 \quad \text{on } [0,2\pi]. \tag{3.7}$$

The equation (3.7) in combination with the Taylor expansion of first and second order of the Dirichlet data v_k around the current boundary Γ_k, associated with the radial function r_k, will provide the desired update rules of the free boundary Γ_k.

3.2.1 First order update equation

The first order update equation results from the linearization of the equation (3.7) around $\boldsymbol{\gamma}_k$. Hence, in view of $\boldsymbol{\gamma}_{k+1} = \boldsymbol{\gamma}_k + \delta\mathsf{r}_{1k}\mathbf{e}_r$, we obtain

$$\mathrm{v}_k \circ (\boldsymbol{\gamma}_k + \delta\mathsf{r}_{1k}\mathbf{e}_r) \approx \mathrm{v}_k \circ \boldsymbol{\gamma}_k + \Big(\frac{\partial \mathrm{v}_k}{\partial \mathbf{e}_r} \circ \boldsymbol{\gamma}_k\Big)\delta\mathsf{r}_{1k}.$$

Due to (3.7), this yields the linear equation

$$\mathrm{v}_k \circ \boldsymbol{\gamma}_k + \Big(\frac{\partial \mathrm{v}_k}{\partial \mathbf{e}_r} \circ \boldsymbol{\gamma}_k\Big)\delta\mathsf{r}_{1k} \stackrel{!}{=} 0 \tag{3.8}$$

for the unknown update function $\delta\mathsf{r}_{1k}$. We decompose the derivative of v_k in the direction $\mathbf{e}_r$ in its normal and tangential components:

$$\frac{\partial \mathrm{v}_k}{\partial \mathbf{e}_r} \circ \boldsymbol{\gamma}_k = \Big(\frac{\partial \mathrm{v}_k}{\partial \mathbf{n}} \circ \boldsymbol{\gamma}_k\Big)\langle \mathbf{e}_r, \mathbf{n}\rangle + \Big(\frac{\partial \mathrm{v}_k}{\partial \mathbf{t}} \circ \boldsymbol{\gamma}_k\Big)\langle \mathbf{e}_r, \mathbf{t}\rangle. \tag{3.9}$$

By inserting (3.9) into equation (3.8) and considering the Neumann boundary condition $\partial \mathrm{v}_k/\partial \mathbf{n} = h$, cf. (3.3), (3.8) becomes equivalent to

$$\mathrm{v}_k \circ \boldsymbol{\gamma}_k + \left[(h \circ \boldsymbol{\gamma}_k)\langle \mathbf{e}_r, \mathbf{n}\rangle + \Big(\frac{\partial \mathrm{v}_k}{\partial \mathbf{t}} \circ \boldsymbol{\gamma}_k\Big)\langle \mathbf{e}_r, \mathbf{t}\rangle\right]\delta\mathsf{r}_{1k} = 0. \tag{3.10}$$

Provided that $\partial \mathrm{v}_k/\partial \mathbf{e}_r \neq 0$ for all $s \in [0, 2\pi]$, we finally arrive at

$$\delta\mathsf{r}_{1k} = -\frac{\mathrm{v}_k \circ \boldsymbol{\gamma}_k}{(h \circ \boldsymbol{\gamma}_k)\langle \mathbf{e}_r, \mathbf{n}\rangle + \Big(\frac{\partial \mathrm{v}_k}{\partial \mathbf{t}} \circ \boldsymbol{\gamma}_k\Big)\langle \mathbf{e}_r, \mathbf{t}\rangle}. \tag{3.11}$$

Here, the tangential derivative of v_k at the boundary Γ_k is expressed via the ansatz (3.4) by

$$\frac{\partial \mathrm{v}_k}{\partial \mathbf{t}} = \frac{\partial v_k}{\partial \mathbf{t}} + \frac{\partial N_f}{\partial \mathbf{t}}. \tag{3.12}$$

Since the Newton potential is given analytically, we are able to compute all its necessary derivatives. Moreover, the tangential derivate of v_k is given by

$$\frac{\partial v_k}{\partial \mathbf{t}} \circ \boldsymbol{\gamma}_k = \frac{1}{\|\boldsymbol{\gamma}_k'\|}\frac{\partial (v_k \circ \boldsymbol{\gamma}_k)}{\partial s},$$

in which the right hand side is computed by differentiating the trigonometric representation of the approximation v_k with respect to s (see Chapter 2, Section 2.3.3).

Relation (3.10) corresponds to the most common update rule and has, for example, been used in [36, 56, 75]. However, there the update is performed in the normal direction rather than the radial direction which might lead to a degeneration of the domain.

3.2.2 Second order update equation

The second order update rule is derived from a second order Taylor's expansion of $\mathrm{v}_k \circ (\boldsymbol{\gamma}_k + \delta \mathsf{r}_{2k}\mathbf{e}_r)$ with respect to $\delta \mathsf{r}_{2k}$, i.e.,

$$\mathrm{v}_k \circ (\boldsymbol{\gamma}_k + \delta \mathsf{r}_{2k}\mathbf{e}_r) \approx \mathrm{v}_k \circ \boldsymbol{\gamma}_k + \Big(\frac{\partial \mathrm{v}_k}{\partial \mathbf{e}_r} \circ \boldsymbol{\gamma}_k\Big)\delta \mathsf{r}_{2k} + \frac{1}{2}\Big(\frac{\partial^2 \mathrm{v}_k}{\partial \mathbf{e}_r^2} \circ \boldsymbol{\gamma}_k\Big)\delta \mathsf{r}_{2k}^2. \tag{3.13}$$

Since (3.7) should be satisfied for the new boundary Γ_{k+1}, we conclude to the following second order update equation:

$$\mathrm{v}_k \circ \boldsymbol{\gamma}_k + \Big(\frac{\partial \mathrm{v}_k}{\partial \mathbf{e}_r} \circ \boldsymbol{\gamma}_k\Big)\delta \mathsf{r}_{2k} + \frac{1}{2}\Big(\frac{\partial^2 \mathrm{v}_k}{\partial \mathbf{e}_r^2} \circ \boldsymbol{\gamma}_k\Big)\delta \mathsf{r}_{2k}^2 \stackrel{!}{=} 0. \tag{3.14}$$

Because of our regularity assumptions at the boundary Γ_k, we are able to compute the derivatives of the twice continuously differentiable function v_k. Notice that, assuming more regularity of Γ_k, even a higher order Taylor expansion can be exploited here.

The directional derivative $\partial \mathrm{v}_k/\partial \mathbf{e}_r$ in (3.14) has been computed in (3.9), whereas for the second order directional derivative $\partial^2 \mathrm{v}_k/\partial \mathbf{e}_r^2$, we refer to the following lemma.

Lemma 3.9. *The second order derivative of* v_k *in the direction* $\mathbf{e}_r$ *is given by*

$$\begin{aligned}\frac{\partial^2 \mathrm{v}_k}{\partial \mathbf{e}_r^2} \circ \boldsymbol{\gamma}_k =& \Big(\frac{\partial^2 \mathrm{v}_k}{\partial \mathbf{t}^2} \circ \boldsymbol{\gamma}_k\Big)\Big(\langle \mathbf{e}_r, \mathbf{t}\rangle^2 - \langle \mathbf{e}_r, \mathbf{n}\rangle^2\Big) - (f \circ \boldsymbol{\gamma}_k)\langle \mathbf{e}_r, \mathbf{n}\rangle^2 \\ &+ 2\Big(\frac{\partial h}{\partial \mathbf{t}} \circ \boldsymbol{\gamma}_k - \kappa\Big(\frac{\partial \mathrm{v}_k}{\partial \mathbf{t}} \circ \boldsymbol{\gamma}_k\Big)\Big)\langle \mathbf{e}_r, \mathbf{n}\rangle\langle \mathbf{e}_r, \mathbf{t}\rangle,\end{aligned} \tag{3.15}$$

where $\kappa = -\langle \boldsymbol{\gamma}_k'', \mathbf{n}\rangle/\|\boldsymbol{\gamma}_k'\|^2$ *stands for the curvature of the boundary* Γ_k.

Proof. We split the second order derivative of v_k in the direction $\mathbf{e}_r$ into its normal and tangential components

$$\begin{aligned}\frac{\partial^2 \mathrm{v}_k}{\partial \mathbf{e}_r^2} \circ \boldsymbol{\gamma}_k &= \langle (\nabla^2 \mathrm{v}_k \circ \boldsymbol{\gamma}_k) \cdot \mathbf{n}, \mathbf{e}_r\rangle\langle \mathbf{e}_r, \mathbf{n}\rangle + \langle (\nabla^2 \mathrm{v}_k \circ \boldsymbol{\gamma}_k) \cdot \mathbf{t}, \mathbf{e}_r\rangle\langle \mathbf{e}_r, \mathbf{t}\rangle \\ &= \Big(\frac{\partial^2 \mathrm{v}_k}{\partial \mathbf{n}^2} \circ \boldsymbol{\gamma}_k\Big)\langle \mathbf{e}_r, \mathbf{n}\rangle^2 + 2\Big(\frac{\partial^2 \mathrm{v}_k}{\partial \mathbf{n}\partial \mathbf{t}} \circ \boldsymbol{\gamma}_k\Big)\langle \mathbf{e}_r, \mathbf{n}\rangle\langle \mathbf{e}_r, \mathbf{t}\rangle \\ &\quad + \Big(\frac{\partial^2 \mathrm{v}_k}{\partial \mathbf{t}^2} \circ \boldsymbol{\gamma}_k\Big)\langle \mathbf{e}_r, \mathbf{t}\rangle^2.\end{aligned} \tag{3.16}$$

The derivative of v_k's Neumann data with respect to s reads

$$\frac{\partial}{\partial s}\Big(\frac{\partial \mathrm{v}_k}{\partial \mathbf{n}} \circ \boldsymbol{\gamma}_k\Big) = \|\boldsymbol{\gamma}_k'\|\Big(\frac{\partial^2 \mathrm{v}_k}{\partial \mathbf{n}\partial \mathbf{t}} \circ \boldsymbol{\gamma}_k\Big) + \Big\langle \nabla \mathrm{v}_k \circ \boldsymbol{\gamma}_k, \frac{\partial \mathbf{n}}{\partial s}\Big\rangle. \tag{3.17}$$

In view of the derivative of the normal vector with respect to s, i.e., $\partial\mathbf{n}/\partial s = \kappa\|\boldsymbol{\gamma}_k'\|\mathbf{t}$, and the Neumann boundary condition at Γ_k, equation (3.17) can be rewritten as

$$\frac{\partial^2 \mathrm{v}_k}{\partial\mathbf{n}\partial\mathbf{t}} \circ \boldsymbol{\gamma}_k = \frac{\partial h}{\partial\mathbf{t}} \circ \boldsymbol{\gamma}_k - \kappa\Big(\frac{\partial \mathrm{v}_k}{\partial\mathbf{t}} \circ \boldsymbol{\gamma}_k\Big). \tag{3.18}$$

According to the smoothness assumptions, the derivatives $\partial^2\mathrm{v}_k/\partial\mathbf{n}^2 = \langle\nabla^2\mathrm{v}_k \cdot \mathbf{n}, \mathbf{n}\rangle$ and $\partial^2\mathrm{v}_k/\partial\mathbf{t}^2 = \langle\nabla^2\mathrm{v}_k \cdot \mathbf{t}, \mathbf{t}\rangle$ are coupled also at the free boundary by the Poisson equation, namely

$$-\Delta\mathrm{v}_k = -\frac{\partial^2\mathrm{v}_k}{\partial\mathbf{n}^2} - \frac{\partial^2\mathrm{v}_k}{\partial\mathbf{t}^2} = f. \tag{3.19}$$

By inserting the relations (3.18) and (3.19) into (3.16), the latter becomes (3.15). This concludes the proof. □

Having the second order derivative of v_k in the direction $\mathbf{e}_r$ (3.15) at hand, we find the update function $\delta\mathsf{r}_{2k}$ as the solution of the following nonlinear equation

$$\begin{aligned}\mathrm{v}_k + \Big[h\langle\mathbf{e}_r, \mathbf{n}\rangle + \frac{\partial \mathrm{v}_k}{\partial\mathbf{t}}\langle\mathbf{e}_r, \mathbf{t}\rangle\Big]\delta\mathsf{r}_{2k} + \frac{1}{2}\Bigg[\frac{\partial^2\mathrm{v}_k}{\partial\mathbf{t}^2}\Big(\langle\mathbf{e}_r, \mathbf{t}\rangle^2 - \langle\mathbf{e}_r, \mathbf{n}\rangle^2\Big) \\ - f\langle\mathbf{e}_r, \mathbf{n}\rangle^2 + 2\Big(\frac{\partial h}{\partial\mathbf{t}} - \kappa\frac{\partial \mathrm{v}_k}{\partial\mathbf{t}}\Big)\langle\mathbf{e}_r, \mathbf{n}\rangle\langle\mathbf{e}_r, \mathbf{t}\rangle\Bigg]\delta\mathsf{r}_{2k}^2 = 0 \quad \text{on } \Gamma_k.\end{aligned} \tag{3.20}$$

In order to assemble the second order update equation it is necessary to express (3.20) by known or computable terms. For this purpose, we will make use of the ansatz (3.4) and the fact that the Newton potential is given analytically, so that one can compute all its required derivatives. Therewith, the tangential derivative of v_k at the boundary Γ_k is given by (3.12) and the second order derivative of v_k in the tangential direction is

$$\frac{\partial^2\mathrm{v}_k}{\partial\mathbf{t}^2} = \frac{\partial^2 v_k}{\partial\mathbf{t}^2} + \frac{\partial^2 N_f}{\partial\mathbf{t}^2}. \tag{3.21}$$

Herein, the second order tangential derivative of the function v_k can be computed by the second order derivative of v_k with respect to s:

$$\begin{aligned}\frac{\partial^2 v_k}{\partial s^2} &= \frac{\partial}{\partial s}\langle\nabla v_k, \boldsymbol{\gamma}_k'\rangle \\ &= \langle\nabla^2 v_k \cdot \boldsymbol{\gamma}_k', \boldsymbol{\gamma}_k'\rangle + \langle\nabla v_k, \boldsymbol{\gamma}_k''\rangle \\ &= \|\boldsymbol{\gamma}_k'\|^2\frac{\partial^2 v_k}{\partial\mathbf{t}^2} + \langle\boldsymbol{\gamma}_k'', \mathbf{t}\rangle\frac{\partial v_k}{\partial\mathbf{t}} + \langle\boldsymbol{\gamma}_k'', \mathbf{n}\rangle\frac{\partial v_k}{\partial\mathbf{n}} \quad \text{on } \Gamma_k.\end{aligned} \tag{3.22}$$

Equation (3.22), along with the given Neumann boundary condition $\partial \mathrm{v}_k/\partial \mathbf{n} = h$, changes to

$$\frac{\partial^2 v_k}{\partial \mathbf{t}^2} \circ \boldsymbol{\gamma}_k = \frac{1}{\|\boldsymbol{\gamma}_k'\|^2} \frac{\partial^2 (v_k \circ \boldsymbol{\gamma}_k)}{\partial s^2} - \frac{\langle \boldsymbol{\gamma}_k'', \mathbf{t} \rangle}{\|\boldsymbol{\gamma}_k'\|^3} \frac{\partial (v_k \circ \boldsymbol{\gamma}_k)}{\partial s} + \kappa \Big(h - \frac{\partial N_f}{\partial \mathbf{n}} \Big) \circ \boldsymbol{\gamma}_k. \quad (3.23)$$

The quantities $\partial(v_k \circ \boldsymbol{\gamma}_k)/\partial s$ and $\partial^2(v_k \circ \boldsymbol{\gamma}_k)/\partial s^2$ which appear in (3.20) are computed by differentiating the trigonometric representation of the approximate Dirichlet data v_k. These analytical computations provide the essential basis for the subsequent numerical implementation of the trial method.

3.3 Solution of the update equations

In this section, we will describe the numerical methods to solve the linear update equation (3.8) and the nonlinear equation (3.14), where $\delta \mathsf{r}_{1k}$ and $\delta \mathsf{r}_{2k}$ are the unknown update functions. The approximate update function will be used to update the free boundary Γ_k. Repeating this update procedure, as the trial method suggests, we shall obtain the solution of the free boundary problem.

We will reformulate the equations (3.8) and (3.14), respectively, as an optimization problem for the unknown update function. Optimization problems governed by partial differential equations are usually solved by the "optimize-then-discretize" approach. Advances in computing power allow us to use an alternative approach, namely the "discretize-then-optimize" approach, which transforms the original problem into a larger discrete optimization problem. The "discretize-then-optimize" approach corresponds to the pointwise update of the free boundary, while an update in variational form is achieved by applying the "optimize-then-discretize" approach. From a structural point of view these two approaches are completely different. Namely:

1. In the "discretize-then-optimize" approach, all the quantities of the problem are first discretized which results in a finite dimensional minimization problem.
2. In the "optimize-then-discretize" approach, first the minimization problem is derived from the given continuous problem which is then discretized and solved numerically.

There is no rule of thumb which approach has to be preferred. It depends on the application and computational method which approach should be taken for

tackling the numerical solution of the optimization problem. In this chapter, we develop and implement both approaches in order to use in the sequel the more efficient one.

Note 3.10. In the following sections, to simplify the notation, we drop the iteration index k from the update function $\delta\mathsf{r}_k$ and from all other functions which are defined relative to the boundary Γ_k.

3.3.1 "Discretize-then-optimize" approach

For the numerical computations, we discretize the radial function $r \in C^2_{\mathrm{per}}\big([0, 2\pi]\big)$ associated with the free boundary Γ by a finite Fourier series according to

$$r(s_i) = a_0 + \sum_{m=1}^{\nu-1} \Big(a_m \cos(ms_i) + b_m \sin(ms_i) \Big) + a_\nu \cos(\nu s_i).$$

Hence, the update function $\delta\mathsf{r}$ should be also represented by a respective Fourier series. In the current simulation, we assume the real set of trigonometric basis functions expressed by

$$\{\phi_j(s)\}_{j=1}^{2\nu} = \{\sin((\nu-1)s), \ldots, \sin(s), 1, \cos(s), \ldots, \cos(\nu s)\}. \tag{3.24}$$

Therefore the discretized update function can be also written as

$$\delta\mathsf{r}^\nu(s_i) = \sum_{j=1}^{2\nu} \widehat{\delta\mathsf{r}^\nu_j}\,\phi_j(s_i). \tag{3.25}$$

We aim now at the solution of the update equations (3.8) and (3.14) in $2n$ equidistantly distributed points $s_i = \pi i/n,\ i = 1, \ldots, 2n$, where $n \geq \nu$. To that end, we define the residual vector function $\mathbf{F}$ from $\mathbb{R}^{2\nu}$ to $\mathbb{R}^{2n}$ as

$$\mathbf{F}(\delta\mathsf{r}^\nu) := \Big[\mathrm{v}(s_i) + \frac{\partial \mathrm{v}}{\partial \mathbf{e}_r}(s_i)\delta\mathsf{r}^\nu(s_i) \Big]_{i=1,\ldots,2n} \tag{3.26}$$

and as

$$\mathbf{F}(\delta\mathsf{r}^\nu) := \Big[\mathrm{v}(s_i) + \frac{\partial \mathrm{v}}{\partial \mathbf{e}_r}(s_i)\delta\mathsf{r}^\nu(s_i) + \frac{1}{2}\frac{\partial^2 \mathrm{v}}{\partial \mathbf{e}_r^2}(s_i)\big(\delta\mathsf{r}^\nu(s_i)\big)^2 \Big]_{i=1,\ldots,2n}, \tag{3.27}$$

respectively. Note that all the terms contained in the residual vector functions (3.26) and (3.27) have been computed in Section 3.2. Subsequently, we consider the least-squares method which consists in minimizing $\|\mathbf{F}(\delta\mathsf{r}^\nu)\|_2^2$. This is equivalent to looking for

$$\delta\mathsf{r}^\dagger = \underset{\delta\mathsf{r}^\nu}{\operatorname{argmin}}\{\mathcal{F}(\delta\mathsf{r}^\nu)\}, \tag{3.28}$$

where $\mathcal{F} : \mathbb{R}^{2n} \to \mathbb{R}$ is the objective function given by

$$\mathcal{F}(\delta \mathsf{r}^\nu) := \left\|\mathbf{F}(\delta \mathsf{r}^\nu)\right\|_2^2 = \left(\mathbf{F}(\delta \mathsf{r}^\nu)\right)^T \mathbf{F}(\delta \mathsf{r}^\nu). \tag{3.29}$$

The discrete optimization problem (3.28) and (3.29) can now be solved numerically with the help of appropriate algorithms, which are briefly described below.

The linear discrete least-squares method

The discrete least-squares method for the linear residual vector function (3.26) leads to the well known normal equations. Namely, we find the minimizer $\delta \mathsf{r}^\dagger$ of (3.29) by solving directly the normal equations, which can be expressed as

$$\mathbf{J}^T \mathbf{J} \boldsymbol{\delta \mathbf{r}}^\dagger = -\mathbf{J}^T \mathbf{F}(0), \tag{3.30}$$

where $\boldsymbol{\delta \mathbf{r}}^\dagger = [\widehat{\delta \mathsf{r}_j^\nu}]_{j=1,\dots,2\nu}$. Here, $\mathbf{J} \in \mathbb{R}^{2n \times 2\nu}$ is the Jacobian matrix which contains the partial derivatives with respect to the components of the update function, i.e.,

$$\mathbf{J} = \left[\frac{\partial \mathbf{F}(\delta \mathsf{r}^\nu)}{\partial \widehat{\delta \mathsf{r}_j^\nu}}\right]_{j=1,\dots,2\nu}. \tag{3.31}$$

Note that $\mathbf{J}$ does not depend on $\delta \mathsf{r}^\nu$ since $\mathbf{F}$ is only linear in $\delta \mathsf{r}^\nu$. Applying the chain rule, the Jacobian matrix (3.31) of the linear residual function (3.26) reads

$$\mathbf{J} = \left[\frac{\partial \mathrm{v}}{\partial \mathbf{e}_r}(s_i) \frac{\partial \delta \mathsf{r}^\nu}{\partial \widehat{\delta \mathsf{r}_j^\nu}}\right]_{\substack{i=1,\dots,2n \\ j=1,\dots,2\nu}}. \tag{3.32}$$

As $\mathbf{F}$ is a linear function, $\mathcal{F}$ is certainly convex, and Theorem 3.7 applies.

The nonlinear discrete least-squares method

We now describe the Gauss-Newton method (see [58]) for minimizing the objective function (3.29) in case of the nonlinear residual function (3.27). The Gauss-Newton method is an iterative method and based on a linear approximation of the components of $\mathbf{F}$ in the neighborhood of $\delta \mathsf{r}^\nu$. For an arbitrary small p with trigonometric coefficients $\mathbf{p} = [\widehat{p_j}]_{j=1,\dots,2\nu}$, Taylor's expansion yields

$$\mathbf{L}(p) := \mathbf{F}(\delta \mathsf{r}^\nu + p) \approx \mathbf{F}(\delta \mathsf{r}^\nu) + \mathbf{J}(\delta \mathsf{r}^\nu)\mathbf{p},$$

where $\mathbf{J} \in \mathbb{R}^{2n\times 2\nu}$ is the Jacobian matrix (3.31), given by

$$\mathbf{J}(\delta \mathsf{r}^\nu) = \left[\Big(\frac{\partial \mathrm{v}}{\partial \mathbf{e}_r}(s_i) + \frac{\partial^2 \mathrm{v}}{\partial \mathbf{e}_r^2}(s_i)\delta \mathsf{r}^\nu(s_i) \Big) \frac{\partial \delta \mathsf{r}^\nu}{\partial \widehat{\delta \mathsf{r}}_j} \right]_{\substack{i=1,\dots,2n \\ j=1,\dots,2\nu}}. \tag{3.33}$$

Replacing $\mathbf{F}$ in (3.29) by this Taylor expansion, we obtain

$$\begin{aligned} \mathcal{F}(\delta \mathsf{r}^\nu + p) &= \big(\mathbf{F}(\delta \mathsf{r}^\nu + p)\big)^T \mathbf{F}(\delta \mathsf{r}^\nu + p) \\ &\approx \big(\mathbf{F}(\delta \mathsf{r}^\nu)\big)^T \mathbf{F}(\delta \mathsf{r}^\nu) + \mathbf{p}^T \big(\mathbf{J}(\delta \mathsf{r}^\nu)\big)^T \mathbf{J}(\delta \mathsf{r}^\nu)\mathbf{p} \\ &\quad + 2\mathbf{p}^T \big(\mathbf{J}(\delta \mathsf{r}^\nu)\big)^T \mathbf{F}(\delta \mathsf{r}^\nu) =: \mathcal{L}(p). \end{aligned} \tag{3.34}$$

A single iteration of the Gauss-Newton method consists in finding p which minimizes the quadratic functional $\mathcal{L}(p)$. The gradient of $\mathcal{L}$ is

$$\nabla \mathcal{L}(p) = 2\big(\mathbf{J}(\delta \mathsf{r}^\nu)\big)^T \mathbf{J}(\delta \mathsf{r}^\nu)\mathbf{p} + 2\big(\mathbf{J}(\delta \mathsf{r}^\nu)\big)^T \mathbf{F}(\delta \mathsf{r}^\nu)$$

and the Hessian of $\mathcal{L}$ is

$$\nabla^2 \mathcal{L}(p) = 2\big(\mathbf{J}(\delta \mathsf{r}^\nu)\big)^T \mathbf{J}(\delta \mathsf{r}^\nu). \tag{3.35}$$

We notice that $\nabla \mathcal{L}(0) = \nabla \mathcal{F}(\delta \mathsf{r}^\nu)$. If $\mathbf{J}(\delta \mathsf{r}^\nu)$ has full rank, then the Hessian (3.35) is positive definite. According to Theorems 3.6 and 3.7, the functional $\mathcal{L}(p)$ admits a unique minimizer when the gradient of $\mathcal{L}(p)$ is equal to zero. This minimizer p is thus found by solving

$$\big(\mathbf{J}(\delta \mathsf{r}^\nu)\big)^T \mathbf{J}(\delta \mathsf{r}^\nu)\mathbf{p} = -\big(\mathbf{J}(\delta \mathsf{r}^\nu)\big)^T \mathbf{F}(\delta \mathsf{r}^\nu). \tag{3.36}$$

The direction p is a descent direction for $\mathcal{F}$. Indeed, it holds

$$\mathbf{p}^T \nabla \mathcal{F}(\delta \mathsf{r}^\nu) = \mathbf{p}^T \big(\mathbf{J}(\delta \mathsf{r}^\nu)\big)^T \mathbf{F}(\delta \mathsf{r}^\nu) = -\mathbf{p}^T \big(\mathbf{J}(\delta \mathsf{r}^\nu)\big)^T \mathbf{J}(\delta \mathsf{r}^\nu)\mathbf{p} = -\|\mathbf{J}(\delta \mathsf{r}^\nu)\mathbf{p}\|^2 < 0.$$

The next step of the iterative Gauss-Newton method is to update $\delta \mathsf{r}^\nu$ according to $\delta \mathsf{r}^\nu + p$ and to repeat the procedure by linearizing around this updated $\delta \mathsf{r}^\nu$. We stop the iteration when a suitable criterion can guarantee that the minimizer $\delta \mathsf{r}^\dagger = \delta \mathsf{r}^\nu$ is found. This stopping criterion should hence reflect that the actual gradient of the objective function $\mathcal{F}$ is zero, see Theorem 3.4. This means that

$$\nabla \mathcal{F}(\delta \mathsf{r}^\dagger) = \big(\mathbf{J}(\delta \mathsf{r}^\dagger)\big)^T \mathbf{F}(\delta \mathsf{r}^\dagger) = \mathbf{0},$$

or in other words that

$$R(\delta \mathsf{r}^\dagger) := \big\| \big(\mathbf{J}(\delta \mathsf{r}^\dagger)\big)^T \mathbf{F}(\delta \mathsf{r}^\dagger) \big\| < \mathrm{tol} \tag{3.37}$$

for a small positive tolerance chosen by the user. For further details we refer to [71].

Implementations of the Gauss-Newton method for nonlinear equations have shown that the method might take bad steps by being too long. This suggests two ways of improving the Gauss-Newton algorithm; using either a line search or a trust region strategy. That way, the so-called damped Gauss-Newton method is introduced, see [23]. Since the damped Gauss-Newton method shall take descent steps which satisfy the line search criterion, it is locally convergent for almost all nonlinear least-squares problems. In our simulation, we choose a damping parameter $\xi_0 = 1$, which we halve in each step until a descent direction is found.

The iterative procedure starts with $\delta\mathsf{r}^\nu = 0$. For this value of the update function $\delta\mathsf{r}^\nu$ we determine the residual function from (3.27) and the Jacobian matrix from (3.33). By plugging them into (3.36), we obtain the update direction p. The next step is to successively increase $\imath = 0, 1, 2, \ldots$ until $\mathcal{F}(\delta\mathsf{r}^\nu + 2^{-\imath}p) < \mathcal{F}(\delta\mathsf{r}^\nu)$ holds. Then, we update $\delta\mathsf{r}^\nu$ correspondingly by adding $2^{-\imath}p$ and check if the stopping criterion (3.37) is fulfilled for a specific tolerance. If the stopping criterion is not satisfied, we repeat the same process. Otherwise, we terminate since the desired minimizer $\delta\mathsf{r}^\dagger$ is found.

3.3.2 "Optimize-then-discretize" approach

In Section 3.3.1, we got involved with the problem of minimizing some cost function $\mathcal{F}$ for a trigonometric polynomial $\delta\mathsf{r}$ at the discrete points $s_1, \ldots, s_{2n}$ for some $n \geq \nu$. Instead, suppose now we simply wish to minimize $\mathcal{F}$ throughout all points of $[0, 2\pi]$. To that end, we define the (continuous) residual function F, which either results from the first order update equation

$$F(\delta\mathsf{r}) := \mathrm{v} + \frac{\partial \mathrm{v}}{\partial \mathbf{e}_r}\delta\mathsf{r} \tag{3.38}$$

or results from the second order update equation

$$F(\delta\mathsf{r}) := \mathrm{v} + \frac{\partial \mathrm{v}}{\partial \mathbf{e}_r}\delta\mathsf{r} + \frac{1}{2}\frac{\partial^2 \mathrm{v}}{\partial \mathbf{e}_r^2}\delta\mathsf{r}^2. \tag{3.39}$$

Thus, questions like "How should one pick the points s_i?" or "What value should n take?" arise. Assume that we uniformly distribute the points s_i equispaced over $[0, 2\pi]$ by $s_i = \pi i/n$. The least-squares formula, when scaled by π/n, takes the form of a Riemann sum that, in the $n \to \infty$ limit, approximates an integral:

$$\lim_{n\to\infty} \frac{\pi}{n} \sum_{i=0}^{n} \Big(\big(F(\delta\mathsf{r})\big)(s_i)\Big)^2 = \int_0^{2\pi} \Big(\big(F(\delta\mathsf{r})\big)(s)\Big)^2 \mathrm{d}s. \tag{3.40}$$

That is, in the limit we are actually minimizing an integral, rather than a sum.

We shall equip the linear space $C\big([0,2\pi]\big)$ with an inner-product.

Definition 3.11. *The inner-product of two functions $f, g \in C\big([0,2\pi]\big)$ is given by*

$$\langle f, g\rangle := \int_0^{2\pi} f(s)g(s)\mathrm{d}s.$$

The inner-product induces a norm via

$$\|f\|_{L^2} := \langle f, f\rangle^{1/2} = \Big(\int_0^{2\pi} \big(f(s)\big)^2 \mathrm{d}s\Big)^{1/2}.$$

Thus, in view of (3.40), the minimization of (3.40) gives rise to the continuous least-squares method with the objective function $\mathcal{F} : C\big([0,2\pi]\big) \to \mathbb{R}$ given by

$$\mathcal{F}(\delta\mathsf{r}) := \langle F(\delta\mathsf{r}), F(\delta\mathsf{r})\rangle = \|F(\delta\mathsf{r})\|_{L^2}^2 = \int_0^{2\pi} \Big(\big(F(\delta\mathsf{r})\big)(s)\Big)^2 \mathrm{d}s. \tag{3.41}$$

The Galerkin method is a powerful and flexible tool for finding approximate solutions in a variational formulation like (3.41). Moreover, it is a member of the larger class of methods known as methods of weighted residuals [34]. In such methods equations are solved, the solution of which is assumed to be well approximated by a function of a particular form having a finite number of degrees of freedom that it depends on. We have so far used the assumption that the solution $\delta\mathsf{r}$ is expressed by a Fourier series (3.25) with orthonormal basis function set $\{\phi_j(s)\}$ given by (3.24), i.e.,

$$\delta\mathsf{r}(s) = \sum_{j=1}^{2\nu} \widehat{\delta\mathsf{r}}_j \phi_j(s), \quad s \in [0,2\pi]. \tag{3.42}$$

Consequently, $\delta\mathsf{r} \in V_\nu$, where $V_\nu = \mathrm{span}\{\phi_j,\ j = 1,\ldots,2\nu\}$. If the ansatz (3.42) is inserted into the variational functional (3.41), the variational problem reduces to a finite dimensional optimization problem. In order to reach a minimum of the cost functional (3.41) we require that the derivative of $\mathcal{F}$ in the direction ϕ satisfies

$$\mathrm{d}\mathcal{F}[\phi](\delta\mathsf{r}) = \lim_{\varepsilon\to 0} \frac{\mathcal{F}\big(\delta\mathsf{r} + \varepsilon\phi\big) - \mathcal{F}\big(\delta\mathsf{r}\big)}{\varepsilon} = 2\int_0^{2\pi} F(\delta\mathsf{r}) \frac{\partial F(\delta\mathsf{r})}{\partial \delta\mathsf{r}} \phi \mathrm{d}s = 0 \tag{3.43}$$

for all ϕ. If we demand (3.43) only for all ϕ in V_ν, then we arrive at the Galerkin method:

$$\text{Find } \delta\mathsf{r} \in V_\nu \text{ such that } \mathrm{d}\mathcal{F}[\phi](\delta\mathsf{r}) = 0 \text{ for all } \phi \in V_\nu.$$

When numerical integration is used to calculate the involved integrals for the residuals (3.38) and (3.39), we end up with a possibly nonlinear system of equations. For the approximation of the integrals, the trapezoidal rule will be used. In what follows, we elaborate separately on the linear residual function (3.38) and the nonlinear one (3.39).

Linear Galerkin method

The (linear) first order update equation (3.8) leads to a linear optimization problem. Considering the function (3.38), the update $\delta\mathsf{r}^\dagger(s)$, which is the minimizer of $\mathcal{F}(\delta\mathsf{r})$, is found by directly solving the equation

$$\left[\mathrm{d}\mathcal{F}\left[\phi_\ell\right](\delta\mathsf{r}^\dagger)\right]_{\ell=1}^{2\nu} = \mathbf{0} \tag{3.44}$$

where $\phi_\ell,\ \ell = 1,\ldots,2\nu$, are the basis functions in V_ν. Equation (3.44) for the residual function (3.38) reads as

$$\left[\left\langle\left(\mathrm{v} + \frac{\partial \mathrm{v}}{\partial \mathbf{e}_r}\delta\mathsf{r}^\dagger\right)\frac{\partial \mathrm{v}}{\partial \mathbf{e}_r}, \phi_\ell\right\rangle\right]_{\ell=1}^{2\nu} = \mathbf{0},$$

which is equivalent to

$$\left[\left\langle\left(\frac{\partial \mathrm{v}}{\partial \mathbf{e}_r}\right)^2\psi_l, \phi_\ell\right\rangle\right]_{l,\ell=1}^{2\nu}\boldsymbol{\delta}\mathbf{r}^\dagger = -\left[\left\langle \mathrm{v}\frac{\partial \mathrm{v}}{\partial \mathbf{e}_r}, \phi_\ell\right\rangle\right]_{\ell=1}^{2\nu}, \tag{3.45}$$

where $\boldsymbol{\delta}\mathbf{r}^\dagger$ is the vector containing the Fourier coefficients of the trigonometric representation of the function $\delta\mathsf{r}^\dagger$. We assemble the linear system of equations (3.45) with the help of the trapezoidal rule and the Fast Fourier Transform.

Nonlinear Galerkin method

In case of the nonlinear residual function (3.39), we employ Newton's iterative method to solve (3.44). The first order directional derivative of the objective function $\mathcal{F}$ is given by (3.43), while its second order derivative in the directions ψ and ϕ is

$$\begin{aligned}\mathrm{d}^2\mathcal{F}[\psi,\phi](\delta\mathsf{r}) &= \lim_{\varepsilon\to 0}\frac{\mathrm{d}\mathcal{F}[\phi](\delta\mathsf{r}+\varepsilon\psi) - \mathrm{d}\mathcal{F}[\phi](\delta\mathsf{r})}{\varepsilon},\\ &= 2\int_0^{2\pi}\left[\left(\frac{\partial F(\delta\mathsf{r})}{\partial\delta\mathsf{r}}\right)^2 + \frac{\partial^2 F(\delta\mathsf{r})}{\partial\delta\mathsf{r}^2}F(\delta\mathsf{r})\right]\psi\phi\mathrm{d}s.\end{aligned} \tag{3.46}$$

Here, only the trigonometric basis functions in V_ν need to be considered. More precisely, for the residual function (3.39), the first order directional derivatives are expressed by the gradient

$$\begin{aligned}\mathbf{G}(\delta\mathsf{r}) &= \left[\mathrm{d}\mathcal{F}\left[\phi_\ell\right](\delta\mathsf{r})\right]_{\ell=1}^{2\nu} \\ &= \left[2\int_0^{2\pi}\Big(\mathrm{v}+\frac{\partial \mathrm{v}}{\partial \mathbf{e}_r}\delta\mathsf{r}+\frac{1}{2}\frac{\partial^2\mathrm{v}}{\partial\mathbf{e}_r^2}\delta\mathsf{r}^2\Big)\Big(\frac{\partial\mathrm{v}}{\partial\mathbf{e}_r}+\frac{\partial^2\mathrm{v}}{\partial\mathbf{e}_r^2}\delta\mathsf{r}\Big)\phi_\ell\mathrm{d}s\right]_{\ell=1}^{2\nu},\end{aligned}$$

and the second order directional derivatives are expressed by the Hessian

$$\begin{aligned}\mathbf{H}(\delta\mathsf{r}) &= \left[\mathrm{d}^2\mathcal{F}\left[\psi_l,\phi_\ell\right](\delta\mathsf{r})\right]_{l,\ell=1}^{2\nu} \\ &= \left[2\int_0^{2\pi}\left(\Big(\frac{\partial\mathrm{v}}{\partial\mathbf{e}_r}+\frac{\partial^2\mathrm{v}}{\partial\mathbf{e}_r^2}\delta\mathsf{r}\Big)^2+\Big(\mathrm{v}+\frac{\partial\mathrm{v}}{\partial\mathbf{e}_r}\delta\mathsf{r}+\frac{1}{2}\frac{\partial^2\mathrm{v}}{\partial\mathbf{e}_r^2}\delta\mathsf{r}^2\Big)\frac{\partial^2\mathrm{v}}{\partial\mathbf{e}_r^2}\right)\psi_l\phi_\ell\mathrm{d}s\right]_{l,\ell=1}^{2\nu}.\end{aligned}$$

For the Newton method one has then to compute

$$\mathbf{p} = -\big(\mathbf{H}(\delta\mathsf{r})\big)^{-1}\mathbf{G}(\delta\mathsf{r}), \tag{3.47}$$

where the vector $\mathbf{p}$ contains the Fourier coefficients of the Newton update $p = \delta\mathsf{r}_{\mathrm{new}} - \delta\mathsf{r}$. If the Hessian is positive definite, then it follows that $\delta\mathsf{r}$ is downhill. Further, if $\mathbf{H}(\delta\mathsf{r})$ stays positive definite in all the steps and if the starting point is sufficiently close to a minimizer, then the Newton method converges rapidly towards the solution.

Nevertheless, due to a series of drawbacks, the basic version of the Newton method is not suitable for a general purpose optimization algorithm. For instance, the Hessian may not always be positive definite when $\delta\mathsf{r}$ is far from the solution. In this case, the sequence of iterates might be heading towards a saddle point or even a maximizer. Moreover, the Newton method is well defined only if Hessian remains non-singular. For these reasons, the use of the Hessian matrix might be impractical.

As an alternative, the Quasi-Newton method is suggested. The idea underlying Quasi-Newton method is to use an approximation to the inverse Hessian. Since second derivatives are not required, the Quasi-Newton method is sometimes more efficient than the Newton method. The most popular Quasi-Newton algorithm is the BFGS method, named for its discoverers Broyden, Fletcher, Goldfarb, and Shanno, see [12, 58]. Here, the search direction has the form

$$\mathbf{p} = -\mathbf{B}\mathbf{G}(\delta\mathsf{r}), \tag{3.48}$$

where $\mathbf{B}$ is a suitable approximation of the inverse Hessian matrix $\mathbf{H}^{-1}$. The iterative scheme usually starts with $\mathbf{B} = \mathbf{I}$ and $\delta\mathsf{r} = 0$ and the new approximation

of the inverse Hessian matrix $\mathbf{B}$ is given by

$$\mathbf{B}_{\text{new}} = \mathbf{B} + \frac{\big(\mathbf{p} - \mathbf{B}\mathbf{y}\big)\mathbf{p}^T + \mathbf{p}\big(\mathbf{p} - \mathbf{B}\mathbf{y}\big)^T}{\mathbf{y}^T\mathbf{p}} - \frac{\big(\mathbf{p} - \mathbf{B}\mathbf{y}\big)^T\mathbf{y}\mathbf{p}\mathbf{p}^T}{\big(\mathbf{y}^T\mathbf{p}\big)^2}$$

with $\mathbf{y} = \mathbf{G}(\delta\mathsf{r}_{\text{new}}) - \mathbf{G}(\delta\mathsf{r})$.

In each step of both, the Newton method and the Quasi-Newton method, it is necessary to validate the descent direction. Namely, we compute the residual function $F(\delta\mathsf{r}_{\text{new}})$ and check if

$$\big(\mathcal{F}(\delta\mathsf{r}_{\text{new}})\big)(s) = \int_0^{2\pi} \Big(\big(F(\delta\mathsf{r}_{\text{new}})\big)(s)\Big)^2 \mathrm{d}s < \int_0^{2\pi} \Big(\big(F(\delta\mathsf{r})\big)(s)\Big)^2 \mathrm{d}s = \big(\mathcal{F}(\delta\mathsf{r})\big)(s). \tag{3.49}$$

The trapezoidal rule for the computation of the integrals in (3.49) yields the following condition for the descent direction:

$$\frac{\pi}{n}\sum_{i=1}^{2n} \Big(\big(F(\delta\mathsf{r}_{\text{new}})\big)(s_i)\Big)^2 < \frac{\pi}{n}\sum_{i=1}^{2n} \Big(\big(F(\delta\mathsf{r})\big)(s_i)\Big)^2.$$

If the inequality holds, we examine the stopping criterion $\|\mathrm{d}\mathcal{F}[\phi](\delta\mathsf{r}_{\text{new}})\| < \text{tol}$. Otherwise we perform a line search analogously to Section 3.3.1 until the descent direction and thus $\delta\mathsf{r}_{\text{new}}$ is found. This iterative procedure is performed until we finally find $\delta\mathsf{r}^\dagger = \delta\mathsf{r}_{\text{new}}$ which satisfies the stopping criterion.

After the brief description of the algorithms and the presentation of their basic theoretical properties we proceed to the numerical implementation.

3.4 Numerical examples

In this section, we perform numerical tests in order to compare the trial method based on the first and on the second order update equation. The free boundary is updated according to the update rule (3.6). Exploiting the starshapeness of the domain, this update rule contains in fact only the radial function of the boundary Γ_k, i.e.,

$$r_{k+1} = r_k + \delta\mathsf{r}(r_k). \tag{3.50}$$

Note that, for the Poisson equation with right hand side f equal to a constant, an appropriate Newton potential is given by the function

$$N_f(x, y) = -f(x^2 + y^2)/4.$$

This Newton potential enables the analytical computation of all the necessary derivatives which are contained in the update equations (3.8) and (3.14).

Example 3.12. For the first example, we assume a kite-shaped fixed boundary Σ with parametrization

$$\boldsymbol{\gamma}_\Sigma : [0, 2\pi] \to \Sigma, \quad s \mapsto \boldsymbol{\gamma}_\Sigma(s) = \begin{bmatrix} -0.1\cos(s) + 0.065\cos(2s) \\ 0.15\sin(s) \end{bmatrix}.$$

The initial guess Γ_0 of the free boundary is a slightly perturbed ellipse which is parametrized by

$$\boldsymbol{\gamma}_0 : [0, 2\pi] \to \Gamma_0, \quad s \mapsto \boldsymbol{\gamma}_0(s) = \sqrt{0.04\cos^2(2s) + 0.06\sin^2(2s)} \begin{bmatrix} \cos(s) \\ \sin(s) \end{bmatrix}.$$

We solve the generalized Bernoulli free boundary problem with respect to the data

$$f(x, y) = 60, \quad g(x, y) = x^2 + y^2 + 1, \quad h(x, y) = -\lambda(x^2 + y^2 + 1),$$

where λ is a positive constant. The Newton potential is analytically determined by $N_f(x, y) = -15(x^2+y^2)$. The numerical setting is as follows. We use 80 degrees of freedom to represent the unknown boundary Γ_k (i.e., $\nu = 40$) and 600 boundary elements per boundary. The trial method stops when the update function satisfies $\|\delta \mathsf{r}\| \leq 10^{-8}$. Figure 3.1 shows the boundary Σ and the solutions $\Gamma^\star$ of the free boundary problem for different values of the parameter λ. The outermost boundary corresponds to $\lambda = 20$ and the innermost boundary to $\lambda = 40$.

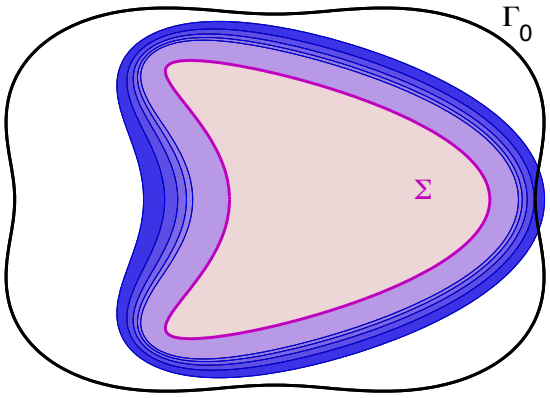

Figure 3.1: Solutions of the generalized Bernoulli free boundary problem in case of a kite-shaped interior boundary.

In Table 3.1, we present the number of boundary updates that the trial method requires in order to reach the optimal free boundary $\Gamma^\star$ when the discrete least-squares method is used for the solution of the update equations. Recall that this

corresponds to the normal equations for the solution of the first order update equation (3.8) (see Algorithm 3.1) and to the Gauss-Newton method in case of the second order update equation (3.14) (see Algorithm 3.2).

parameter λ	20	25	30	35	40
1st order update	23	31	–	–	–
1st order with damping ($\alpha = 0.8$)	23	22	21	20	19
1st order with damping ($\alpha = 0.5$)	42	41	39	37	36
2nd order update	27	28	29	29	31

Table 3.1: Number of boundary updates of the trial methods for a kite-shaped interior boundary in case of pointwise updates.

The results in Table 3.1 suggest that the trial method based on the first order update rule converges only if the parameter λ is small enough (row entitled "1st order update"). Whereas, the trial method based on the second order update rule converges for all choices of the parameter λ (row entitled "2nd order update"). We observe that a modification of the update rule by introducing an appropriate damping parameter α can help to enforce convergence in case of the first order update also for large values of λ. Namely, for $0 < \alpha \leq 1$, the update of the radial function is calculated by $r_{k+1} = r_k + \alpha\delta\mathsf{r}$. Then, as it is seen in Table 3.1, convergence for all values of λ is achieved for the particular choices $\alpha = 0.5$ and $\alpha = 0.8$ (rows entitled "1st order with damping"). Nevertheless, even if we can always attain convergence for the trial method based on the first order update with a proper damping parameter, there is no systematic rule for choosing this parameter.

Algorithm 3.1: Trial method for updating the free boundary according to the Dirichlet data based on the first order update equation and the "discretize-then-optimize" approach.

Data: The mixed BVP with Dirichlet data on Σ, Neumann data on the free boundary and an initial free boundary Γ_0.

Set $k = 0$ and $\|\delta\mathsf{r}_0^\dagger\| = 1$.

while $\|\delta\mathsf{r}_k^\dagger\| > \text{tol}$ **do**

1. Solve the BIE (2.16) to determine the missing Dirichlet boundary data of v_k on Γ_k.
2. Compute the terms of the update equation (3.8).
3. Solve the normal equations (3.30) to find the update function $\delta\mathsf{r}_k^\dagger$.
4. Update the free boundary according to $\boldsymbol{\gamma}_{k+1} = \boldsymbol{\gamma}_k + \delta\mathsf{r}_k^\dagger \mathbf{e}_r$.
5. Set $k = k + 1$.

end

Result: The solution $\Gamma^\star$ of the free boundary problem.

Algorithm 3.2: Trial method for updating the free boundary according to the Dirichlet data based on the second order update equation and the "discretize-then-optimize" approach.

Data: The mixed BVP with Dirichlet data on Σ, Neumann data on the free boundary and an initial free boundary Γ_0.

Set $k = 0$ and $\|\delta \mathsf{r}_0^\dagger\| = 1$.

while $\|\delta \mathsf{r}_k^\dagger\| > \text{tol}$ **do**

1. Solve the BIE (2.16) to determine the missing Dirichlet boundary data of v_k on Γ_k.

2. Compute the terms of the update equation (3.14) and set $\delta \mathsf{r}_k = 0$.

3. Use the damped Gauss-Newton method (3.36) to find the update function $\delta \mathsf{r}_k^\dagger$.

4. Update the free boundary according to $\boldsymbol{\gamma}_{k+1} = \boldsymbol{\gamma}_k + \delta \mathsf{r}_k^\dagger \mathbf{e}_r$.

5. Set $k = k + 1$.

end

Result: The solution $\Gamma^\star$ of the free boundary problem.

Figure 3.2 displays the error between the actual iterate r_k and the optimal radial function $r^\star$ versus the number of iterations. What we note is that both the trial method based on the first order update rule and the trial method based on the second order update rule converge linearly. However, the latter is more robust unless we use a suitable damping for the first one, see Table 3.1.

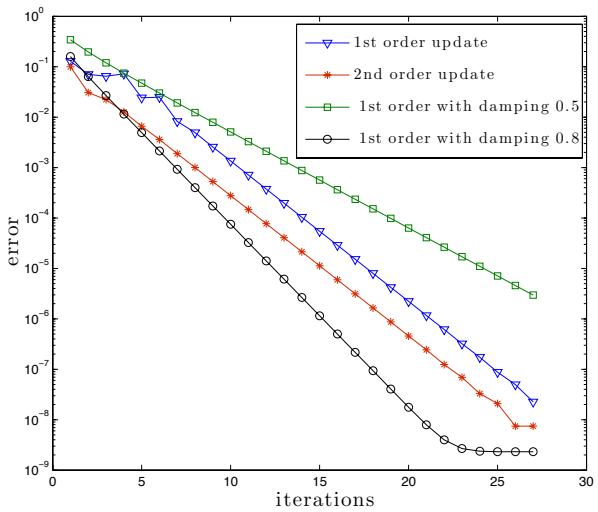

Figure 3.2: Convergence history of the trial methods for a kite-shaped interior boundary and $\lambda = 25$ in case of pointwise updates.

We now solve the same free boundary problem for the same values of the pa-

rameter λ using the "optimize-then-discretize" approach, as it was described in Section 3.3.2. The solution of the linear equation (3.8) is found by the gradient method (see Algorithm 3.3) while the nonlinear equation (3.14) is solved by the Newton/Quasi-Newton method (see Algorithm 3.4). The number of iterations in the trial method are shown in Table 3.2. For the solution of the nonlinear equation (3.14) we have distinguished between the Newton method and the Quasi-Newton method. For the convergence of the Newton method it is necessary that we are already close to the solution of (3.14). This is a condition that can be satisfied for some value of the parameter λ but not in general. Therefore, our strategy consists in either applying directly the Newton method when we are close to the solution or employing first the Quasi-Newton method until the norm of the gradient (3.37) is relatively small and switching then to the Newton method so that we can benefit from its quadratic convergence rate. Nevertheless, the convergence order of the trial method is still only linear. A plot of the error with respect to the number of boundary updates would be similar to Figure 3.2.

parameter λ	20	25	30	35	40
1st order update	23	–	–	–	–
1st order with damping ($\alpha = 0.8$)	23	22	21	20	19
1st order with damping ($\alpha = 0.5$)	42	41	39	37	36
2nd order update	27	28	29	–	–

Table 3.2: Number of boundary updates of the trial methods for a kite-shaped interior boundary in case of variational updates.

Algorithm 3.3: Trial method for updating the free boundary according to the Dirichlet data based on the first order update equation and the "optimize-then-discretize" approach.

Data: The mixed BVP with Dirichlet data on Σ, Neumann data on the free boundary and an initial free boundary Γ_0.

Set $k = 0$ and $\|\delta \mathsf{r}_0^\dagger\| = 1$.

while $\|\delta \mathsf{r}_k^\dagger\| > \text{tol}$ **do**

1. Solve the BIE (2.16) to determine the missing Dirichlet boundary data of v_k on Γ_k.

2. Compute the terms of the update equation (3.8).

3. Use equation (3.45) to find the update function $\delta \mathsf{r}_k^\dagger$.

4. Update the free boundary according to $\boldsymbol{\gamma}_{k+1} = \boldsymbol{\gamma}_k + \delta \mathsf{r}_k^\dagger \mathbf{e}_r$.

5. Set $k = k + 1$.

end

Result: The solution $\Gamma^\star$ of the free boundary problem.

Algorithm 3.4: Trial method for updating the free boundary according to the Dirichlet data based on the second order update equation and the "optimize-then-discretize" approach.

Data: The mixed BVP with Dirichlet data on Σ, Neumann data on the free boundary and an initial free boundary Γ_0.

Set $k = 0$ and $\|\delta \mathsf{r}_0^\dagger\| = 1$.

while $\|\delta \mathsf{r}_k^\dagger\| > \text{tol}$ **do**

1. Solve the BIE (2.16) to determine the missing Dirichlet boundary data of v_k on Γ_k.

2. Compute the terms of the update equation (3.14) and set $\delta \mathsf{r}_k = 0$.

3. Use the Newton method (3.47) or the Quasi-Newton method (3.48) to find the update function $\delta \mathsf{r}_k^\dagger$.

4. Update the free boundary according to $\boldsymbol{\gamma}_{k+1} = \boldsymbol{\gamma}_k + \delta \mathsf{r}_k^\dagger \mathbf{e}_r$.

5. Set $k = k + 1$.

end

Result: The solution $\Gamma^\star$ of the free boundary problem.

By comparing the results from the pointwise and the variational formulation of the update equations (3.8) and (3.14), we notice that, when the trial method is converging for both cases, then it requires the same number of boundary updates. Another observation is that, after having performed several tests variational updates are more unstable and create more oscillations on the approximations of the free boundary during the iterative process compared to the pointwise updates. The consequence of these oscillations is that the trial method is not converging for particular values of the parameter λ.

In connection with the previous chapter on the boundary element method we present some more results concerning the Dirichlet data of $\mathrm{v}^\star$ computed by the Neumann-to-Dirichlet map on the optimal boundary $\Gamma^\star$. In Section 2.4, we have seen that the accuracy of the Dirichlet data of v at the free boundary Γ depends on the number of the boundary elements that have been used for the boundary element method. Moreover, a valid optimal boundary $\Gamma^\star$ is that, for which the requirement (3.7) is satisfied. Here, for the parameter $\lambda = 20$, we solve the free boundary value problem for different numbers of boundary elements (# of BE) and degrees of freedom for the representation of the boundary curve (dof Γ). In Figure 3.3, the L^2-norm of the Dirichet data of $\mathrm{v}^\star$ at $\Gamma^\star$ with respect to the "# of BE" and the "dof Γ" is depicted.

Table 3.3 contains the respective values of this norm. It is clearly seen that both, the number of boundary elements and the degrees of freedom for the representation of the free boundary, have to be increased in order to raise the accuracy of the finite approximation of $\mathrm{v}^\star$. △

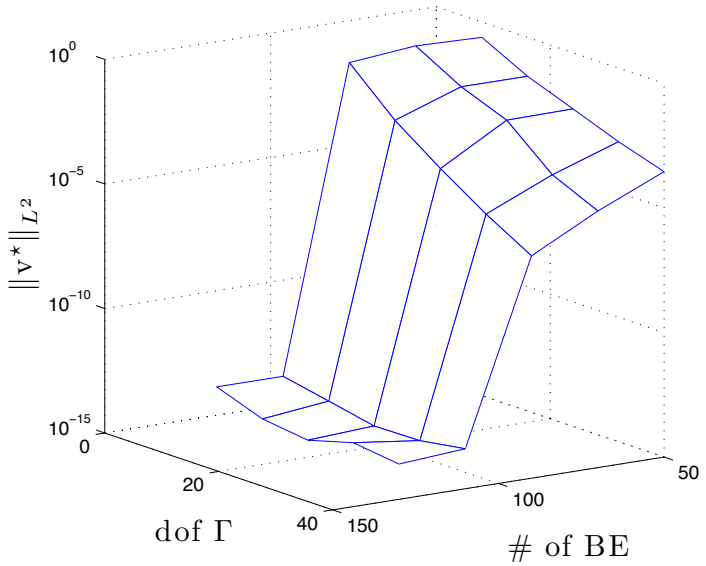

Figure 3.3: The L^2-norm of the Dirichlet data of $v^\star$ at the optimal approximate free boundary $\Gamma^\star$ with respect to the degrees of freedom for the representation of the boundary Γ (dof Γ) and the number of boundary elements (# of BE).

# of BE \ dof Γ	8	16	24	32	40
50	0.242	0.0275	0.00551	0.00111	$2.88 \cdot 10^{-4}$
70	0.293	0.0276	0.00514	$1.36 \cdot 10^{-4}$	$2.01 \cdot 10^{-5}$
90	0.164	0.00325	$1.56 \cdot 10^{-4}$	$9.57 \cdot 10^{-6}$	$8.45 \cdot 10^{-7}$
110	$1.12 \cdot 10^{-13}$	$4.7 \cdot 10^{-14}$	$1.92 \cdot 10^{-14}$	$2.05 \cdot 10^{-14}$	$3.98 \cdot 10^{-14}$
130	$1.12 \cdot 10^{-13}$	$2.41 \cdot 10^{-14}$	$1.37 \cdot 10^{-14}$	$4.48 \cdot 10^{-14}$	$2.58 \cdot 10^{-14}$

Table 3.3: The L^2-norm of the Dirichlet data of $v^\star$ at the optimal approximate free boundary $\Gamma^\star$.

Example 3.13. In our second example, we solve the free boundary problem (1.1) in case of the Laplace equation ($f = 0$) and non-constant boundary data

$$g(x, y) = x^2 + y^2 + 1 \quad \text{and} \quad h(x, y) = -\lambda(x^2 + y^2 + 1),$$

where λ is again a positive constant. The fixed boundary Σ is assumed to be peanut-shaped, parametrized by

$$\boldsymbol{\gamma}_\Sigma : [0, 2\pi] \to \Sigma, \quad s \mapsto \boldsymbol{\gamma}_\Sigma(s) = \begin{bmatrix} 0.03\sin(s)\big(1.25 + \cos(2s)\big) \\ 0.045\cos(s) \end{bmatrix}.$$

The initial guess Γ_0 of the free boundary is a flower-shaped boundary, whose

parametrization reads

$$\boldsymbol{\gamma}_0 : [0, 2\pi] \to \Gamma_0, \quad s \mapsto \boldsymbol{\gamma}_0(s) = \sqrt{0.004\cos^2(6s) + 0.003\sin^2(6s)} \begin{bmatrix} \cos(s) \\ \sin(s) \end{bmatrix}.$$

This time the numerical setting consists of 60 degrees of freedom for the representation of the unknown boundary Γ_k (i.e., $\nu = 30$) and 600 boundary elements per boundary. The trial method is terminated when the norm of the update function $\delta\mathsf{r}$ is smaller than 10^{-8}. The solutions of the free boundary problem are shown in Figure 3.4 for different values of the parameter λ.

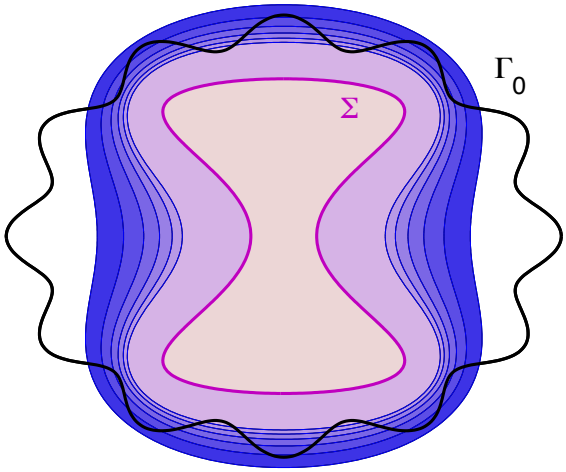

Figure 3.4: Solutions of the Bernoulli free boundary problem in case of a peanut-shaped interior boundary.

In Table 3.4, we present the number of executed boundary updates until the solution of the free boundary problem is achieved. We perform both, first and second order updates as well as pointwise and variational updates. The results are consistent with what we already observed in Example 3.12. Namely, the second order update is more robust than the first order update.

In all cases the trial method converges linearly, see Figure 3.5. In view of the fact that the trial method based on the approach "discretize-then-optimize" is converging for particular values of the parameter λ, while the method based on the approach "optimize-then-discretize" does not, we can deduce that the first approach is more efficient than the second one. However, for those values of the parameter λ where the trial method converges for the pointwise as well as the variational formulation, it is noteworthy that in both cases the optimal free boundary is detected after the same number of iterations. △

	parameter λ	40	50	60	70	80	90
pointwise updates	1st order update	27	28	27	27	25	–
	1st order with damping ($\alpha = 0.8$)	16	19	22	23	24	25
	1st order with damping ($\alpha = 0.5$)	27	32	36	39	41	42
	2nd order update	29	28	27	26	25	23
variational updates	1st order update	27	28	–	–	–	–
	1st order with damping ($\alpha = 0.8$)	16	19	22	–	–	–
	1st order with damping ($\alpha = 0.5$)	27	32	36	38	40	40
	2nd order update	29	28	27	26	25	23

Table 3.4: Number of boundary updates of the trial methods in case of a peanut-shaped interior boundary.

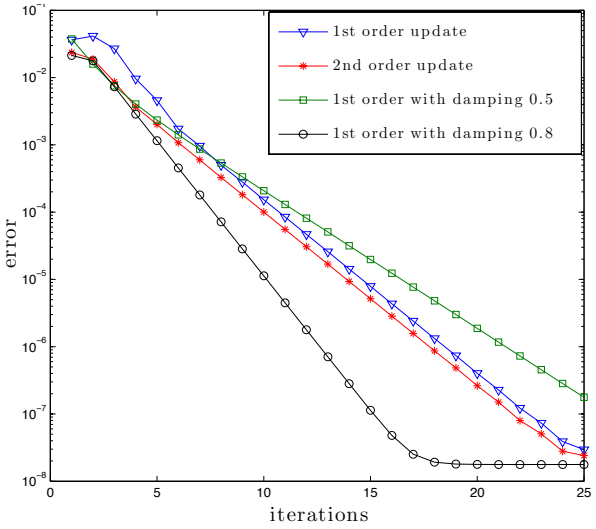

Figure 3.5: Convergence history of the trial methods for a peanut-shaped interior boundary and $\lambda = 50$ in case of variational updates.

Example 3.14. The last example of this chapter is for a flower-shaped fixed boundary Σ, parametrized by

$$\boldsymbol{\gamma}_\Sigma : [0, 2\pi] \to \Sigma, \quad s \mapsto \boldsymbol{\gamma}_\Sigma(s) = \sqrt{0.3\cos^2(3s) + 0.5\sin^2(3s)} \begin{bmatrix} \cos(s) \\ \sin(s) \end{bmatrix}.$$

We consider the original Bernoulli free boundary problem which corresponds to the Laplace equation ($f = 0$) and constant boundary data

$$g(x, y) = 1 \quad \text{and} \quad h(x, y) = -\lambda, \ \lambda > 0.$$

The boundary value problem is solved for 60 degrees of freedom to represent the boundary Γ and 500 boundary elements per boundary. Moreover, a random

boundary is used as initial guess Γ_0. The solutions of the free boundary problem for the chosen values of the parameter λ and the number of boundary updates that the trial method requires in order to achieve convergence are presented in Figure 3.6 and Table 3.5, respectively. The outermost boundary corresponds to $\lambda = 6$ and the innermost boundary to $\lambda = 16$.

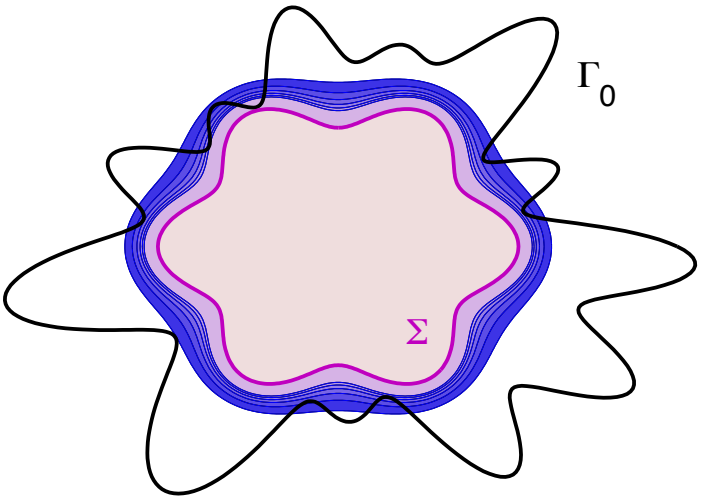

Figure 3.6: Solutions of the original Bernoulli free boundary problem in case of a flower-shaped interior boundary.

	parameter λ	6	8	10	12	14	16
pointwise updates	1st order update	–	–	–	–	–	–
	1st order with damping ($\alpha = 0.4$)	41	44	47	49	50	51
	2nd order update	21	20	18	17	16	16
variational updates	1st order update	–	–	–	–	–	–
	1st order with damping ($\alpha = 0.4$)	41	44	47	49	50	51
	2nd order update	21	20	18	17	16	16

Table 3.5: Number of boundary updates of the trial methods in case of a flower-shaped interior boundary.

For the chosen values of the parameter λ, we observe that the trial method based on the first order update rule is not converging. Therefore, a damping parameter is introduced. After having performed many tests in order to find a suitable damping parameter α for this example, we come up with the value $\alpha = 0.4$. In contrast to the previous two examples, we observe that the method based on the first order update rule demands considerably more iterations for the solution of the free boundary problem. The prompt convergence of the trial method based

on the second order update rule validates that this method is very efficient to solve the free boundary problem. △

Chapter 4

Convergence of the trial method

In this chapter, we investigate the convergence of the trial method. Following the lines of [75], we explore under which conditions we gain convergence and what is its rate. We review first some preliminary results from shape calculus and the theory of the fixed-point iteration method. By exploiting results from shape sensitivity analysis [22, 46, 68] we derive update rules for which the trial method shows a better performance. The novelty of the suggested method, compared to the already existing ones [36, 39, 75], is that this method does not require a change of the state equation (3.3). Furthermore, a fixed-point iterative scheme based on the Newton method is developed. In this case, the trial method is converging quadratically provided that the iterative process starts with an initial approximation which is close to the solution of the free boundary problem. The efficiency of the proposed trial methods is verified by numerical results at the end of this chapter.

4.1 Shape calculus

Shape calculus is the study of changes with respect to the shape of geometrical objects. It has been mostly developed in the field of shape optimization for applications such as optimal shape design, free boundary problems etc. In practice, shape sensitivity analysis corresponds to the calculation of partial derivatives with respect to the parameters that specify the geometry. As a valuable source of the theory related with shape optimization, we refer to [22, 25, 46, 68].

4.1.1 Domain variations

To carry out the sensitivity analysis of the solution v of the boundary value problem

$$\begin{aligned} -\Delta \mathrm{v} &= f \quad \text{in} \quad \Omega \\ \mathrm{v} &= g \quad \text{on} \quad \Sigma \\ \frac{\partial \mathrm{v}}{\partial \mathbf{n}} &= h \quad \text{on} \quad \Gamma \end{aligned} \tag{4.1}$$

one needs to introduce a family of perturbations $\{\Omega_\varepsilon\}$ of the given domain $\Omega \subset \mathbb{R}^2$ for small $\varepsilon > 0$. In order to construct a family of transformations, one uses the velocity method [22, 68] and its special case, the perturbation of the identity. An important subclass of the perturbation of identity involves perturbations in a specific direction only. In this case, although the direction is fixed, the magnitude of the perturbation is prescribed by a scalar field at the boundary.

In this thesis, we consider perturbations of the identity and more specifically perturbations in the radial direction. For a sufficiently smooth perturbation field $\mathbf{V} : \Omega \to \mathbb{R}^2$, we can define the perturbed domain Ω_ε as

$$\Omega_\varepsilon := \big\{(\mathbf{I} + \varepsilon \mathbf{V})(\mathbf{x}) : \mathbf{x} \in \Omega\big\}. \tag{4.2}$$

Consequently, the perturbation of the boundary Γ in the direction $\mathbf{V}$ is given by

$$\Gamma_\varepsilon := \big\{\big(\mathbf{I} + \varepsilon \mathbf{V}\big)(\mathbf{x}) : \mathbf{x} \in \Gamma\big\}.$$

We denote by $\mathbf{T}_\varepsilon$ the transformation

$$\mathbf{T}_\varepsilon(\mathbf{x}) = \mathbf{x} + \varepsilon \mathbf{V}(\mathbf{x}), \quad \mathbf{x} \in \Omega, \tag{4.3}$$

which deforms the domain Ω into the domain $\Omega_\varepsilon = \mathbf{T}_\varepsilon(\Omega)$ with boundary Γ_ε as illustrated in Figure 4.1. It is assumed that the domains Ω and Ω_ε have the same topological properties and possess the same regularity, e.g. Ω and Ω_ε are simply connected domains of class C^2. The perturbation of identity is introduced and studied in [57, 65]. Due to the fact that the perturbation of the identity is equivalent to the velocity method with respect to first order derivatives, we can still use the velocity method and the related notation to present further theoretical results and details from shape calculus.

4.1.2 Shape calculus for the state

Shape sensitivity analysis is a fundamental tool in shape optimization to analyze the relationship between the geometry and the solution of the state equation.

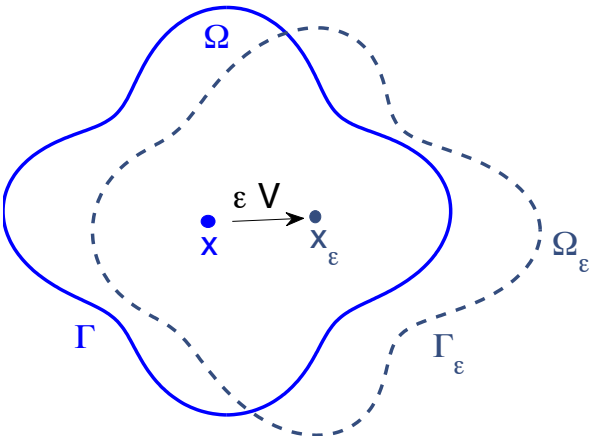

Figure 4.1: Variation of the domain.

Recall that the solution v of the boundary value problem (4.1) is defined with respect to the domain Ω. Compared with this, in the perturbed domain Ω_ε with boundaries Γ_ε and Σ, the solution of the boundary value problem satisfies

$$\begin{aligned} -\Delta \mathrm{v}_\varepsilon &= f \quad && \text{in} \quad \Omega_\varepsilon \\ \mathrm{v}_\varepsilon &= g \quad && \text{on} \quad \Sigma \\ \frac{\partial \mathrm{v}_\varepsilon}{\partial \mathbf{n}} &= h \quad && \text{on} \quad \Gamma_\varepsilon. \end{aligned} \tag{4.4}$$

Hence, when the deformation $\mathbf{x}_\varepsilon = \mathbf{x} + \varepsilon \mathbf{V}$ is interpreted as a flow with initial velocity field $\mathbf{V}$, the following definition becomes conclusive.

Definition 4.1. *Let* $\mathbf{V}$ *be a vector field in* $C^2(\mathbb{R}^2)$. *A shape functional* $J : \Omega \to \mathbb{R}$ *is called shape differentiable at the domain* Ω, *if the Eulerian derivative*

$$\mathrm{d}J[\mathbf{V}](\Omega) = \lim_{\varepsilon \to 0} \frac{J(\Omega_\varepsilon) - J(\Omega)}{\varepsilon}, \quad \Omega_\varepsilon = \mathbf{T}_\varepsilon(\Omega)$$

exists for all directions $\mathbf{V}$ *and the mapping* $\mathbf{V} \mapsto \mathrm{d}J[\mathbf{V}](\Omega)$ *is linear and continuous. The expression* $\mathrm{d}J[\mathbf{V}](\Omega)$ *is called the shape derivative of* J *at* Ω *in the direction* $\mathbf{V}$.

Additionally, partial derivatives of the state v which occur because of the transformation (4.3) of the domain Ω appear. As an important concept, the material derivative $\dot{\mathrm{v}}$ is introduced. It is computed by pulling back v_ε to the reference domain Ω, thus by differentiating $\mathrm{v}^\varepsilon(\mathbf{x}) := \mathrm{v}_\varepsilon \circ (\mathbf{I} + \varepsilon \mathbf{V})(\mathbf{x}) = \mathrm{v}_\varepsilon(\mathbf{x}_\varepsilon)$.

Definition 4.2. *The material derivative of* v *in the direction* $\mathbf{V}$ *is defined as the limit*

$$\dot{\mathrm{v}}[\mathbf{V}](\mathbf{x}) := \frac{\mathrm{d}\mathrm{v}^\varepsilon[\mathbf{V}](\mathbf{x})}{\mathrm{d}\varepsilon}\Big|_{\varepsilon=0} = \lim_{\varepsilon \to 0} \frac{\mathrm{v}^\varepsilon(\mathbf{x}) - \mathrm{v}(\mathbf{x})}{\varepsilon}, \quad \mathbf{x} \in \Omega.$$

In contrast, the linearization of the state v alone, without considering that the point where the state is being evaluated has been moved, leads to the local shape derivative. The local shape derivative $\mathrm{dv}[\mathbf{V}]$ at a point $\mathbf{x}$ is defined by differentiating $\mathrm{v}_\varepsilon(\mathbf{x})$ directly.

Definition 4.3. *The local shape derivative of* v *at* Ω *in the direction* $\mathbf{V}$ *is given by*

$$\mathrm{dv}[\mathbf{V}](\mathbf{x}) := \frac{\mathrm{d}\mathrm{v}_\varepsilon[\mathbf{V}](\mathbf{x})}{\mathrm{d}\varepsilon}\Big|_{\varepsilon=0} = \lim_{\varepsilon\to 0}\frac{\mathrm{v}_\varepsilon(\mathbf{x})-\mathrm{v}(\mathbf{x})}{\varepsilon}, \quad \mathbf{x}\in\Omega.$$

The relation between the material and the local shape derivative is expressed in the following remark.

Remark 4.4. The chain rule combines the material and the local shape derivative by the relation

$$\dot{\mathrm{v}}[\mathbf{V}] = \mathrm{dv}[\mathbf{V}] + \langle\nabla \mathrm{v}, \mathbf{V}\rangle. \tag{4.5}$$

In our forthcoming computations, beside the material derivative of the function v, we will also need the material derivative of the unit normal vector. To that end, we will remind the definition of the unit normal vector in the context of shape calculus as it was introduced in [22, 68], and we will derive its material derivative.

4.1.3 Material derivative of the normal vector

Let $\{\mathbf{e}_1,\dots,\mathbf{e}_N\}$ be the canonic orthonormal basis in $\mathbb{R}^N$. We use the notation $\boldsymbol{\zeta} = (\boldsymbol{\zeta}', \zeta_N)$ for a point $\boldsymbol{\zeta} = (\zeta_1,\dots,\zeta_N)$ in $\mathbb{R}^N$, where $\boldsymbol{\zeta}' = (\zeta_1,\dots,\zeta_{N-1})$. The open unit ball in $\mathbb{R}^N$ is denoted by B and we define the sets

$$\begin{aligned} B_+ &:= \{\boldsymbol{\zeta}\in B : \zeta_N > 0\},\\ B_- &:= \{\boldsymbol{\zeta}\in B : \zeta_N < 0\},\\ B_0 &:= \{\boldsymbol{\zeta}\in B : \zeta_N = 0\}. \end{aligned}$$

Lemma 4.5. *Let the domain* Ω *be a subset of* $\mathbb{R}^N$ *such that* $\partial\Omega\neq\emptyset$ *and let* $k>0$ *be an integer. If* Ω *is locally of class* C^k *at* $\mathbf{x}\in\partial\Omega$*, then there exist a neighborhood* $U(\mathbf{x})$ *of* $\mathbf{x}$ *and a bijective map* $\mathbf{c}_\mathbf{x} : U(\mathbf{x})\to B$ *with the following properties:*

(i) $\mathbf{c}_\mathbf{x}\in C^k\big(U(\mathbf{x}); B\big)$ *(ii)* $\mathbf{z}_\mathbf{x} := \mathbf{c}_\mathbf{x}^{-1}\in C^k\big(B; U(\mathbf{x})\big)$,

(iii) $\mathrm{int}\,\Omega\cap U(\mathbf{x}) = \mathbf{z}_\mathbf{x}(B_+)$, *(iv)* $\Gamma_\mathbf{x} := \partial\Omega\cap U(\mathbf{x}) = \mathbf{z}_\mathbf{x}(B_0)$,

(v) $B_0 = \mathbf{c}_\mathbf{x}(\Gamma_\mathbf{x})$.

More information about the properties stated in Lemma 4.5 can be found in [22]. Especially, for sets of class C^1, the normal vector at the boundary $\partial\Omega$ can be characterized through the Jacobian matrices of $\mathbf{c}_\mathbf{x}$ and $\mathbf{z}_\mathbf{x}$. By definition of B_0, it holds $\{\mathbf{e}_1, \dots, \mathbf{e}_{N-1}\} \subset B_0$ and the tangent space $T_\mathbf{y}\Gamma_\mathbf{x}$, at $\mathbf{y}$ to $\Gamma_\mathbf{x}$ is the vector space spanned by the $N-1$ vectors

$$\{D\mathbf{z}_\mathbf{x}(\boldsymbol{\zeta}', 0)\mathbf{e}_i : 1 \le i \le N-1\}, \quad (\boldsymbol{\zeta}', 0) = \mathbf{c}_\mathbf{x}(\mathbf{y}) \in B_0, \tag{4.6}$$

where $D\mathbf{z}_\mathbf{x}(\boldsymbol{\zeta})$ is the Jacobian matrix of $\mathbf{z}_\mathbf{x}$ at the point $\boldsymbol{\zeta}$:

$$(D\mathbf{z}_\mathbf{x})_{\ell,m} := \partial_m(\mathbf{z}_\mathbf{x})_\ell.$$

Due to (4.6), a normal vector field to $\Gamma_\mathbf{x}$ at $\mathbf{y} \in \Gamma_\mathbf{x}$ is given by

$$\mathbf{m}_\mathbf{x}(\mathbf{y}) = (D\mathbf{z}_\mathbf{x})^{-T}(\boldsymbol{\zeta}', 0)\mathbf{e}_N = (D\mathbf{z}_\mathbf{x})^{-T}\big(\mathbf{z}_\mathbf{x}^{-1}(\mathbf{y})\big)\mathbf{e}_N,$$

since

$$\langle \mathbf{m}_\mathbf{x}(\mathbf{y}), D\mathbf{z}_\mathbf{x}(\boldsymbol{\zeta}', 0)\mathbf{e}_i\rangle = \langle \mathbf{e}_N, \mathbf{e}_i\rangle = \delta_{iN}, \quad 1 \le i \le N.$$

Thus, the unit normal field $\mathbf{n}(\mathbf{y})$ at $\mathbf{y} \in \Gamma_\mathbf{x}$ is given by

$$\mathbf{n}(\mathbf{y}) = \frac{(D\mathbf{z}_\mathbf{x})^{-T}\big(\mathbf{z}_\mathbf{x}^{-1}(\mathbf{y})\big)\mathbf{e}_N}{\big\|(D\mathbf{z}_\mathbf{x})^{-T}\big(\mathbf{z}_\mathbf{x}^{-1}(\mathbf{y})\big)\mathbf{e}_N\big\|} \quad \text{for all } \mathbf{y} \in \Gamma_\mathbf{x}. \tag{4.7}$$

We consider the perturbation of the domain Ω as it was described in (4.2) and the associated transformation being given by (4.3). For Ω_ε and $\mathbf{x}_\varepsilon = \mathbf{T}_\varepsilon(\mathbf{x})$, we choose the following new neighborhood and local diffeomorphism:

$$\begin{aligned} \mathbf{z}_\varepsilon &:= \mathbf{T}_\varepsilon \circ \mathbf{z}_\mathbf{x} : B \to U_\varepsilon := \mathbf{T}_\varepsilon\big(U(\mathbf{x})\big) \\ \mathbf{z}_\varepsilon^{-1} &:= (\mathbf{T}_\varepsilon \circ \mathbf{z}_\mathbf{x})^{-1} = \ \mathbf{c}_\varepsilon = \mathbf{c}_\mathbf{x} \circ \mathbf{T}_\varepsilon^{-1} : U_\varepsilon \to B. \end{aligned} \tag{4.8}$$

The normal vector on $\Gamma_\varepsilon \cap U_\varepsilon$ is given by the same expression as in (4.7) but with $\mathbf{z}_\varepsilon$ in place of $\mathbf{z}_\mathbf{x}$:

$$\mathbf{n}_\varepsilon(\mathbf{y}) = \frac{(D\mathbf{z}_\varepsilon)^{-T}\big(\mathbf{z}_\varepsilon^{-1}(\mathbf{y})\big)\mathbf{e}_N}{\big\|(D\mathbf{z}_\varepsilon)^{-T}\big(\mathbf{z}_\varepsilon^{-1}(\mathbf{y})\big)\mathbf{e}_N\big\|} \quad \text{for all } \mathbf{y} \in \Gamma_\varepsilon. \tag{4.9}$$

In view of (4.8), the following relations hold for the enumerator of (4.9):

$$\begin{aligned} D\mathbf{z}_\varepsilon = D(\mathbf{T}_\varepsilon \circ \mathbf{z}_\mathbf{x}) &= (D\mathbf{T}_\varepsilon \circ \mathbf{z}_\mathbf{x})D\mathbf{z}_\mathbf{x}, \\ D(\mathbf{T}_\varepsilon \circ \mathbf{z}_\mathbf{x}) \circ (\mathbf{T}_\varepsilon \circ \mathbf{z}_\mathbf{x})^{-1} &= [D\mathbf{T}_\varepsilon D\mathbf{z}_\mathbf{x} \circ \mathbf{z}_\mathbf{x}^{-1}] \circ \mathbf{T}_\varepsilon^{-1} \\ (D\mathbf{T}_\varepsilon \circ \mathbf{z}_\mathbf{x})^{-T} \circ (\mathbf{T}_\varepsilon \circ \mathbf{z}_\mathbf{x})^{-1}\mathbf{e}_N &= [(D\mathbf{T}_\varepsilon)^{-T}(D\mathbf{z}_\mathbf{x})^{-T} \circ \mathbf{z}_\mathbf{x}^{-1}\mathbf{e}_N] \circ \mathbf{T}_\varepsilon^{-1}. \end{aligned} \tag{4.10}$$

We recognize the enumerator of the normal vector at $\mathbf{y} \in \Gamma_\mathbf{x}$ on the right hand side of equation (4.10) when we compare it with (4.7). Therefore, inserting (4.7)

into (4.10) and the resulting expression into (4.9), the normal vector $\mathbf{n}^\varepsilon := \mathbf{n}_\varepsilon(\mathbf{T}_\varepsilon)$ is given by

$$\mathbf{n}^\varepsilon = \frac{(D\mathbf{T}_\varepsilon)^{-T}\mathbf{n}}{\|(D\mathbf{T}_\varepsilon)^{-T}\mathbf{n}\|}. \tag{4.11}$$

Having the definition of the normal vector $\mathbf{n}^\varepsilon$ at hand, we report Remark 4.6 and Lemma 4.7 which provide essential results for the computation of the material derivative of the normal vector in Lemma 4.8.

Remark 4.6. Let $\mathbf{A}(\varepsilon) \in \mathbb{R}^{m\times m}$ be a matrix where each entry is a differentiable function with respect to ε such that $\mathbf{A}(\varepsilon)^{-1}$ exists for some $\varepsilon > 0$. Then, the derivative of the inverse matrix with respect to ε is given by

$$\frac{\mathrm{d}}{\mathrm{d}\varepsilon}\mathbf{A}(\varepsilon)^{-1} = -\mathbf{A}(\varepsilon)^{-1}\frac{\mathrm{d}\mathbf{A}(\varepsilon)}{\mathrm{d}\varepsilon}\mathbf{A}(\varepsilon)^{-1}.$$

Lemma 4.7. *For the transformation* (4.3) *of the domain* Ω *and a velocity field* $\mathbf{V}$*, the following identities are valid:*

(i) $D\mathbf{T}_\varepsilon|_{\varepsilon=0} = \mathbf{I}$ *(ii)* $\dfrac{\mathrm{d}}{\mathrm{d}\varepsilon}\mathbf{T}_\varepsilon\Big|_{\varepsilon=0} = \mathbf{V}$

(iii) $\dfrac{\mathrm{d}}{\mathrm{d}\varepsilon}D\mathbf{T}_\varepsilon\Big|_{\varepsilon=0} = D\mathbf{V}$ *(iv)* $\dfrac{\mathrm{d}}{\mathrm{d}\varepsilon}(D\mathbf{T}_\varepsilon)^T\Big|_{\varepsilon=0} = (D\mathbf{V})^T$

(v) $\dfrac{\mathrm{d}}{\mathrm{d}\varepsilon}(D\mathbf{T}_\varepsilon^{-1})\Big|_{\varepsilon=0} = -D\mathbf{V}.$

Proof. For the proof of these identities, we address the reader to [68]. □

The following lemma presents the material derivative of the normal vector at the boundary Γ.

Lemma 4.8. *The material derivative of the normal vector in the direction* $\mathbf{V}$ *is given by*

$$\dot{\mathbf{n}}[\mathbf{V}](\mathbf{x}) = \big\langle \big(D\mathbf{V}(\mathbf{x})\big)^T\mathbf{n}(\mathbf{x}), \mathbf{n}(\mathbf{x})\big\rangle\mathbf{n}(\mathbf{x}) - \big(D\mathbf{V}(\mathbf{x})\big)^T\mathbf{n}(\mathbf{x}), \quad \mathbf{x}\in\Gamma. \tag{4.12}$$

Proof. According to Definition 4.2, the material derivative of the unit normal vector is defined as

$$\dot{\mathbf{n}}[\mathbf{V}](\mathbf{x}) = \frac{\mathrm{d}\mathbf{n}^\varepsilon[\mathbf{V}](\mathbf{x})}{\mathrm{d}\varepsilon}\Big|_{\varepsilon=0} \tag{4.13}$$

with $\mathbf{n}^\varepsilon$ being given by (4.11). Since $D\mathbf{T}_0(\mathbf{x}) = \mathbf{I}$ (cf. Lemma 4.7, relation (i)), the quotient rule for the computation of the derivative in (4.13) yields

$$\dot{\mathbf{n}}[\mathbf{V}](\mathbf{x}) = \frac{\mathrm{d}}{\mathrm{d}\varepsilon}\big[\big(D\mathbf{T}_\varepsilon(\mathbf{x})\big)^{-T}\mathbf{n}(\mathbf{x})\big]\Big|_{\varepsilon=0} - \mathbf{n}(\mathbf{x})\frac{\mathrm{d}}{\mathrm{d}\varepsilon}\big\|\big(D\mathbf{T}_\varepsilon(\mathbf{x})\big)^{-T}\mathbf{n}(\mathbf{x})\big\|_2\Big|_{\varepsilon=0}. \tag{4.14}$$

Using Remark 4.6 and the relations (iv) and (v) from Lemma 4.7, the expression (4.14) is equivalent to

$$\dot{\mathbf{n}}[\mathbf{V}](\mathbf{x}) = -\mathbf{n}(\mathbf{x})\frac{\mathrm{d}}{\mathrm{d}\varepsilon}\big\|\big(D\mathbf{T}_\varepsilon(\mathbf{x})\big)^{-T}\mathbf{n}(\mathbf{x})\big\|_2\Big|_{\varepsilon=0} - \big(D\mathbf{V}(\mathbf{x})\big)^T\mathbf{n}(\mathbf{x}). \tag{4.15}$$

For any vector $\mathbf{v}(\varepsilon)$ where the components are differentiable functions, the chain rule gives

$$\frac{\mathrm{d}}{\mathrm{d}\varepsilon}\big\|\mathbf{v}(\varepsilon)\big\|_2\Big|_{\varepsilon=0} = \frac{1}{\|\mathbf{v}(0)\|_2}\Big\langle\frac{\mathrm{d}}{\mathrm{d}\varepsilon}\mathbf{v}(\varepsilon)\big|_{\varepsilon=0}, \mathbf{v}(0)\Big\rangle.$$

Hence, for $\mathbf{v}(\varepsilon) = \big(D\mathbf{T}_\varepsilon(\mathbf{x})\big)^{-T}\mathbf{n}(\mathbf{x})$, one has $\mathbf{v}(0) = \mathbf{n}(\mathbf{x})$ and thus, again due to Remark 4.6

$$\frac{\mathrm{d}}{\mathrm{d}\varepsilon}\mathbf{v}(\varepsilon)\Big|_{\varepsilon=0} = -\big(D\mathbf{V}(\mathbf{x})\big)^T\mathbf{n}(\mathbf{x}).$$

Moreover, the first term on the right hand side of (4.15) reads as

$$-\mathbf{n}(\mathbf{x})\frac{\mathrm{d}}{\mathrm{d}\varepsilon}\big\|\big(D\mathbf{T}_\varepsilon(\mathbf{x})\big)^{-T}\mathbf{n}(\mathbf{x})\big\|_2\Big|_{\varepsilon=0} = \mathbf{n}(\mathbf{x})\big\langle\big(D\mathbf{V}(\mathbf{x})\big)^T\mathbf{n}(\mathbf{x}), \mathbf{n}(\mathbf{x})\big\rangle.$$

This leads finally to the desired expression. □

At this point we like to mention that a smooth boundary variation $\mathbf{V} : \Gamma \to \mathbb{R}^2$ which acts on the free boundary Γ can always smoothly be extended to a domain perturbation $\widetilde{\mathbf{V}} : \Omega \to \mathbb{R}^2$ such that $\widetilde{\mathbf{V}}|_\Gamma = \mathbf{V}$. This is important for our subsequent analysis since each iteration of the trial method imposes a boundary variation in the direction $\mathbf{V} = q\mathbf{e}_r$, where q stands for an arbitrary scalar function in $C^2_{\mathrm{per}}\big([0, 2\pi]\big)$. For this reason, it makes sense to determine the material derivative of the normal vector also in the case of a vector field of the form $\mathbf{V} = q\mathbf{e}_r$.

Lemma 4.9. *Let $\mathbf{V} = q\mathbf{e}_r$ be the direction of the perturbation field at the boundary Γ. Then, the material derivative of the unit normal vector in the direction $\mathbf{V}$ is given by*

$$\dot{\mathbf{n}}[q\mathbf{e}_r] = q\frac{\langle\mathbf{e}_r, \mathbf{t}\rangle}{\|\boldsymbol{\gamma}'\|}\mathbf{t} - q'\frac{\langle\mathbf{e}_r, \mathbf{n}\rangle}{\|\boldsymbol{\gamma}'\|}\mathbf{t}. \tag{4.16}$$

Proof. The material derivative of the unit normal vector in case of an arbitrary vector field $\mathbf{V}$ is given by (4.12). Moreover, the definition of the normal vector does not depend on the actual domain which means that its local shape derivative vanishes. In accordance with Remark 4.4, the material derivative of the normal vector is equal to its directional derivative. Since $(D\mathbf{V})^T = \nabla\mathbf{V}$, [1] this yields the identity

$$\dot{\mathbf{n}}[\mathbf{V}] = \frac{\partial \mathbf{n}}{\partial \mathbf{V}} = -\langle \nabla\mathbf{V} \cdot \mathbf{n}, \mathbf{t}\rangle \mathbf{t}. \tag{4.17}$$

For the subsequent computations, we require an extension $\widetilde{q}$ of q into the neighborhood of Γ. Given a point $\mathbf{x} = \boldsymbol{\gamma}(s) + t\mathbf{n}(s) \subset \mathbb{R}^2$ with t being sufficiently small, we thus set $\widetilde{q}(\mathbf{x}) = q(s)$. Hence, the gradient of the vector field $\widetilde{\mathbf{V}} = \widetilde{q}\mathbf{e}_r$ can be written as

$$\nabla\widetilde{\mathbf{V}} = \widetilde{q}\nabla\mathbf{e}_r + (\nabla\widetilde{q})\mathbf{e}_r^T. \tag{4.18}$$

By inserting (4.18) into (4.17) we obtain

$$\frac{\partial \mathbf{n}}{\partial(\widetilde{q}\mathbf{e}_r)} = -\widetilde{q}\langle \nabla\mathbf{e}_r \cdot \mathbf{n}, \mathbf{t}\rangle \mathbf{t} - \langle (\nabla\widetilde{q})\mathbf{e}_r^T \cdot \mathbf{n}, \mathbf{t}\rangle \mathbf{t}. \tag{4.19}$$

We compute the terms included in (4.19) as follows. The gradient of the unit radial vector $\mathbf{e}_r = \boldsymbol{\gamma}/\|\boldsymbol{\gamma}\|$ in polar coordinates [2] is given by

$$\nabla\mathbf{e}_r(s) = \frac{1}{\|\boldsymbol{\gamma}(s)\|} \begin{bmatrix} -\sin(s) \\ \cos(s) \end{bmatrix} \frac{\partial \mathbf{e}_r(s)}{\partial s} = \frac{\mathbf{e}_r^{\perp}(s)\big(\mathbf{e}_r^{\perp}(s)\big)^T}{\|\boldsymbol{\gamma}(s)\|}, \tag{4.20}$$

where

$$\mathbf{e}_r^{\perp}(s) = \begin{bmatrix} -\sin(s) \\ \cos(s) \end{bmatrix}.$$

Hence, it holds

$$\langle \nabla\mathbf{e}_r \cdot \mathbf{n}, \mathbf{t}\rangle \mathbf{t} = \left\langle \frac{\mathbf{e}_r^{\perp}(\mathbf{e}_r^{\perp})^T}{\|\boldsymbol{\gamma}\|} \cdot \mathbf{n}, \mathbf{t} \right\rangle \mathbf{t} = \frac{\mathbf{t}^T\mathbf{e}_r^{\perp}(\mathbf{e}_r^{\perp})^T\mathbf{n}}{\|\boldsymbol{\gamma}\|}\mathbf{t} = \frac{\langle \mathbf{e}_r^{\perp}, \mathbf{t}\rangle\langle \mathbf{e}_r^{\perp}, \mathbf{n}\rangle}{\|\boldsymbol{\gamma}\|}\mathbf{t}. \tag{4.21}$$

[1] Given a vector $\mathbf{V} = (V_1, V_2)$, it holds that

$$D\mathbf{V} = \begin{bmatrix} \frac{\partial V_1}{\partial x} & \frac{\partial V_1}{\partial y} \\ \frac{\partial V_2}{\partial x} & \frac{\partial V_2}{\partial y} \end{bmatrix}, \quad \nabla\mathbf{V} = \begin{bmatrix} \frac{\partial V_1}{\partial x} & \frac{\partial V_2}{\partial x} \\ \frac{\partial V_1}{\partial y} & \frac{\partial V_2}{\partial y} \end{bmatrix}.$$

[2] The gradient of a function $f(r, s)$ given in polar coordinates is computed as

$$\nabla f(r, s) = \frac{1}{r} \begin{bmatrix} r\cos(s) & -\sin(s) \\ r\sin(s) & \cos(s) \end{bmatrix} \begin{bmatrix} \frac{\partial f}{\partial r} \\ \frac{\partial f}{\partial s} \end{bmatrix}.$$

Exploiting the identities

$$\langle \mathbf{e}_r^\perp, \mathbf{t}\rangle = -\langle \mathbf{e}_r, \mathbf{n}\rangle, \quad \langle \mathbf{e}_r^\perp, \mathbf{n}\rangle = \langle \mathbf{e}_r, \mathbf{t}\rangle \quad \text{and} \quad \frac{\langle \mathbf{e}_r, \mathbf{n}\rangle}{\|\boldsymbol{\gamma}\|} = \frac{1}{\|\boldsymbol{\gamma}'\|},$$

(4.21) can be further simplified to

$$\langle \nabla \mathbf{e}_r \cdot \mathbf{n}, \mathbf{t}\rangle \mathbf{t} = -\frac{\langle \mathbf{e}_r, \mathbf{n}\rangle \langle \mathbf{e}_r, \mathbf{t}\rangle}{\|\boldsymbol{\gamma}\|}\mathbf{t} = -\frac{\langle \mathbf{e}_r, \mathbf{t}\rangle}{\|\boldsymbol{\gamma}'\|}\mathbf{t}. \tag{4.22}$$

Employing again polar coordinates, the gradient of $\widetilde{q}$ is seen to be

$$\nabla \widetilde{q}\big(\boldsymbol{\gamma}(s) + t\mathbf{n}(s)\big) = \frac{1}{\|\boldsymbol{\gamma}(s)\|} \begin{bmatrix} -\sin(s) \\ \cos(s) \end{bmatrix} \frac{\partial q(s)}{\partial s} = -\frac{\mathbf{e}_r^\perp}{\|\boldsymbol{\gamma}\|} q(s)',$$

and thus the second term on the right hand side of (4.19) becomes

$$\langle (\nabla \widetilde{q}) \mathbf{e}_r^T \cdot \mathbf{n}, \mathbf{t}\rangle \mathbf{t} = -\frac{q'}{\|\boldsymbol{\gamma}\|} \langle \mathbf{e}_r^\perp, \mathbf{t}\rangle \langle \mathbf{e}_r, \mathbf{n}\rangle \mathbf{t} = q' \frac{\langle \mathbf{e}_r, \mathbf{n}\rangle}{\|\boldsymbol{\gamma}'\|}\mathbf{t}. \tag{4.23}$$

Finally, the validity of (4.16) follows from plugging (4.22) and (4.23) into (4.19). □

This form of the material derivative of the normal vector constitutes a valuable tool for the forthcoming analysis of the local shape derivative of the state. Additionally, it will be useful for the convergence analysis of the trial method and the numerical solution of the free boundary problem.

4.1.4 Shape derivative of the state

What remains to be analyzed in this brief review of shape calculus is the local shape derivative of the mixed boundary value problem (4.1). The subsequent lemma refers to this derivative.

Lemma 4.10. *The local shape derivative* dv *under the perturbation* $\mathbf{V}$ *is given as the solution of the boundary value problem*

$$\Delta \mathrm{dv}[\mathbf{V}] = 0 \qquad \text{in} \quad \Omega \tag{4.24a}$$

$$\mathrm{dv}[\mathbf{V}] = 0 \qquad \text{on} \quad \Sigma \tag{4.24b}$$

$$\frac{\partial \mathrm{dv}[\mathbf{V}]}{\partial \mathbf{n}} = \langle \nabla h, \mathbf{V}\rangle - \langle \nabla^2 \mathrm{v} \cdot \mathbf{V}, \mathbf{n}\rangle - \langle \nabla \mathrm{v}, \dot{\mathbf{n}}[\mathbf{V}]\rangle \qquad \text{on} \quad \Gamma. \tag{4.24c}$$

Proof. The functions v from (4.1) and v_ε from (4.4) satisfy both the Poisson equation with the same inhomogeneity. Due to the linearity of the Laplace operator and taking into account Definition 4.3, it follows that

$$\Delta \mathrm{dv}[\mathbf{V}](\mathbf{x}) = \lim_{\varepsilon \to 0} \frac{\Delta \mathrm{v}_\varepsilon(\mathbf{x}) - \Delta \mathrm{v}(\mathbf{x})}{\varepsilon} = 0, \qquad \mathbf{x} \in \Omega.$$

Besides the boundary data g at the fixed boundary Σ, also the functions f and h are invariant of the geometry of the domain Ω. This implies that their local shape derivative is zero and, due to Remark 4.4, their material derivative is equal to their derivative in the direction $\mathbf{V}$, i.e.,

$$\dot{h}[\mathbf{V}] = \langle \nabla h, \mathbf{V} \rangle \quad \text{and} \quad \dot{f}[\mathbf{V}] = \langle \nabla f, \mathbf{V} \rangle. \tag{4.25}$$

The Neumann data at $\mathbf{x}_\varepsilon = \mathbf{T}_\varepsilon(\mathbf{x}) \in \Gamma_\varepsilon$ read as

$$h(\mathbf{x}_\varepsilon) = \langle \nabla \mathrm{v}_\varepsilon, \mathbf{n}_\varepsilon \rangle \circ \mathbf{x}_\varepsilon = \langle \nabla \mathrm{v}_\varepsilon, \mathbf{n}_\varepsilon \rangle \circ \mathbf{T}_\varepsilon(\mathbf{x}) = \langle (\nabla \mathrm{v}_\varepsilon) \circ \mathbf{T}_\varepsilon(\mathbf{x}), \mathbf{n}_\varepsilon(\mathbf{x}_\varepsilon) \rangle. \tag{4.26}$$

We remind that $\nabla \mathrm{v} = (D\mathrm{v})^T$ and apply the chain rule to obtain

$$\begin{aligned} \nabla\big(\mathrm{v}_\varepsilon(\mathbf{x}_\varepsilon)\big) &= \Big(D\big(\mathrm{v}_\varepsilon(\mathbf{x}_\varepsilon)\big)\Big)^T \\ &= \Big(\big((D\mathrm{v}_\varepsilon) \circ \mathbf{T}_\varepsilon(\mathbf{x})\big) D\mathbf{T}_\varepsilon(\mathbf{x})\Big)^T \\ &= \big(D\mathbf{T}_\varepsilon(\mathbf{x})\big)^T \big((\nabla \mathrm{v}_\varepsilon) \circ \mathbf{T}_\varepsilon(\mathbf{x})\big). \end{aligned}$$

Thus, the first factor of the resulting inner product in (4.26) is given by

$$(\nabla \mathrm{v}_\varepsilon) \circ \mathbf{T}_\varepsilon(\mathbf{x}) = \big(D\mathbf{T}_\varepsilon(\mathbf{x})\big)^{-T} \nabla\big(\mathrm{v}_\varepsilon(\mathbf{x}_\varepsilon)\big).$$

The boundary data h from (4.26) become

$$\begin{aligned} h(\mathbf{x}_\varepsilon) &= \Big\langle \big(D\mathbf{T}_\varepsilon(\mathbf{x})\big)^{-T} \nabla\big(\mathrm{v}_\varepsilon(\mathbf{x}_\varepsilon)\big), \mathbf{n}_\varepsilon(\mathbf{x}_\varepsilon) \Big\rangle \\ &= \Big(\big(D\mathbf{T}_\varepsilon(\mathbf{x})\big)^{-T} \nabla\big(\mathrm{v}_\varepsilon(\mathbf{x}_\varepsilon)\big)\Big)^T \mathbf{n}_\varepsilon(\mathbf{x}_\varepsilon) \\ &= \big(\nabla \mathrm{v}_\varepsilon(\mathbf{x}_\varepsilon)\big)^T \big(D\mathbf{T}_\varepsilon(\mathbf{x})\big)^{-1} \mathbf{n}_\varepsilon(\mathbf{x}_\varepsilon). \end{aligned}$$

We take the derivative of $h(\mathbf{x}_\varepsilon)$ with respect to ε at $\varepsilon = 0$ and use Remark 4.6 and Lemma 4.7 to obtain

$$\dot{h}[\mathbf{V}] = \big(\nabla \dot{\mathrm{v}}[\mathbf{V}]\big)^T \mathbf{n} - (\nabla \mathrm{v})^T (D\mathbf{V})\mathbf{n} + \langle \nabla \mathrm{v}, \dot{\mathbf{n}}[\mathbf{V}] \rangle. \tag{4.27}$$

Rewriting equation (4.27) shows that the normal derivative of the material derivative of v is given by

$$\frac{\partial \dot{\mathrm{v}}[\mathbf{V}]}{\partial \mathbf{n}} = \dot{h}[\mathbf{V}] + \langle \nabla \mathrm{v}, (D\mathbf{V})\mathbf{n} \rangle - \langle \nabla \mathrm{v}, \dot{\mathbf{n}}[\mathbf{V}] \rangle. \tag{4.28}$$

Alternatively, we can also compute the normal derivative of (4.5), which gives

$$\frac{\partial \dot{\mathrm{v}}[\mathbf{V}]}{\partial \mathbf{n}} = \frac{\partial \mathrm{dv}[\mathbf{V}]}{\partial \mathbf{n}} + \langle \nabla^2 \mathrm{v} \cdot \mathbf{V}, \mathbf{n} \rangle + \langle \nabla \mathrm{v}, (D\mathbf{V})\mathbf{n} \rangle. \tag{4.29}$$

Hence, combining (4.28) and (4.29), we obtain an equation which leads to the Neumann data of the local shape derivative $\mathrm{dv}[\mathbf{V}]$ at Γ. Namely, it holds that

$$\begin{aligned} \frac{\partial \mathrm{dv}[\mathbf{V}]}{\partial \mathbf{n}} &= \dot{h}[\mathbf{V}] + \langle \nabla \mathrm{v}, (D\mathbf{V})\mathbf{n} \rangle - \langle \nabla \mathrm{v}, \dot{\mathbf{n}}[\mathbf{V}] \rangle - \langle \nabla^2 \mathrm{v} \cdot \mathbf{V}, \mathbf{n} \rangle - \langle \nabla \mathrm{v}, (D\mathbf{V})\mathbf{n} \rangle \\ &= \dot{h}[\mathbf{V}] - \langle \nabla \mathrm{v}, \dot{\mathbf{n}}[\mathbf{V}] \rangle - \langle \nabla^2 \mathrm{v} \cdot \mathbf{V}, \mathbf{n} \rangle. \end{aligned} \tag{4.30}$$

Inserting (4.25) into (4.30) concludes the proof. □

If we consider the specific perturbation $\mathbf{V} = q\mathbf{e}_r$, the material derivative of the normal vector is given by (4.16). By decomposing the derivatives included in (4.24c) into the normal and the tangential direction, the Neumann boundary condition (4.24c) can be rewritten as

$$\begin{aligned} \frac{\partial \mathrm{dv}[q\mathbf{e}_r]}{\partial \mathbf{n}} = \Big(\frac{\partial h}{\partial \mathbf{n}} - \frac{\partial^2 \mathrm{v}}{\partial \mathbf{n}^2}\Big)\langle q\mathbf{e}_r, \mathbf{n} \rangle + \Big(\frac{\partial h}{\partial \mathbf{t}} - \frac{\partial^2 \mathrm{v}}{\partial \mathbf{t} \partial \mathbf{n}}\Big)\langle q\mathbf{e}_r, \mathbf{t} \rangle \\ - \frac{\partial \mathrm{v}}{\partial \mathbf{t}}\Big(q\frac{\langle \mathbf{e}_r, \mathbf{t} \rangle}{\|\boldsymbol{\gamma}'\|} - q'\frac{\langle \mathbf{e}_r, \mathbf{n} \rangle}{\|\boldsymbol{\gamma}'\|}\Big). \end{aligned} \tag{4.31}$$

Having derived all the necessary information from sensitivity analysis, we will get a deeper insight into the convergence behavior of the trial method via Banach's fixed-point theorem.

4.2 Banach's fixed-point theorem

The trial method corresponds to a fixed-point iteration method. This provides an elegant basis for its convergence analysis. Let us assume that the update rule

$$r_{k+1} = r_k + \delta \mathsf{r}(r_k), \qquad k = 0, 1, 2, \ldots \tag{4.32}$$

defines a mapping $\Phi : C^2_{\mathrm{per}}\big([0, 2\pi]\big) \to C^2_{\mathrm{per}}\big([0, 2\pi]\big)$ given by

$$\Phi(r_k) = r_k + \delta \mathsf{r}(r_k), \qquad r_k \in C^2_{\mathrm{per}}\big([0, 2\pi]\big), \tag{4.33}$$

where $\delta \mathsf{r}$ stands for the update function. Our interest is to review the theoretical properties of fixed-point iteration methods, particularly the convergence analysis.

For sake of notational convenience we assume that $X := C^2_{\mathrm{per}}\big([0,2\pi]\big)$ denotes the Banach space equipped with the norm $\|\cdot\|_X = \|\cdot\|_{C^2_{\mathrm{per}}([0,2\pi])}$ as defined in (2.1). We indicate the fixed-point of (4.33) by $r^\star$, i.e., $\Phi(r^\star) = r^\star$, and state the following definition.

Definition 4.11. *We say an operator $\Phi : X \to X$ is contractive with contractivity constant $\vartheta \in [0,1)$ if*

$$\|\Phi(x) - \Phi(y)\|_X \leq \vartheta \|x - y\|_X \quad \textit{for all} \quad x,\ y \in X.$$

The most important method to analyze the solvability theory of equations such as (4.32) is Banach's fixed-point theorem, see [10, 41] for details.

Theorem 4.12 (**Banach's fixed-point theorem**). *Assume that $\Phi : X \to X$ is a contractive mapping with contractivity constant $\vartheta < 1$. Then, the following results hold.*

(i) ***Existence and uniqueness:*** *There exists a unique $r^\star \in X$ such that*

$$r^\star = \Phi(r^\star).$$

(ii) ***Convergence and error estimates of the iteration:*** *For any $r_0 \in X$, the sequence $\{r_k\} \subset X$ which is defined recursively by the iteration $r_{k+1} = \Phi(r_k)$, $k = 0, 1, \ldots$, converges to the fixed-point $r^\star$:*

$$\|r_k - r^\star\|_X \to 0 \quad \textit{as} \quad k \to \infty.$$

For the error, the following bounds are valid:

$$\begin{aligned} \|r_k - r^\star\|_X &\leq \frac{\vartheta^k}{1-\vartheta} \|r_0 - r_1\|_X, \\ \|r_k - r^\star\|_X &\leq \frac{\vartheta}{1-\vartheta} \|r_{k-1} - r_k\|_X, \\ \|r_{k+1} - r^\star\|_X &\leq \vartheta \|r_k - r^\star\|_X. \end{aligned} \tag{4.34}$$

Proof. For the proof we address the reader to [10, Theorem 5.1.3]. □

We close this compact summary of the theory of the fixed-point iteration method with some remarks about the rates of convergence. We say that the sequence r_k converges linearly to $r^\star$ if there exists a $\vartheta \in (0,1)$ such that

$$\lim_{k\to\infty} \frac{\|r_{k+1} - r^\star\|_X}{\|r_k - r^\star\|_X} = \vartheta.$$

The number ϑ is called the rate of convergence. If there holds $\vartheta = 0$, then the sequence is said to converge superlinearly. Moreover, if we have

$$\lim_{k\to\infty} \frac{\|r_{k+1} - r^\star\|_X}{\|r_k - r^\star\|_X^2} = \vartheta,$$

for a $\vartheta > 0$, then the sequence converges quadratically. In particular, we notice that the inequality (4.34) implies linear convergence of the fixed-point iteration method.

4.3 Convergence rate of the trial method

According to Banach's fixed-point theorem, there exists a unique solution of the fixed-point iteration if the mapping Φ is contractive. The convergence rate is established by computing the limit

$$\lim_{k\to\infty} \frac{\|r_{k+1} - r^\star\|_X}{\|r_k - r^\star\|_X} = \lim_{k\to\infty} \frac{\|\Phi(r_k) - \Phi(r^\star)\|_X}{\|r_k - r^\star\|_X}.$$

By considering arbitrary perturbations of the optimal free boundary $\Gamma^\star$ in the radial direction $q\mathbf{e}_r$, with $\|q\|_X = 1$, this limit can be estimated by

$$\begin{aligned}\lim_{k\to\infty} \frac{\|r_{k+1} - r^\star\|_X}{\|r_k - r^\star\|_X} &\leq \sup_{\|q\|_X=1} \lim_{\varepsilon\to 0} \frac{\|\Phi(r^\star + \varepsilon q) - \Phi(r^\star)\|_X}{\varepsilon} \\ &= \sup_{\|q\|_X=1} \|\mathrm{d}\Phi[q](r^\star)\|_X \,. \end{aligned} \tag{4.35}$$

As firstly stated in [75], we can thus deduce a sufficient condition for the convergence of the trial method. Namely, if $\sup_{\|q\|_X=1} \|\mathrm{d}\Phi[q](r^\star)\|_X < 1$, then the trial method converges. If it holds in addition that $\inf_{\|q\|_X=1} \|\mathrm{d}\Phi[q](r^\star)\|_X > 0$, then the convergence rate is only linear.

In what follows, we define admissible perturbed domains $\Omega_\varepsilon^\star$ with boundaries $\Gamma_\varepsilon^\star$ and Σ by the connection

$$\Gamma_\varepsilon^\star \leftrightarrow r_\varepsilon^\star = r^\star + \varepsilon q,$$

with $q \in C^2_{\mathrm{per}}\big([0, 2\pi]\big)$ and $\varepsilon > 0$ being sufficiently small, and investigate the convergence rate of the trial method based on the first order update rule by using (4.35).

4.3.1 Convergence in case of the first order update rule

As we have seen in Chapter 3, the first order update equation

$$\mathrm{v} \circ \boldsymbol{\gamma} + \Big(\frac{\partial \mathrm{v}}{\partial \mathbf{e}_r} \circ \boldsymbol{\gamma} \Big) \delta \mathsf{r}(r) = 0 \tag{4.36}$$

results from the first order Taylor expansion of the Dirichlet data at the boundary Γ and leads to the update function

$$\delta \mathsf{r}(r) = - \frac{\mathrm{v} \circ \boldsymbol{\gamma}}{\dfrac{\partial \mathrm{v}}{\partial \mathbf{e}_r} \circ \boldsymbol{\gamma}} \tag{4.37}$$

provided that $\partial \mathrm{v} / \partial \mathbf{e}_r(s) \neq 0$ for all $s \in [0, 2\pi]$. In this case, the mapping

$$\Phi_D : C^2_{\mathrm{per}}\big([0,2\pi]\big) \to C^2_{\mathrm{per}}\big([0,2\pi]\big), \quad r \mapsto \Phi_D(r) = r + \delta \mathsf{r}(r) \tag{4.38}$$

is well defined. We intend to prove convergence for the respective fixed-point iteration method by estimating the directional derivative $\mathrm{d}\Phi_D[q]$ on $\Gamma^\star$. Since, the mapping Φ_D contains the update function $\delta \mathsf{r}$, we start by presenting a theorem about the directional derivative of $\delta \mathsf{r}$.

Theorem 4.13. *Consider the trial method based on the first order update equation* (4.36)*. Then, the derivative of the update function* $\delta \mathsf{r}$ *in the direction* $q \in X$ *is given by*

$$\mathrm{d}\delta \mathsf{r}[q](r) = - \frac{\mathrm{dv}[q\mathbf{e}_r] \circ \boldsymbol{\gamma}}{\dfrac{\partial \mathrm{v}}{\partial \mathbf{e}_r} \circ \boldsymbol{\gamma}} - q + \frac{(\mathrm{v} \circ \boldsymbol{\gamma}) \left(\dfrac{\partial \mathrm{dv}[q\mathbf{e}_r]}{\partial \mathbf{e}_r} \circ \boldsymbol{\gamma} \right)}{\left(\dfrac{\partial \mathrm{v}}{\partial \mathbf{e}_r} \circ \boldsymbol{\gamma} \right)^2} + q(\mathrm{v} \circ \boldsymbol{\gamma}), \tag{4.39}$$

where $\mathrm{dv}[q\mathbf{e}_r]$ *denotes the local shape derivative of* v *in the direction* $\mathbf{V} = q\mathbf{e}_r$*.*

Proof. Let the perturbed boundary Γ_ε be parametrized by $\boldsymbol{\gamma}_\varepsilon = r_\varepsilon \mathbf{e}_r = (r + \varepsilon q)\mathbf{e}_r$. Denote the solutions to the underlying boundary value problems (4.1) relative to the domains Ω and Ω_ε by v and v_ε , i.e.,

$$\begin{aligned} -\Delta \mathrm{v} &= f \quad \text{in} \quad \Omega, \\ \mathrm{v} &= g \quad \text{on} \quad \Sigma, \\ \frac{\partial \mathrm{v}}{\partial \mathbf{n}} &= h \quad \text{on} \quad \Gamma, \end{aligned} \qquad \begin{aligned} -\Delta \mathrm{v}_\varepsilon &= f \quad \text{in} \quad \Omega_\varepsilon \\ \mathrm{v}_\varepsilon &= g \quad \text{on} \quad \Sigma \\ \frac{\partial \mathrm{v}_\varepsilon}{\partial \mathbf{n}_\varepsilon} &= h \quad \text{on} \quad \Gamma_\varepsilon. \end{aligned}$$

Then, the derivative of $\delta\mathsf{r}$ in the direction q is given by

$$\begin{aligned}
\mathrm{d}\delta\mathsf{r}[q](r) &= \lim_{\varepsilon\to 0}\frac{\delta\mathsf{r}(r_\varepsilon)-\delta\mathsf{r}(r)}{\varepsilon}\\
&= -\lim_{\varepsilon\to 0}\frac{1}{\varepsilon}\left(\frac{\mathrm{v}_\varepsilon\circ\boldsymbol{\gamma}_\varepsilon}{\dfrac{\partial \mathrm{v}_\varepsilon}{\partial \mathbf{e}_r}\circ\boldsymbol{\gamma}_\varepsilon}-\frac{\mathrm{v}\circ\boldsymbol{\gamma}}{\dfrac{\partial \mathrm{v}}{\partial \mathbf{e}_r}\circ\boldsymbol{\gamma}}\right)\\
&= -\lim_{\varepsilon\to 0}\frac{1}{\varepsilon}\frac{(\mathrm{v}_\varepsilon\circ\boldsymbol{\gamma}_\varepsilon)\Big(\dfrac{\partial \mathrm{v}}{\partial \mathbf{e}_r}\circ\boldsymbol{\gamma}\Big)-(\mathrm{v}\circ\boldsymbol{\gamma})\Big(\dfrac{\partial \mathrm{v}_\varepsilon}{\partial \mathbf{e}_r}\circ\boldsymbol{\gamma}_\varepsilon\Big)}{\Big(\dfrac{\partial \mathrm{v}}{\partial \mathbf{e}_r}\circ\boldsymbol{\gamma}\Big)\Big(\dfrac{\partial \mathrm{v}_\varepsilon}{\partial \mathbf{e}_r}\circ\boldsymbol{\gamma}_\varepsilon\Big)}\\
&= -\lim_{\varepsilon\to 0}\frac{1}{\varepsilon}\frac{\Big(\dfrac{\partial \mathrm{v}}{\partial \mathbf{e}_r}\circ\boldsymbol{\gamma}\Big)(\mathrm{v}_\varepsilon\circ\boldsymbol{\gamma}_\varepsilon-\mathrm{v}\circ\boldsymbol{\gamma})-(\mathrm{v}\circ\boldsymbol{\gamma})\Big(\dfrac{\partial \mathrm{v}_\varepsilon}{\partial \mathbf{e}_r}\circ\boldsymbol{\gamma}_\varepsilon-\dfrac{\partial \mathrm{v}}{\partial \mathbf{e}_r}\circ\boldsymbol{\gamma}\Big)}{\Big(\dfrac{\partial \mathrm{v}}{\partial \mathbf{e}_r}\circ\boldsymbol{\gamma}\Big)\Big(\dfrac{\partial \mathrm{v}_\varepsilon}{\partial \mathbf{e}_r}\circ\boldsymbol{\gamma}_\varepsilon\Big)}.
\end{aligned}\tag{4.40}$$

We treat the terms in the enumerator of (4.40) separately. The first term is rewritten as

$$\begin{aligned}
\lim_{\varepsilon\to 0}\frac{\mathrm{v}_\varepsilon\circ\boldsymbol{\gamma}_\varepsilon-\mathrm{v}\circ\boldsymbol{\gamma}}{\varepsilon} &= \lim_{\varepsilon\to 0}\frac{\mathrm{v}_\varepsilon\circ\boldsymbol{\gamma}_\varepsilon-\mathrm{v}\circ\boldsymbol{\gamma}_\varepsilon+\mathrm{v}\circ\boldsymbol{\gamma}_\varepsilon-\mathrm{v}\circ\boldsymbol{\gamma}}{\varepsilon}\\
&= \lim_{\varepsilon\to 0}\frac{\mathrm{v}_\varepsilon\circ\boldsymbol{\gamma}_\varepsilon-\mathrm{v}\circ\boldsymbol{\gamma}_\varepsilon}{\varepsilon}+\lim_{\varepsilon\to 0}\frac{\mathrm{v}\circ\boldsymbol{\gamma}_\varepsilon-\mathrm{v}\circ\boldsymbol{\gamma}}{\varepsilon}\\
&= \mathrm{dv}[q\mathbf{e}_r]\circ\boldsymbol{\gamma}+q\Big(\frac{\partial \mathrm{v}}{\partial \mathbf{e}_r}\circ\boldsymbol{\gamma}\Big).
\end{aligned}\tag{4.41}$$

Equation (4.41) includes the local shape derivative $\mathrm{dv}[q\mathbf{e}_r]$ and the directional derivative $\partial\mathrm{v}/\partial\mathbf{e}_r$. The first occurs from the change of the geometry of the boundary Γ due to its perturbation in the direction $\mathbf{V}=q\mathbf{e}_r$, and satisfies the boundary value problem (4.24). For the second term of the enumerator in (4.40) we get

$$\begin{aligned}
\lim_{\varepsilon\to 0}\frac{\dfrac{\partial \mathrm{v}_\varepsilon}{\partial \mathbf{e}_r}\circ\boldsymbol{\gamma}_\varepsilon-\dfrac{\partial \mathrm{v}}{\partial \mathbf{e}_r}\circ\boldsymbol{\gamma}}{\varepsilon} &= \lim_{\varepsilon\to 0}\frac{\dfrac{\partial \mathrm{v}_\varepsilon}{\partial \mathbf{e}_r}\circ\boldsymbol{\gamma}_\varepsilon-\dfrac{\partial \mathrm{v}}{\partial \mathbf{e}_r}\circ\boldsymbol{\gamma}_\varepsilon+\dfrac{\partial \mathrm{v}}{\partial \mathbf{e}_r}\circ\boldsymbol{\gamma}_\varepsilon-\dfrac{\partial \mathrm{v}}{\partial \mathbf{e}_r}\circ\boldsymbol{\gamma}}{\varepsilon}\\
&= \lim_{\varepsilon\to 0}\frac{\dfrac{\partial \mathrm{v}_\varepsilon}{\partial \mathbf{e}_r}\circ\boldsymbol{\gamma}_\varepsilon-\dfrac{\partial \mathrm{v}}{\partial \mathbf{e}_r}\circ\boldsymbol{\gamma}_\varepsilon}{\varepsilon}+\lim_{\varepsilon\to 0}\frac{\dfrac{\partial \mathrm{v}}{\partial \mathbf{e}_r}\circ\boldsymbol{\gamma}_\varepsilon-\dfrac{\partial \mathrm{v}}{\partial \mathbf{e}_r}\circ\boldsymbol{\gamma}}{\varepsilon}\\
&= \frac{\partial \mathrm{dv}[q\mathbf{e}_r]}{\partial \mathbf{e}_r}\circ\boldsymbol{\gamma}+\frac{\partial}{\partial(q\mathbf{e}_r)}\Big(\frac{\partial \mathrm{v}}{\partial \mathbf{e}_r}\circ\boldsymbol{\gamma}\Big)\\
&= \Big(\frac{\partial \mathrm{dv}[q\mathbf{e}_r]}{\partial \mathbf{e}_r}+q\frac{\partial^2 \mathrm{v}}{\partial \mathbf{e}_r^2}\Big)\circ\boldsymbol{\gamma}+q\langle\nabla\mathrm{v}\circ\boldsymbol{\gamma},\nabla\mathbf{e}_r\cdot\mathbf{e}_r\rangle.
\end{aligned}\tag{4.42}$$

The directional derivative of the local shape derivative $\partial \mathrm{dv}[q\mathbf{e}_r]/\partial \mathbf{e}_r$ and the second order directional derivative of the state $\partial^2 \mathrm{v}/\partial \mathbf{e}_r^2$ are contained in (4.42). Making use of the fact that the gradient of $\mathbf{e}_r$ is expressed in polar coordinates by (4.20), the third term of (4.42) vanishes, i.e.,

$$\langle \nabla \mathrm{v} \circ \boldsymbol{\gamma}, \nabla \mathbf{e}_r \cdot \mathbf{e}_r \rangle = \left\langle \nabla \mathrm{v} \circ \boldsymbol{\gamma}, \frac{\mathbf{e}_r^{\perp} (\mathbf{e}_r^{\perp})^T \mathbf{e}_r}{\|\boldsymbol{\gamma}\|} \right\rangle = 0.$$

If we insert (4.41) and (4.42) into (4.40), we obtain finally (4.39). □

We shall return now to (4.35) and focus on the derivation of the directional derivative $\mathrm{d}\Phi_D[q]$ at the optimal boundary $\Gamma^\star$.

Proposition 4.14. *Let the trial method be based on the first order update equation* (4.36)*. Then, for a given perturbation $q \in X$, it holds that*

$$\mathrm{d}\Phi_D[q](r^\star) = -\frac{\mathrm{dv}^\star[q\mathbf{e}_r] \circ \boldsymbol{\gamma}^\star}{(h \circ \boldsymbol{\gamma}^\star)\langle \mathbf{e}_r, \mathbf{n} \rangle}, \tag{4.43}$$

where $\boldsymbol{\gamma}^\star = r^\star \mathbf{e}_r$ and $\mathrm{dv}^\star[q\mathbf{e}_r]$ denotes the local shape derivative of $\mathrm{v}^\star$ into the direction $\mathbf{V} = q\mathbf{e}_r$. Especially, the latter satisfies the boundary value problem

$$\begin{aligned}
\Delta \mathrm{dv}^\star[q\mathbf{e}_r] &= 0 && \text{in} \quad \Omega^\star && \text{(4.44a)}\\
\mathrm{dv}^\star[q\mathbf{e}_r] &= 0 && \text{on} \quad \Sigma && \text{(4.44b)}\\
\frac{\partial \mathrm{dv}^\star[q\mathbf{e}_r]}{\partial \mathbf{n}} &= \Big(\kappa h + \frac{\partial h}{\partial \mathbf{n}} + f\Big)\langle q\mathbf{e}_r, \mathbf{n} \rangle && \text{on} \quad \Gamma^\star. && \text{(4.44c)}
\end{aligned}$$

Proof. On the optimal boundary $\Gamma^\star$, the following identities are valid

$$\mathrm{v}^\star \circ \boldsymbol{\gamma}^\star = 0, \qquad \frac{\partial \mathrm{v}^\star}{\partial \mathbf{t}} \circ \boldsymbol{\gamma}^\star = 0 \qquad \text{and} \qquad \frac{\partial \mathrm{v}^\star}{\partial \mathbf{n}} \circ \boldsymbol{\gamma}^\star = h \circ \boldsymbol{\gamma}^\star. \tag{4.45}$$

Therefore, in view of Theorem 4.13, the derivative of Φ_D in the direction q reads as

$$\begin{aligned}
\mathrm{d}\Phi_D[q](r^\star) &= \lim_{\varepsilon \to 0} \frac{\Phi_D(r^\star + \varepsilon q) - \Phi_D(r^\star)}{\varepsilon} \\
&= q + \mathrm{d}\delta \mathrm{r}[q](r^\star) \\
&= -\frac{\mathrm{dv}^\star[q\mathbf{e}_r] \circ \boldsymbol{\gamma}^\star}{\dfrac{\partial \mathrm{v}^\star}{\partial \mathbf{e}_r} \circ \boldsymbol{\gamma}^\star},
\end{aligned} \tag{4.46}$$

where the local shape derivative $\mathrm{dv}^\star[q\mathbf{e}_r]$ is the solution of the boundary value problem (4.24) at the optimal domain $\Omega^\star$. Note that, due to equation (3.9) and

the relations in (4.45), the derivative of $\mathrm{v}^\star$ in the direction $\mathbf{e}_r$ satisfies at the optimal boundary $\Gamma^\star$

$$\frac{\partial \mathrm{v}^\star}{\partial \mathbf{e}_r} \circ \boldsymbol{\gamma}^\star = (h \circ \boldsymbol{\gamma}^\star)\langle \mathbf{e}_r, \mathbf{n}\rangle.$$

With this result, (4.46) changes to the desired equation (4.43).

That the Neumann boundary condition of the boundary value problem (4.24) is written at the optimal boundary $\Gamma^\star$ as in (4.44c) is seen from equation (4.31) when we take into account the relations from (4.45) and additionally insert (3.18) and (3.19). □

Proposition 4.14 shows that equation (4.43) yields the norm

$$\big\|\mathrm{d}\Phi_D[q](r^\star)\big\|_X = \left\| \frac{\mathrm{dv}^\star[q\mathbf{e}_r] \circ \boldsymbol{\gamma}^\star}{(h \circ \boldsymbol{\gamma}^\star)\langle \mathbf{e}_r, \mathbf{n}\rangle} \right\|_X.$$

The requirement for a (local) convergence of the trial method is that the mapping Φ_D is contractive, i.e.,

$$\left\| \frac{\mathrm{dv}^\star[q\mathbf{e}_r] \circ \boldsymbol{\gamma}^\star}{(h \circ \boldsymbol{\gamma}^\star)\langle \mathbf{e}_r, \mathbf{n}\rangle} \right\|_X \overset{!}{<} 1. \tag{4.47}$$

From this result, it is obvious that the question whether the trial method based on the first order update equation is (locally) converging or not can be answered by inspecting the local shape derivative.

Since it holds in general

$$\Big(\kappa h + \frac{\partial h}{\partial \mathbf{n}} + f\Big) \neq 0 \quad \text{almost everywhere on } \Gamma^\star,$$

and consequently the Neumann data (4.44c) and the local shape derivative $\mathrm{dv}^\star[q\mathbf{e}_r]$ are nonzero for all directions $0 \neq q \in X$. The reasoning for this is that $\mathrm{dv}^\star[q\mathbf{e}_r]$ satisfies the Laplace equation with a homogeneous boundary condition on Σ and, hence, the Dirichlet data $\mathrm{dv}^\star[q\mathbf{e}_r]$ can only vanish if it holds $\mathrm{dv}^\star[q\mathbf{e}_r] = 0$ in $\Omega^\star$. Therefore, we generally expect only linear convergence of the trial method, as already observed in the numerical experiments of Section 3.4.

Remark 4.15. The update $\delta\mathsf{r}_2 = \delta\mathsf{r}_2(r)$ computed from the second order update equation

$$\mathrm{v} \circ \boldsymbol{\gamma} + \Big(\frac{\partial \mathrm{v}}{\partial \mathbf{e}_r} \circ \boldsymbol{\gamma}\Big)\delta\mathsf{r}_2(r) + \frac{1}{2}\Big(\frac{\partial^2 \mathrm{v}}{\partial \mathbf{e}_r^2} \circ \boldsymbol{\gamma}\Big)\delta\mathsf{r}_2^2(r) = 0 \tag{4.48}$$

coincides with the update $\delta\mathsf{r}_1 = \delta\mathsf{r}_1(r)$ computed from the first order update equation (4.36) except for a higher order term, i.e., $\delta\mathsf{r}_2(r) = \delta\mathsf{r}_1(r) + \epsilon(r)$ with

$\|\epsilon(r)\|_X = \mathcal{O}\big(\|\delta \mathsf{r}_1(r)\|_X^2\big)$. Hence, all the results about the convergence remain essentially valid also in the case where the trial method is based on the second order update equation (4.48).

4.3.2 Improved trial method

In Section 4.3.1 we have shown that the computation of the local shape derivative $\mathrm{dv}^\star[q\mathbf{e}_r]$ enables the evaluation of the convergence rate of the trial method. Hence, a question of great importance arises. What happens if $\|\mathrm{d}\Phi_D[q](r^\star)\|_X \geq 1$? Can we then enforce convergence of the trial method or is it possible to obtain even superlinear convergence? A superlinearly convergent trial method for interior Bernoulli's free boundary problem has been proposed in [36], called the implicit Neumann method. Results on a quadratically convergent trial method can be found in [39, 52, 73, 75], where the solution of a Robin boundary value problem was suggested. Unfortunately, this Robin boundary value problem is only well-posed if the free boundary is convex. In contrast, our objective is to avoid the solution of a boundary value problem other than (4.1) since this would require the change of the boundary element method.

Until now we have seen that the convergence of the trial method is closely related to the update rule of the free boundary, namely, the definition of the self-mapping Φ_D. Due to this observation, we suggest to modify the initially proposed mapping Φ_D in (4.38) by introducing a constant damping parameter α as follows

$$\Phi_D : X \to X, \quad r \mapsto \Phi_D(r) = r + \alpha \delta \mathsf{r}(r). \tag{4.49}$$

Thus, the derivative (4.43) becomes

$$\mathrm{d}\Phi_D[q](r^\star) = (1-\alpha)q - \alpha \frac{\mathrm{dv}^\star[q\mathbf{e}_r] \circ \boldsymbol{\gamma}^\star}{(h \circ \boldsymbol{\gamma}^\star)\langle \mathbf{e}_r, \mathbf{n}\rangle}.$$

From this expression, it is not obvious how to choose the damping parameter α to ensure that $\|\mathrm{d}\Phi_D[q](r^\star)\|_X < 1$. This result, established for a constant parameter α, triggers the idea of considering a function $\alpha(r) : [0, 2\pi] \to \mathbb{R}$ instead of a constant. Within this framework, the self-mapping Φ_D is modified according to

$$\Phi_D : X \to X, \quad r \mapsto \Phi_D(r) = r + \alpha(r) \delta \mathsf{r}(r). \tag{4.50}$$

Notice that $r^\star$ is still a fixed-point of Φ_D. We shall now determine the function $\alpha(r) : [0, 2\pi] \to \mathbb{R}$ such that superlinear convergence of the method is ensured. In other words, we seek a function $\alpha(r)$ for which

$$\lim_{k\to\infty} \frac{\|r_{k+1} - r^\star\|_X}{\|r_k - r^\star\|_X} = \lim_{k\to\infty} \frac{\|\Phi_D(r_k) - \Phi_D(r^\star)\|_X}{\|r_k - r^\star\|_X} = 0. \tag{4.51}$$

We remind that the parametrization of the perturbed boundary $\Gamma_\varepsilon^\star$ is $\gamma_\varepsilon^\star = r_\varepsilon^\star \mathbf{e}_r = (r^\star + \varepsilon q)\mathbf{e}_r$. Following the same procedure as in the proof of Proposition 4.14, the derivative of the mapping Φ_D with respect to a given direction q is computed by

$$\begin{aligned}
\mathrm{d}\Phi_D[q](r^\star) &= \lim_{\varepsilon\to 0} \frac{\Phi_D(r^\star + \varepsilon q) - \Phi_D(r^\star)}{\varepsilon} \\
&= \lim_{\varepsilon\to 0} \frac{r^\star + \varepsilon q + \alpha(r_\varepsilon^\star)\delta\mathsf{r}(r_\varepsilon^\star) - r^\star - \alpha(r^\star)\delta\mathsf{r}(r^\star)}{\varepsilon} \\
&= q + \mathrm{d}(\alpha\delta\mathsf{r})[q](r^\star) \\
&= q + \mathrm{d}\alpha[q](r^\star)\delta\mathsf{r}(r^\star) + \alpha(r^\star)\mathrm{d}\delta\mathsf{r}[q](r^\star). \qquad (4.52)
\end{aligned}$$

Recall Theorem 4.13 and that by construction $\delta\mathsf{r}(r^\star) = 0$. Thus, (4.52) yields

$$\mathrm{d}\Phi_D[q](r^\star) = q - \alpha(r^\star)\Big(\frac{\mathrm{dv}^\star[q\mathbf{e}_r]\circ\boldsymbol{\gamma}^\star}{\langle\nabla \mathrm{v}^\star\circ\boldsymbol{\gamma}^\star, \mathbf{e}_r\rangle} + q\Big). \qquad (4.53)$$

A superlinearly convergent scheme is derived if we define the function $\alpha(r)$ such that (4.51) is satisfied for the direction $q := \lim_{k\to\infty}(r_k - r^\star)/\|r_k - r^\star\|_X$ provided that this limit exists. Nevertheless, since $r^\star$ is unknown, q would not be accessible even in the case of existence. Hence, we choose just $q = 1$ which corresponds to the radial direction $\mathbf{V} = \mathbf{e}_r$. This leads to

$$\alpha(r) = \frac{\dfrac{\partial \mathrm{v}}{\partial \mathbf{e}_r}\circ\boldsymbol{\gamma}}{\mathrm{dv}[\mathbf{e}_r]\circ\boldsymbol{\gamma} + \dfrac{\partial \mathrm{v}}{\partial \mathbf{e}_r}\circ\boldsymbol{\gamma}}. \qquad (4.54)$$

The expression (4.54) depends on the actual state v and on its local shape derivative. The local shape derivative $\mathrm{dv}[\mathbf{e}_r]$ can be evaluated in complete analogy to the solution of the mixed boundary value problem (4.24) by using the Neumann-to-Dirichlet map as it was described in Section 2.2. Hence, one additional solve of the Neumann-to-Dirichlet map is necessary per iteration step.

Remark 4.16. The condition

$$\Big(\kappa h + \frac{\partial h}{\partial \mathbf{n}} + f\Big) < 0 \quad \text{on } \Gamma^\star \qquad (4.55)$$

is very often required in connection with the convergence theory of free boundary problems, see e.g. [30, 31, 77, 78]. Since it holds also $\langle \mathbf{e}_r, \mathbf{n}\rangle > 0$ in case of a starlike domain, the prescribed Neumann data of the local shape derivative $\mathrm{dv}[\mathbf{e}_r]$ are negative at $\Gamma^\star$, cf. (4.44c). Hence, under the condition (4.55), there holds $\mathrm{dv}[\mathbf{e}_r] < 0$ in $\Omega^\star$ and thus $\mathrm{dv}[\mathbf{e}_r] < 0$ at $\Gamma^\star$. As a consequence, the denominator of $\big(\alpha(r^\star)\big)(s)$ is negative for all $s \in [0, 2\pi]$. We finally conclude that $\alpha(r)$ is well defined at least in a neighborhood of $r^\star$ if (4.55) holds.

The convergence rate of the trial method with damping parameter α from (4.54), as it is demonstrated by numerical examples in Section 4.5, is an improved linear one. However, the goal of deriving a quadratically convergent trial method can be realized and we present the corresponding update rule in the next section.

4.3.3 Newton method

A quadratically convergent trial method is derived by use of Newton's method. It is obtained by demanding that the update function $\delta\mathsf{r}(r_k)$ on the boundary Γ_k, given by (4.37), becomes zero, i.e.,

$$\delta\mathsf{r}(r_k) \stackrel{!}{=} 0.$$

Linearizing the update function around the actual boundary Γ_k gives

$$\delta\mathsf{r}(r_{k+1}) \approx \delta\mathsf{r}(r_k) + \mathrm{d}\delta\mathsf{r}[q](r_k) \stackrel{!}{=} 0.$$

The derivative of the update function $\delta\mathsf{r}$ with respect to a direction $q \in X$ is given by equation (4.39), namely,

$$\mathrm{d}\delta\mathsf{r}[q](r_k) = -\frac{\mathrm{dv}_k[q\mathbf{e}_r] \circ \boldsymbol{\gamma}_k}{\dfrac{\partial \mathrm{v}_k}{\partial \mathbf{e}_r} \circ \boldsymbol{\gamma}_k} - q + \frac{(\mathrm{v}_k \circ \boldsymbol{\gamma}_k)\Big(\dfrac{\partial \mathrm{dv}_k[q\mathbf{e}_r]}{\partial \mathbf{e}_r} \circ \boldsymbol{\gamma}_k\Big)}{\Big(\dfrac{\partial \mathrm{v}_k}{\partial \mathbf{e}_r} \circ \boldsymbol{\gamma}_k\Big)^2} + q(\mathrm{v}_k \circ \boldsymbol{\gamma}_k), \tag{4.56}$$

where $\mathrm{dv}_k[q\mathbf{e}_r]$ is the local shape derivative of the state v_k associated with the domain Ω_k. Hence, the Newton update q is determined as the solution of the equation

$$\mathrm{d}\delta\mathsf{r}[q](r_k) \stackrel{!}{=} -\delta\mathsf{r}(r_k). \tag{4.57}$$

To solve this equation, we perform the fixed-point iteration

$$q_{\ell+1} = \delta\mathsf{r}(r_k) - \frac{\mathrm{dv}_k[q_\ell\mathbf{e}_r] \circ \boldsymbol{\gamma}_k}{\dfrac{\partial \mathrm{v}_k}{\partial \mathbf{e}_r} \circ \boldsymbol{\gamma}_k} + \frac{(\mathrm{v}_k \circ \boldsymbol{\gamma}_k)\Big(\dfrac{\partial \mathrm{dv}_k[q_\ell\mathbf{e}_r]}{\partial \mathbf{e}_r} \circ \boldsymbol{\gamma}_k\Big)}{\Big(\dfrac{\partial \mathrm{v}_k}{\partial \mathbf{e}_r} \circ \boldsymbol{\gamma}_k\Big)^2} + q_\ell(\mathrm{v}_k \circ \boldsymbol{\gamma}_k), \tag{4.58}$$

for $\ell = 0, 1, 2, \ldots$. A good initial guess is $q_0 = \delta\mathsf{r}(r_k)$ which would be the first iterate when starting with $q_{-1} = 0$. Nevertheless, several of these inner iterations will be performed, each of which requires one solve of the Neumann-to-Dirichlet map to calculate the local shape derivative $\mathrm{dv}_k[q_\ell\mathbf{e}_r]$. Finally, the free boundary will be updated in each iteration according to the update rule $r_{k+1} = r_k + q_\ell$.

4.3.4 Inexact Newton method

Rather than computing the exact directional derivative (4.56) one could use an approximation instead in the equation (4.57) for the Newton update. This simplification leads to the well-known inexact Newton method.

Given a function F, the exact Newton method to solve the equation $F(x) = 0$ is calculated by

$$-\frac{F(x)}{F'(x)} = \Delta x.$$

Now, in place of the previous equation, we consider the perturbed equation

$$-\frac{F(x)}{F'(x)+\varepsilon} = \widetilde{\Delta x}.$$

The Taylor expansion with respect to the perturbation leads to

$$-\frac{F(x)}{F'(x)+\varepsilon} = -\frac{F(x)}{F'(x)} + \varepsilon\frac{F(x)}{\big(F'(x)\big)^2} + \mathcal{O}(\varepsilon^2).$$

When $\varepsilon = \mathcal{O}(\|F(x)\|)$, we get thus the equation

$$\widetilde{\Delta x} = \Delta x + \mathcal{O}(\|F(x)\|^2). \tag{4.59}$$

Relation (4.59) indicates that the update obtained by the exact Newton method and the inexact Newton method is essentially the same for a perturbation of order $\mathcal{O}(\|F(x)\|)$. In particular, both methods are known to converge quadratically, see [47, 58].

In our problem, we denote by $E(q)$ the third and forth term on the right hand side of equation (4.56). In view of (4.37) it can be rewritten as

$$E(q) = -\delta\mathsf{r}(r_k)\frac{\dfrac{\partial \mathrm{dv}_k[q\mathbf{e}_r]}{\partial \mathbf{e}_r}\circ\boldsymbol{\gamma}_k + q\Big(\dfrac{\partial \mathrm{v}_k}{\partial \mathbf{e}_r}\circ\boldsymbol{\gamma}_k\Big)}{\dfrac{\partial \mathrm{v}_k}{\partial \mathbf{e}_r}\circ\boldsymbol{\gamma}_k},$$

which is obviously a term of order $\mathcal{O}(\|\delta\mathsf{r}\|_X)$ provided that $\|q\|_X = 1$. The inexact Newton method consists of using the inexact derivative of the update function in the direction q. This means that we employ $\mathrm{d}\delta\mathsf{r}[q] - E(q)$ instead of $\mathrm{d}\delta\mathsf{r}[q]$ to solve the update equation. As it has been shown in (4.59), we obtain then essentially the same update in both cases. More precisely, the inexact Newton update q is determined by the fixed-point iteration

$$q_{\ell+1} = \delta\mathsf{r}(r_k) - \frac{\mathrm{dv}_k[q_\ell\mathbf{e}_r]\circ\boldsymbol{\gamma}_k}{\dfrac{\partial \mathrm{v}_k}{\partial \mathbf{e}_r}\circ\boldsymbol{\gamma}_k}, \quad \ell = 0, 1, 2, \ldots, \tag{4.60}$$

with initial guess $q_0 = \delta\mathsf{r}(r_k)$.

4.4 Trial method for circular boundaries

In this section, by exploiting the properties of circular domains, we intend to analytically validate the results obtained until now.

Let the domain Ω_k be described by the concentric circular boundaries Σ and Γ_k with radius r_Σ and r_k, where $r_k > r_\Sigma$ such that the free boundary Γ_k is outer to the fixed boundary Σ. We consider the mixed boundary value problem for the Laplace equation with Dirichlet boundary condition $g(r_k) = 1$ at the boundary Σ and Neumann boundary condition $h(r_k)$ at the boundary Γ_k:

$$\begin{aligned} -\frac{\partial^2 \mathrm{v}_k}{\partial r^2} - \frac{1}{r}\frac{\partial \mathrm{v}_k}{\partial r} &= 0 \qquad \text{in} \quad \Omega_k \\ \mathrm{v}_k &= 1 \qquad \text{on} \quad \Sigma \\ \frac{\partial \mathrm{v}_k}{\partial r} &= h \qquad \text{on} \quad \Gamma_k. \end{aligned} \tag{4.61}$$

The solution to this boundary value problem reads

$$\mathrm{v}_k(r_k) = h(r_k) r_k \log \frac{r_k}{r_\Sigma} + 1.$$

In case of circular boundaries, the following identities hold

$$\langle \mathbf{e}_r, \mathbf{n} \rangle = 1, \qquad \langle \mathbf{e}_r, \mathbf{t} \rangle = 0 \qquad \text{and} \qquad \kappa = \frac{1}{r_k}.$$

The trial method for the problem under consideration corresponds to the fixed-point iteration

$$\Phi_D(r_k) = r_k + \delta \mathsf{r}(r_k).$$

Since the first order update equation (3.11) yields $\delta \mathsf{r}(r_k) = -\mathrm{v}_k(r_k)/h(r_k)$, the mapping Φ_D is explicitly written as

$$\Phi_D(r_k) = r_k - \frac{1}{h(r_k)} - r_k \log \frac{r_k}{r_\Sigma}. \tag{4.62}$$

As we have seen in Section 4.3 the norm of the derivative of the mapping Φ_D in the direction q is required to study the convergence of the trial method. In the special case of concentric circular boundaries, where we assume that the free boundary moves only in the radial direction $\mathbf{V} = q\mathbf{e}_r$ with $q = 1$, the directional derivative $\mathrm{d}\Phi_D[q](r^\star)$ is equivalent to the derivative of the Φ_D with respect to the radius of the boundary Γ_k evaluated at the boundary $\Gamma^\star$. This means that the convergence of the trial method depends on the derivative

$$\frac{\partial \Phi_D}{\partial r}(r^\star) = -\log \frac{r^\star}{r_\Sigma} + \frac{1}{\big(h(r^\star)\big)^2} \frac{\partial h}{\partial r}(r^\star). \tag{4.63}$$

Alternatively, we can find the derivative of Φ_D with respect to r_k also by (4.43), which leads to

$$\frac{\partial \Phi_D}{\partial r}(r^\star) = -\frac{\mathrm{dv}^\star[\mathbf{e}_r](r^\star)}{h(r^\star)}. \tag{4.64}$$

The local shape derivative $\mathrm{dv}^\star[\mathbf{e}_r]$ is the solution of the boundary value problem (4.24), which for circular boundaries reads

$$\begin{aligned} -\frac{\partial^2 \mathrm{dv}^\star[\mathbf{e}_r]}{\partial r^2} - \frac{1}{r}\frac{\partial \mathrm{dv}^\star[\mathbf{e}_r]}{\partial r} &= 0 && \text{in} \quad \Omega^\star \\ \mathrm{dv}^\star[\mathbf{e}_r] &= 0 && \text{on} \quad \Sigma \\ \frac{\partial \mathrm{dv}^\star[\mathbf{e}_r]}{\partial r} &= \frac{h}{r^\star} + \frac{\partial h}{\partial r} && \text{on} \quad \Gamma^\star. \end{aligned} \tag{4.65}$$

This yields the solution $\mathrm{dv}^\star[\mathbf{e}_r]$ of the boundary value problem (4.65) being written at the boundary $\Gamma^\star$ as

$$\mathrm{dv}^\star[\mathbf{e}_r](r^\star) = -\Big(h(r^\star) + r^\star \frac{\partial h}{\partial r}(r^\star)\Big) \log \frac{r_\Sigma}{r^\star},$$

which, in view of the Dirichlet boundary condition at the optimal boundary and the identity $h(r^\star) = -\Big(r^\star \log \dfrac{r^\star}{r_\Sigma}\Big)^{-1}$, can be rewritten as

$$\mathrm{dv}^\star[\mathbf{e}_r](r^\star) = -h(r^\star) \log \frac{r_\Sigma}{r^\star} - \frac{1}{h(r^\star)} \frac{\partial h}{\partial r}(r^\star).$$

Inserting this into (4.64), we get the derivative of Φ_D:

$$\frac{\partial \Phi_D}{\partial r}(r^\star) = \frac{h(r^\star) \log \dfrac{r_\Sigma}{r^\star} + \dfrac{1}{h(r^\star)} \dfrac{\partial h}{\partial r}(r^\star)}{h(r^\star)} = -\log \frac{r^\star}{r_\Sigma} + \frac{1}{\big(h(r^\star)\big)^2} \frac{\partial h}{\partial r}(r^\star). \tag{4.66}$$

It is clear that (4.66) coincides with (4.63). We can summarize the results from the convergence theory on circular domains as follows:

Convergence: The trial method converges locally with a linear rate if the self-mapping Φ_D is contractive. This holds if $\big\|\partial \Phi_D(r^\star)/\partial r\big\|_X < 1$, which is equivalent to the inequality

$$-1 < -\log \frac{r^\star}{r_\Sigma} + \frac{1}{\big(h(r^\star)\big)^2} \frac{\partial h}{\partial r}(r^\star) < 1.$$

In case of constant Neumann data h and as long as $r^\star > r_\Sigma$, this inequality simplifies to the condition

$$\log \frac{r^\star}{r_\Sigma} < 1 \quad \Leftrightarrow \quad r_\Sigma < r^\star < \mathrm{e}\, r_\Sigma.$$

Damped fixed-point iteration: If we modify the mapping Φ_D from (4.62) in accordance with

$$\Phi_D(r_k) = r_k - \alpha \left(\frac{1}{h(r_k)} + r_k \log \frac{r_k}{r_\Sigma} \right),$$

then we can determine a damping parameter α for which the norm of the derivative of Φ_D is smaller than 1, i.e.,

$$\left\| \frac{\partial \Phi_D}{\partial r}(r^\star) \right\|_X = \left| 1 - \alpha \left(1 + \log \frac{r^\star}{r_\Sigma} - \frac{1}{\big(h(r^\star)\big)^2} \frac{\partial h}{\partial r}(r^\star) \right) \right| \overset{!}{<} 1.$$

This choice would ensure locally linear convergence. For constant Neumann boundary data, a suitable damping parameter α which enforces convergence should satisfy the inequality

$$0 < \alpha < 2 \left(1 + \log \frac{r^\star}{r_\Sigma} \right)^{-1}.$$

Superlinear convergence rate: We achieve quadratic convergence by an r-dependent choice of the damping parameter, i.e. $\alpha = \alpha(r)$, such that the derivative of Φ_D at the optimal boundary becomes zero, i.e.

$$\left\| \frac{\partial \Phi_D}{\partial r}(r^\star) \right\|_X = \left| 1 - \alpha(r^\star) \left(1 + \log \frac{r^\star}{r_\Sigma} - \frac{1}{\big(h(r^\star)\big)^2} \frac{\partial h}{\partial r}(r^\star) \right) \right| = 0.$$

As long as the optimal $\Gamma^\star$ is not a-priori known, we employ the function $\alpha(r)$ being given as

$$a(r) = \left(1 + \log \frac{r}{r_\Sigma} - \frac{1}{\big(h(r)\big)^2} \frac{\partial h}{\partial r}(r) \right)^{-1}$$

in each step of the iterative method. This choice coincides with that of the improved trial method introduced in Section 4.3.2.

Example 4.17. In the numerical example, we consider the concentric circular boundaries Σ and Γ_0 with radius $r_\Sigma = 0.04$ and $r_0 = 0.05$, respectively. We find that for the constant Neumann data $h(r) = -3$ the optimal boundary $\Gamma^\star$ is of radius $r^\star = 0.20$. The topological set-up is found in the left plot of Figure 4.2.

If we apply the update rule without any damping parameter α, then the method is not converging. This result is absolutely justified since

$$\left\| \frac{\partial \Phi_D}{\partial r}(r^\star) \right\|_X = \left| \log \frac{r^\star}{r_\Sigma} \right| = 1.63 > 1.$$

When we perform the damped trial method for the update rule with a constant damping parameter α, we find that the method is converging linearly when the parameter α is chosen between these values

$$0 < \alpha < 2\left(1 + \log \frac{r^\star}{r_\Sigma}\right)^{-1} = 0.76.$$

Finally, in case of using the damping parameter $\alpha(r_k) = \left(1 + \log \frac{r_k}{r_\Sigma}\right)^{-1}$, we obtain quadratic convergence since the direction of the update is always in the radial direction. These observations are validated by the right plot of Figure 4.2, where the convergence rates of the trial method are visualized in case of the update rule with the constant damping parameter $\alpha = 0.6$ and in case of the update rule with the function $\alpha(r)$. We observe quadratic convergence in the first case and the method requires only 5 boundary updates to detect the optimal $\Gamma^\star$. In the second case, the method needs almost 6 times more iterations to reach the desired accuracy. △

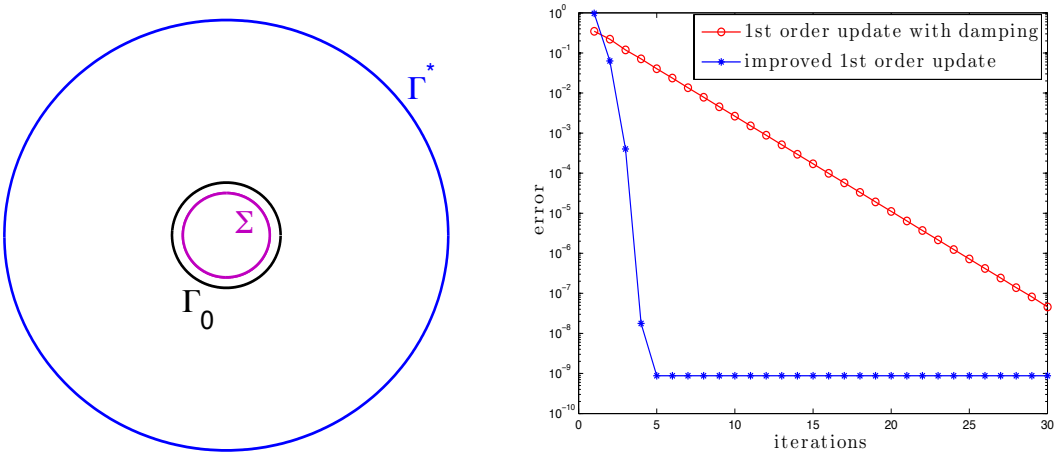

Figure 4.2: The solution of the free boundary problem and the convergence history of the trial methods in case of a circular domain.

4.5 Numerical examples

In the last part of this chapter we wish to illustrate and validate the theoretical findings for the respective trial methods by numerical examples. Our prior interest is concentrated on comparing the different trial methods with respect to their convergence rate. One of the conclusions which has been drawn in Chapter 3 is

that the "discretize-then-optimize" approach performs better than the "optimize-then-discretize" approach. Therefore, the updates are always computed by the discrete least-squares method as it was exhibited in Section 3.3.1.

Example 4.18. The first example concerns Poisson's equation with inhomogeinity $f(x, y) = 5$ and non constant boundary data

$$g(x, y) = x^2 + y^2 + 1 \quad \text{and} \quad h(x, y) = -\lambda(x^2 + y^2 + 1),$$

where λ is a positive constant. The fixed boundary Σ is chosen to be peanut-shaped with parametrization

$$\boldsymbol{\gamma}_\Sigma : [0, 2\pi] \to \Sigma, \quad s \mapsto \boldsymbol{\gamma}_\Sigma(s) = \begin{bmatrix} 0.03\sin(s)\big(1.25 + \cos(2s)\big) \\ 0.045\cos(s) \end{bmatrix}.$$

The solutions of the free boundary problem for different values of the parameter λ are depicted in Figure 4.3. The numerical setting consists in 60 degrees of freedom to represent the unknown boundary Γ_k, 500 boundary elements per boundary, and the stopping criterion $\|\delta \mathsf{r}\| < 10^{-8}$. The random boundary displayed in Figure 4.3 is the initial approximation Γ_0.

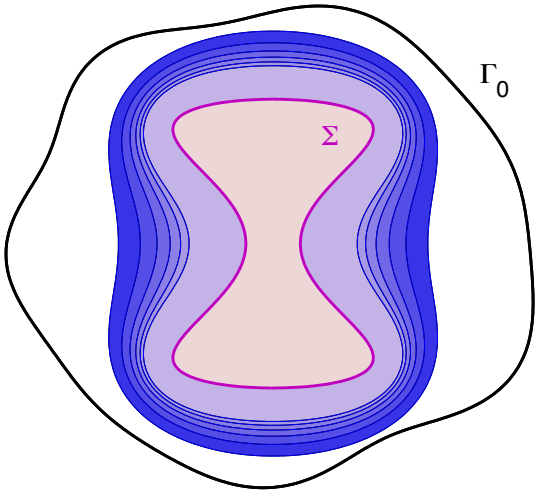

Figure 4.3: Solutions of the free boundary problem in case of a peanut-shaped interior boundary.

It is seen in Table 4.1 that the trial method based on the first order update equation does not converge for all the parameters λ under consideration (row entitled "1st order update"), whereas, the trial method based on the second order update equation always converges (row entitled "2nd order update"). That updating the free boundary by the second order update equation is more robust

has already been our observation from the numerical examples in Chapter 3. Introducing a damping parameter ($\alpha = 0.7$) in the first order update rule enforces the convergence of the respective trial method (row entitled "1st order update with damping"). Moreover, as long as we add the update $\delta\mathsf{r}$ with the suggested parameter $\alpha(r)$ from (4.54), we see that the trial method is converging for both the first order and the second order update equation (rows entitled "improved 1st order update" and "improved 2nd order update", respectively). Indeed, according to Figure 4.4, we obtain a nicely improved (linear) convergence rate.

parameter λ	40	50	60	70	80	90
1st order update	31	29	29	–	–	–
1st order update with damping ($\alpha = 0.7$)	14	17	20	22	23	23
improved 1st order update	11	11	11	14	16	17
Newton & improved 1st order update	6	6	6	6	7	7
2nd order update	31	29	28	27	26	25
improved 2nd order update	12	11	13	24	26	30
Newton & improved 2nd order update	10	10	10	9	9	9
inexact Newton update	5	6	6	6	6	7

Table 4.1: Number of boundary updates of the trial methods in case of a peanut-shaped interior boundary.

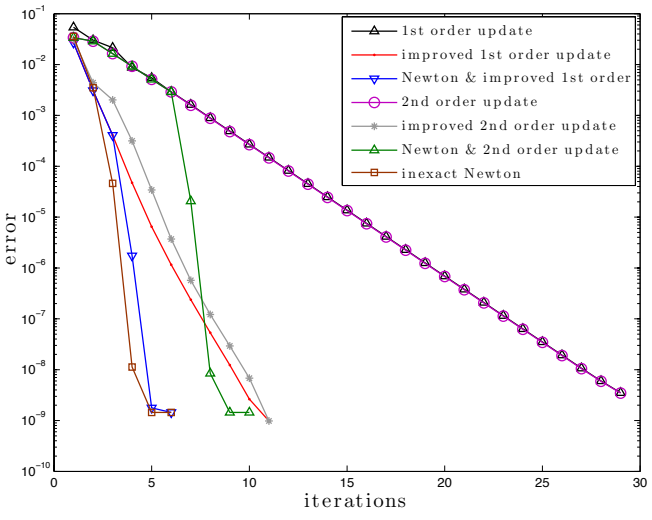

Figure 4.4: Convergence history of the trial methods in case of a peanut-shaped interior boundary and $\lambda = 50$.

The Newton method does not converge for our initial guess. We apply though one of the improved update rules first until the update function $\delta\mathsf{r}$ is small enough, that is $\|\delta\mathsf{r}\| < 10^{-2}$. Then, we start the Newton method. The number of iterations is shown in Table 4.1 in the rows entitled "Newton & improved 1st order update" and "Newton & improved 2nd order update". The associated green, blue and brown graphs in Figure 4.4 validate quadratic convergence.

At last we refer to the inexact Newton method, which, in contrast to the exact Newton method, is converging for the chosen initial guess (row entitled "inexact Newton update") and offers also quadratic convergence as the brown graph validates.

At this point we wish to emphasize that the trial method based on the improved update differs considerably from the trial method based on a Newton type update by the number of times the Neumann-to-Dirichlet map is solved. More precisely, in case of the improved update, the Neumann-to-Dirichlet map is solved twice for every boundary update, once for finding the state v_k and once for finding the local shape derivative dv_k. To compute the Newton update, apart from the solution of the state problem, the solution of the Neumann-to-Dirichlet map for the local shape derivative in the fixed-point iteration (4.58) is repeated until a suitable update function is found. To our experience, we need about 10–20 iterations to obtain the Newton update sufficiently accurate. △

Example 4.19. For the second numerical example we choose a random interior boundary Σ, while the initial guess Γ_0 of the free boundary is assumed to be a slightly perturbed ellipse being parametrized by

$$\boldsymbol{\gamma}_0 : [0, 2\pi] \to \Gamma_0, \quad s \mapsto \boldsymbol{\gamma}_0(s) = \sqrt{0.045\cos^2(2s) + 0.035\sin^2(2s)} \begin{bmatrix} \cos(s) \\ \sin(s) \end{bmatrix}.$$

We consider the Laplace equation and the boundary data given by

$$g(x, y) = x^2 + y^2 + 1 \quad \text{and} \quad h(x, y) = -\lambda(x^2 + y^2 + 1),$$

where λ is a positive constant. This time we use 70 degrees of freedom for the representation of the free boundary and 500 boundary elements per boundary. The stopping criterion for the trial method is again $\|\delta\mathsf{r}\| < 10^{-8}$. In Figure 4.5 we present a visualization of the domain and the solutions $\Gamma^\star$ of the free boundary problem for the different parameters λ.

Table 4.2 contains the number of boundary updates being employed by the different trial method for the solution of the free boundary problem. On the one hand, we notice that neither the first nor the second order update rule converge without any damping parameter for all the values of the parameter λ under consideration.

On the other hand, the improved first and second order updates converge always and require significantly less boundary updates. However, the convergence is linear in both cases as Figure (4.6) shows.

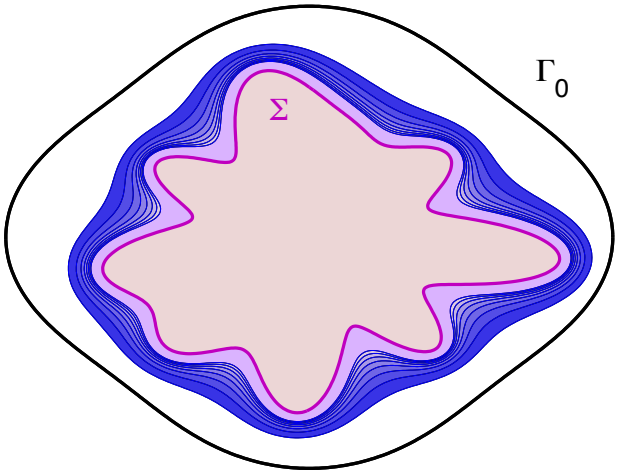

Figure 4.5: Solutions of the free boundary problem in case of a random interior boundary.

parameter λ	30	40	50	60	70	80	90	100
1st order update	30	–	–	–	–	–	–	–
improved 1st order update	10	10	10	11	12	12	11	11
Newton & improved 1st order update	6	6	7	7	7	8	8	8
2nd order update	30	28	25	23	–	–	–	–
improved 2nd order update	10	10	10	11	12	12	12	13
Newton & improved 2nd order update	6	6	7	8	8	8	9	9
inexact Newton update	5	6	6	6	7	7	7	7

Table 4.2: Number of boundary updates of the trial methods in case of random interior boundary.

For all the values of λ under consideration we also discover that the exact Newton method is not converging. On the contrary, if we combine exact Newton updates and improved updates, after some burn-in when the solution is too far away from the optimal boundary $\Gamma^\star$, we still obtain a quadratically convergent trial method. During the tests we have observed for $\lambda = 15$ that the exact Newton method also converges since the initial approximation Γ_0 is close enough to the optimal $\Gamma^\star$. Nevertheless, as we see from Table 4.2, the trial method with inexact Newton update convergences faster than any other trial method.

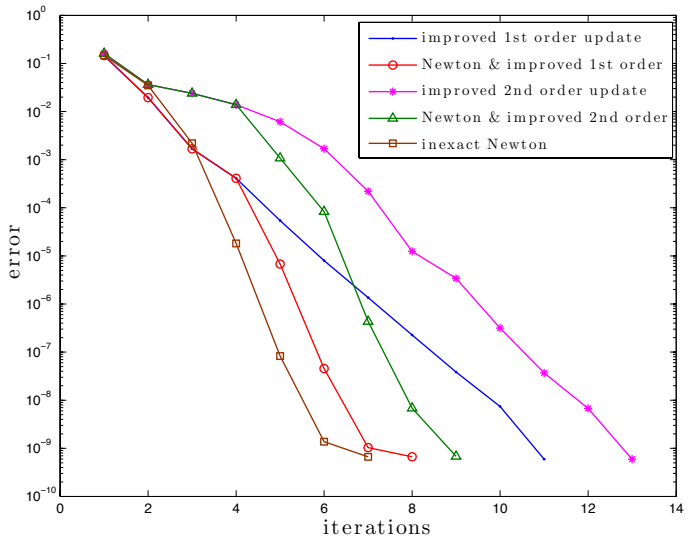

Figure 4.6: Convergence history of the trial methods in case of a random interior boundary and $\lambda = 100$.

But what about the execution time of the trial methods? We see from Table 4.2 that the trial method with improved first order update needs in average slightly less iterations than the trial method with improved second order update. In combination with the simpler computation of the update one can deduce that the trial method with improved first order update is the faster one. In Table 4.3, we thus compare the computing time of the trial method based on the improved first order update and based on the inexact Newton update for different number of degrees of freedom for the representation of the free boundary Γ (dof Γ).

dof Γ	$\|v^\star\|$	improved 1st order	inexact Newton
20	0.0303	5.501587 sec	16.957234 sec
60	0.0020	4.931886 sec	8.683680 sec
100	1.8963e-04	10.414140 sec	7.747184 sec
160	7.2416e-06	24.214333 sec	9.524349 sec

Table 4.3: Comparison of the computing times of the trial method for different numbers of degrees of freedom for the representation of the free boundary.

Note that as we have also explained in Chapter 2, the number of degrees of freedom on Γ can influence the accuracy of the solution of the free boundary problem. What we observe in Table 4.3 is that, for a small number of degrees of freedom for the representation of the free bondary, the trial method with improved update rule is quicker than the inexact Newton method. Whereas, for a large

number of degrees of freedom, which also ensures a smaller value of the Dirichlet data of the state on $\Gamma^\star$, the trial method with improved first order update rule becomes more costly with respect to the time compared to the inexact Newton method. △

Example 4.20. The trial methods we have constructed are also applicable for free boundary problems with several inner boundaries. This is demonstrated by an example where the boundary Σ is composed of the union of four circles as can be seen in Figure 4.7.

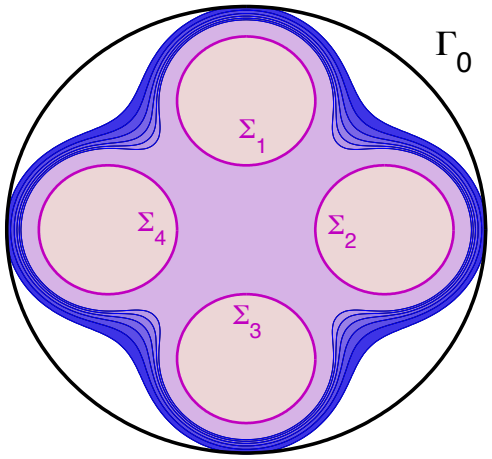

Figure 4.7: Solutions of the original Bernoulli free boundary problem in case of several interior boundaries.

We consider the original Bernoulli free boundary problem which corresponds to the choice

$$f(x,y) = 0, \quad g(x,y) = 1, \quad h(x,y) = -\lambda.$$

The extension of the boundary element method introduced in Chapter 2 to the new topological configuration is straightforward. On each boundary, we apply 400 boundary elements which leads to 2000 boundary elements in all. The free boundary is discretized by 80 degrees of freedom. For the initial approximation of the free boundary, we have chosen a circle. The trial method is again stopped if the update function satisfies $\|\delta \mathsf{r}\| < 10^{-8}$.

In Table 4.4, the number of iterations of the different trial methods are listed. We observe that the trial method is converging for all the suggested update rules and values of the parameter λ. In particular, the standard trial method converges for all chosen parameters λ. Compared to this, the improved first order update converges slightly faster. The same is observed for the related trial methods based

on the second order update equation. The fastest method is again the inexact Newton method which converges immediately for the present initial guess. △

parameter λ	10	12	14	16	18	20
1st order update	18	22	27	32	39	48
improved 1st order update	14	18	21	28	35	38
2nd order update	18	22	26	32	38	47
improved 2nd order update	12	16	22	28	26	44
inexact Newton update	7	8	8	9	10	11

Table 4.4: Number of boundary updates of the trial methods in case of several interior boundaries.

Part II

The trial method for prescribed Dirichlet data

Chapter 5

Solution of the free boundary problem

The last part of this thesis is dedicated to the trial method for the solution of the free boundary problem when the state problem has a Dirichlet boundary condition at the free boundary and the free boundary is updated according to the Neumann boundary condition. Some theoretical results concerning the convergence of the respective trial method can be found in [3]. There is nevertheless, to the best of our knowledge, no article with numerical results on this trial method apart from the case of axially symmetric domains. For instance, in [69], there has been shown that updating the free boundary according to the Neumann boundary condition makes the trial method easier under certain circumstances.

In the previous chapters, we have delivered a detailed analysis of the trial method for the usual technique of updating the free boundary according to the Dirichlet data. The extension of this analysis to the trial method for violated Neumann data is straightforward. Starting from recalling the iterative scheme of the trial method, in complete analogy to the previous chapters, we develop trial methods for the solution of the free boundary problem. Giving a more detailed review of the chapter, this consists of the derivation of an update rule for the unknown boundary and some first numerical tests, from which we observe severe difficulties in the convergence of the respective trial method. This behavior is completely explained by an investigation of the underlying fixed-point iteration method. For this aim a proper theoretical foundation, which includes results from Section 4.1 and the shape derivative of the state, is set. At the end of the chapter, we derive a stabilized version of the trial method and show its efficiency by numerical results.

5.1 Torso of the trial method

The free boundary problem consists in finding the domain Ω and an associated function w such that the overdetermined boundary value problem (1.1) is satisfied. Hence, given a trial free boundary Γ and the Dirichlet data at the free boundary, the state w is uniquely defined by the boundary value problem

$$\begin{aligned} -\Delta \mathrm{w} &= f \quad \text{in} \quad \Omega \\ \mathrm{w} &= g \quad \text{on} \quad \Sigma \\ \mathrm{w} &= 0 \quad \text{on} \quad \Gamma. \end{aligned} \tag{5.1}$$

The trial method for the solution of the free boundary problem is described by the iterative procedure in Algorithm 5.1.

Algorithm 5.1: The trial method with update according to the Neumann data.

1. Choose an initial guess Γ_0 of the free boundary.
2. a) Compute the Neumann data of w_k on Γ_k by applying the boundary element method to the Dirichlet boundary value problem (5.1).
   b) Update the free boundary according to the update rule

$$\boldsymbol{\gamma}_{k+1} = \boldsymbol{\gamma}_k + \beta \delta \mathrm{r}_k \mathbf{e}_r, \tag{5.2}$$

   where the update $\delta \mathrm{r}_k$ is determined by Taylor's expansion of the Neumann data, such that the Neumann boundary condition is approximately satisfied at the new boundary Γ_{k+1}. The parameter β stands for a correction factor.
3. Iterate step 2 until the process becomes stationary up to a specified precision.

Before computing the update rule for the free boundary in detail, we remind in the following the Dirichlet-to-Neumann map and validate the exponential convergence of the collocation-based boundary element method with a numerical result.

As it was described in Chapter 2, we can apply the boundary element method for the solution of the boundary value problem (5.1) by considering the ansatz

$$\mathrm{w} = w + N_f \tag{5.3}$$

for a suitable Newton potential N_f, which satisfies $\Delta N_f = -f$. The harmonic function w has thus to satisfy the boundary value problem

$$\begin{aligned} \Delta w &= 0 && \text{in} \quad \Omega \\ w &= g - N_f && \text{on} \quad \Sigma \\ w &= -N_f && \text{on} \quad \Gamma\,. \end{aligned} \tag{5.4}$$

The associated Dirichlet-to-Neumann map (2.14) is written as

$$\begin{bmatrix} \mathcal{V}_{\Gamma\Gamma} & \mathcal{V}_{\Sigma\Gamma} \\ \mathcal{V}_{\Gamma\Sigma} & \mathcal{V}_{\Sigma\Sigma} \end{bmatrix} \begin{bmatrix} \widetilde{\dfrac{\partial w}{\partial \mathbf{n}}}\Big|_{\Gamma} \\ \widetilde{\dfrac{\partial w}{\partial \mathbf{n}}}\Big|_{\Sigma} \end{bmatrix} = \begin{bmatrix} \dfrac{1}{2} + \mathcal{K}_{\Gamma\Gamma} & \mathcal{K}_{\Sigma\Gamma} \\ \mathcal{K}_{\Gamma\Sigma} & \dfrac{1}{2} + \mathcal{K}_{\Sigma\Sigma} \end{bmatrix} \begin{bmatrix} -N_f|_{\Gamma} \\ g - N_f|_{\Sigma} \end{bmatrix}, \tag{5.5}$$

where $\mathcal{V}_{AB}$ is the single-layer operator (2.11) and $\mathcal{K}_{AB}$ is the double-layer operator (2.12). The numerical approximation of the boundary integral operators leads to the linear system (2.40). Theorem 2.19 about the convergence of the proposed boundary element method remains in force also for the Dirichlet boundary value problem.

Example 5.1. We consider the same domain as in Example 2.20 and the harmonic function

$$w(x,y) = \log\Big(\sqrt{(x-x_0)^2 + (y-y_0)^2}\Big),$$

with $(x_0, y_0) \notin \Omega$ and prescribe the Dirichlet data $w|_{\partial\Omega}$. Then, we compute the Neumann data of w at the boundary Γ numerically by the boundary element method and compare them with the analytically computed Neumann data $\partial w/\partial \mathbf{n}|_{\Gamma}$. The convergence plot in Figure 5.1 validates the exponential convergence order of the collocation method. Additionally, we present in the table on the right side of Figure 5.1 the exact values of the relative L^2-error with respect to the number of boundary elements (# of BE) per boundary.

The analysis of the boundary element method concludes the step 2a of the Algorithm 5.1. We now proceed to step 2b in which the update function $\delta \mathrm{r}_k$ is to be determined. △

5.2 Determining the update rule

As we have already mentioned, our first objective is to solve the free boundary problem by applying the standard update rule, irrespective of the convergence of the trial method. For this, we aim at the determination of the update function $\delta \mathrm{r}_k \in C^2_{\mathrm{per}}\big([0, 2\pi]\big)$ which, due to the starshapness of the boundaries, updates the free boundary according to the rule $r_{k+1} = r_k + \beta \delta \mathrm{r}_k$.

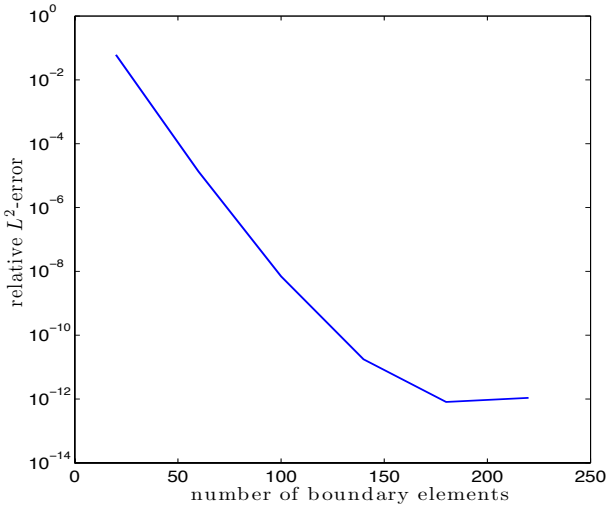

# of BE	error
20	0.06096
60	$1.344{\cdot}10^{-5}$
100	$7.010{\cdot}10^{-9}$
140	$4.446\ 1.762{\cdot}10^{-11}$
180	$9.948\ 8.099{\cdot}10^{-13}$
220	$7.129\ 1.090{\cdot}10^{-12}$

Figure 5.1: Relative L^2-error versus the number of boundary elements.

5.2.1 Update equation

The update function $\delta \mathrm{r}_k$ is found by the requirement that the Neumann boundary condition should be fulfilled at the new boundary Γ_{k+1}, i.e.,

$$\frac{\partial \mathrm{w}_k}{\partial \mathbf{n}} \circ \boldsymbol{\gamma}_{k+1} \stackrel{!}{=} h \circ \boldsymbol{\gamma}_{k+1}. \tag{5.6}$$

The first order Taylor expansion of the Neumann data of w_k around the actual boundary Γ_k

$$\frac{\partial \mathrm{w}_k}{\partial \mathbf{n}} \circ \boldsymbol{\gamma}_{k+1} \approx \frac{\partial \mathrm{w}_k}{\partial \mathbf{n}} \circ \boldsymbol{\gamma}_k + \frac{\partial}{\partial(\delta \mathrm{r}_k \mathbf{e}_r)} \Big(\frac{\partial \mathrm{w}_k}{\partial \mathbf{n}} \circ \boldsymbol{\gamma}_k \Big) \tag{5.7}$$

in combination with equation (5.6) leads to the update equation

$$h \circ \boldsymbol{\gamma}_{k+1} = \frac{\partial \mathrm{w}_k}{\partial \mathbf{n}} \circ \boldsymbol{\gamma}_k + \frac{\partial}{\partial(\delta \mathrm{r}_k \mathbf{e}_r)} \Big(\frac{\partial \mathrm{w}_k}{\partial \mathbf{n}} \circ \boldsymbol{\gamma}_k \Big) \tag{5.8}$$

for the unknown update function $\delta \mathrm{r}_k$. For sake of the subsequent numerical simulation, we intend to express (5.7) by terms which are known or computable.

We start with the computation of the derivative of the Neumann data of the state w_k in the direction $\mathbf{V}$.

Lemma 5.2. *Let the function* w_k *satisfy the boundary value problem* (5.1) *in the domain* Ω_k*. The derivative of the Neumann data of* w_k *in the direction* $\mathbf{V} = \delta \mathrm{r}_k \mathbf{e}_r$

is given by

$$\frac{\partial}{\partial(\delta \mathrm{r}_k \mathbf{e}_r)}\Big(\frac{\partial \mathrm{w}_k}{\partial \mathbf{n}} \circ \boldsymbol{\gamma}_k\Big) = \bigg(\Big(\frac{\partial^2 \mathrm{w}_k}{\partial \mathbf{n}^2} \circ \boldsymbol{\gamma}_k\Big)\langle \mathbf{e}_r, \mathbf{n}\rangle + \Big(\frac{\partial^2 \mathrm{w}_k}{\partial \mathbf{n}\partial \mathbf{t}} \circ \boldsymbol{\gamma}_k\Big)\langle \mathbf{e}_r, \mathbf{t}\rangle\bigg)\delta \mathrm{r}_k. \quad (5.9)$$

Proof. The Neumann data of the function w_k are defined as the inner product of the gradient of the function w_k and the unit normal vector at the boundary Γ_k, that is

$$\frac{\partial \mathrm{w}_k}{\partial \mathbf{n}} \circ \boldsymbol{\gamma}_k = \langle \nabla \mathrm{w}_k \circ \boldsymbol{\gamma}_k, \mathbf{n}\rangle. \quad (5.10)$$

Thus, by applying the product rule, the directional derivative of the Neumann data of w_k is given by

$$\frac{\partial}{\partial(\delta \mathrm{r}_k \mathbf{e}_r)}\Big(\frac{\partial \mathrm{w}_k}{\partial \mathbf{n}} \circ \boldsymbol{\gamma}_k\Big) = \delta \mathrm{r}_k \langle (\nabla^2 \mathrm{w}_k \circ \boldsymbol{\gamma}_k)\cdot \mathbf{n}, \mathbf{e}_r\rangle + \Big\langle \nabla \mathrm{w}_k \circ \boldsymbol{\gamma}_k, \frac{\partial \mathbf{n}}{\partial(\delta \mathrm{r}_k \mathbf{e}_r)}\Big\rangle. \quad (5.11)$$

The first term on the right hand side of equation (5.11) is computed by decomposing the second order directional derivative of w_k into its normal and tangential components as follows

$$\begin{aligned}\langle (\nabla^2 \mathrm{w}_k \circ \boldsymbol{\gamma}_k)\cdot \mathbf{n}, \mathbf{e}_r\rangle &= \langle (\nabla^2 \mathrm{w}_k \circ \boldsymbol{\gamma}_k)\cdot \mathbf{n}, \mathbf{n}\rangle\langle \mathbf{e}_r, \mathbf{n}\rangle + \langle (\nabla^2 \mathrm{w}_k \circ \boldsymbol{\gamma}_k)\cdot \mathbf{n}, \mathbf{t}\rangle\langle \mathbf{e}_r, \mathbf{t}\rangle \\ &= \Big(\frac{\partial^2 \mathrm{w}_k}{\partial \mathbf{n}^2} \circ \boldsymbol{\gamma}_k\Big)\langle \mathbf{e}_r, \mathbf{n}\rangle + \Big(\frac{\partial^2 \mathrm{w}_k}{\partial \mathbf{n}\partial \mathbf{t}} \circ \boldsymbol{\gamma}_k\Big)\langle \mathbf{e}_r, \mathbf{t}\rangle. \end{aligned} \quad (5.12)$$

We exploit formula (4.16) to obtain the directional derivative of the normal as

$$\frac{\partial \mathbf{n}}{\partial(\delta \mathrm{r}_k \mathbf{e}_r)} = \delta \mathrm{r}_k \frac{\langle \mathbf{e}_r, \mathbf{t}\rangle}{\|\boldsymbol{\gamma}_k'\|}\mathbf{t} - \delta \mathrm{r}_k' \frac{\langle \mathbf{e}_r, \mathbf{n}\rangle}{\|\boldsymbol{\gamma}_k'\|}\mathbf{t}. \quad (5.13)$$

Inserting (5.12) and (5.13) into (5.11), we arrive at the directional derivative of the Neumann data of w_k at the boundary Γ_k:

$$\begin{aligned}\frac{\partial}{\partial(\delta \mathrm{r}_k \mathbf{e}_r)}\Big(\frac{\partial \mathrm{w}_k}{\partial \mathbf{n}} \circ \boldsymbol{\gamma}_k\Big) = \bigg[&\Big(\frac{\partial^2 \mathrm{w}_k}{\partial \mathbf{n}^2} \circ \boldsymbol{\gamma}_k\Big)\langle \mathbf{e}_r, \mathbf{n}\rangle + \Big(\frac{\partial^2 \mathrm{w}_k}{\partial \mathbf{n}\partial \mathbf{t}} \circ \boldsymbol{\gamma}_k\Big)\langle \mathbf{e}_r, \mathbf{t}\rangle \\ &+ \Big(\frac{\partial \mathrm{w}_k}{\partial \mathbf{t}} \circ \boldsymbol{\gamma}_k\Big)\frac{\langle \mathbf{e}_r, \mathbf{t}\rangle}{\|\boldsymbol{\gamma}_k'\|}\bigg]\delta \mathrm{r}_k - \Big(\frac{\partial \mathrm{w}_k}{\partial \mathbf{t}} \circ \boldsymbol{\gamma}_k\Big)\frac{\langle \mathbf{e}_r, \mathbf{n}\rangle}{\|\boldsymbol{\gamma}_k'\|}\delta \mathrm{r}_k'. \end{aligned} \quad (5.14)$$

Finally, due to the Dirichlet boundary condition $\mathrm{w}_k = 0$ at Γ_k, the tangential derivative of w_k is equal to zero at Γ_k and (5.9) follows. □

The directional derivative of the Neumann data of the function w_k, as it is described in (5.14), coincides with the derivative which has been proven in [64, Theorem 3.11] in the context of inverse scattering problems. However, by using results from shape sensitivity analysis, we are able to obtain a much simpler proof of this relation.

With the help of equation (5.9), we exhibit in Lemma 5.3 the first order update equation for the unknown function $\delta\mathrm{r}_k$.

Lemma 5.3. *Let the directional derivative of the Neumann data of* w_k *being given by* (5.9)*. Then, the update equation* (5.7) *reads as*

$$h \circ \boldsymbol{\gamma}_{k+1} = \frac{\partial \mathrm{w}_k}{\partial \mathbf{n}} \circ \boldsymbol{\gamma}_k - \left[\left(\left(\kappa \frac{\partial \mathrm{w}_k}{\partial \mathbf{n}} + f \right) \circ \boldsymbol{\gamma}_k \right) \langle \mathbf{e}_r, \mathbf{n} \rangle - \frac{\partial}{\partial \mathbf{t}} \left(\frac{\partial \mathrm{w}_k}{\partial \mathbf{n}} \circ \boldsymbol{\gamma}_k \right) \langle \mathbf{e}_r, \mathbf{t} \rangle \right] \delta \mathrm{r}_k, \tag{5.15}$$

where $\kappa = -\langle \boldsymbol{\gamma}_k'', \mathbf{n} \rangle / \|\boldsymbol{\gamma}_k'\|^2$ *denotes the curvature of the boundary* Γ_k*.*

Proof. Due to (5.9), equation (5.8) can be transformed to

$$h \circ \boldsymbol{\gamma}_{k+1} = \frac{\partial \mathrm{w}_k}{\partial \mathbf{n}} \circ \boldsymbol{\gamma}_k + \left[\left(\frac{\partial^2 \mathrm{w}_k}{\partial \mathbf{n}^2} \circ \boldsymbol{\gamma}_k \right) \langle \mathbf{e}_r, \mathbf{n} \rangle + \left(\frac{\partial^2 \mathrm{w}_k}{\partial \mathbf{n} \partial \mathbf{t}} \circ \boldsymbol{\gamma}_k \right) \langle \mathbf{e}_r, \mathbf{t} \rangle \right] \delta \mathrm{r}_k. \tag{5.16}$$

We compute the second order directional derivative $\partial^2 \mathrm{w}_k / (\partial \mathbf{n} \partial \mathbf{t})$ by differentiating $\partial \mathrm{w}_k / \partial \mathbf{n}$ with respect to s. Namely, we have

$$\frac{\partial}{\partial s} \left(\frac{\partial \mathrm{w}_k}{\partial \mathbf{n}} \circ \boldsymbol{\gamma}_k \right) = \|\boldsymbol{\gamma}_k'\| \frac{\partial^2 \mathrm{w}_k}{\partial \mathbf{n} \partial \mathbf{t}} \circ \boldsymbol{\gamma}_k + \langle \nabla \mathrm{w}_k \circ \boldsymbol{\gamma}_k, \frac{\partial \mathbf{n}}{\partial s} \rangle, \tag{5.17}$$

where $\partial \mathbf{n} / \partial s = \kappa \|\boldsymbol{\gamma}_k'\| \mathbf{t}$. Equation (5.17) implies that

$$\frac{\partial^2 \mathrm{w}_k}{\partial \mathbf{n} \partial \mathbf{t}} \circ \boldsymbol{\gamma}_k = \frac{\partial}{\partial \mathbf{t}} \left(\frac{\partial \mathrm{w}_k}{\partial \mathbf{n}} \circ \boldsymbol{\gamma}_k \right) - \kappa \left(\frac{\partial \mathrm{w}_k}{\partial \mathbf{t}} \circ \boldsymbol{\gamma}_k \right). \tag{5.18}$$

According to the smoothness assumptions, the terms $\partial^2 \mathrm{w}_k / \partial \mathbf{n}^2$ and $\partial^2 \mathrm{w}_k / \partial \mathbf{t}^2$ are coupled via the Poisson equation. As in Chapter 3, from the second order derivative of w_k with respect to s, cf. (3.22), we obtain the derivative $\partial^2 \mathrm{w}_k / \partial \mathbf{n}^2$ in accordance with

$$\frac{\partial^2 \mathrm{w}_k}{\partial \mathbf{n}^2} \circ \boldsymbol{\gamma}_k = -\frac{1}{\|\boldsymbol{\gamma}_k'\|^2} \frac{\partial^2 (\mathrm{w}_k \circ \boldsymbol{\gamma}_k)}{\partial s^2} + \left(\frac{\langle \boldsymbol{\gamma}_k'', \mathbf{t} \rangle}{\|\boldsymbol{\gamma}_k'\|^2} \frac{\partial \mathrm{w}_k}{\partial \mathbf{t}} - \kappa \frac{\partial \mathrm{w}_k}{\partial \mathbf{n}} - f \right) \circ \boldsymbol{\gamma}_k. \tag{5.19}$$

The desired equation (5.15) is now an immediate consequence after inserting the equations (5.18) and (5.19) into (5.16) and taking into account that the Dirichlet data are equal to zero at Γ_k. □

Equation (5.15) is now an implicit equation for the update function $\delta \mathrm{r}_k$ since the term $h \circ \boldsymbol{\gamma}_{k+1}$ also depends on it. Hence, we should also linearize the given Neumann data with respect to $\delta \mathrm{r}_k$. With this approach we introduce a new approximation error in our numerical solution but we still avoid to solve the equation implicitly. The Taylor expansion of h around $\boldsymbol{\gamma}_k$ is given by

$$\begin{aligned} h \circ \boldsymbol{\gamma}_{k+1} &= h \circ \boldsymbol{\gamma}_k + \Big(\frac{\partial h}{\partial \mathbf{e}_r} \circ \boldsymbol{\gamma}_k\Big)\delta \mathrm{r}_k \\ &= h \circ \boldsymbol{\gamma}_k + \bigg[\Big(\frac{\partial h}{\partial \mathbf{n}} \circ \boldsymbol{\gamma}_k\Big)\langle \mathbf{e}_r, \mathbf{n}\rangle + \Big(\frac{\partial h}{\partial \mathbf{t}} \circ \boldsymbol{\gamma}_k\Big)\langle \mathbf{e}_r, \mathbf{t}\rangle\bigg]\delta \mathrm{r}_k. \end{aligned} \tag{5.20}$$

Considering (5.20), the update equation (5.15) for the free boundary Γ_k is expressed as

$$\Big(\frac{\partial \mathrm{w}_k}{\partial \mathbf{n}} - h\Big) - \bigg[\Big(\kappa \frac{\partial \mathrm{w}_k}{\partial \mathbf{n}} + f + \frac{\partial h}{\partial \mathbf{n}}\Big)\langle \mathbf{e}_r, \mathbf{n}\rangle + \Big(\frac{\partial}{\partial \mathbf{t}}\Big(\frac{\partial \mathrm{w}_k}{\partial \mathbf{n}}\Big) - \frac{\partial h}{\partial \mathbf{t}}\Big)\langle \mathbf{e}_r, \mathbf{t}\rangle\bigg]\delta \mathrm{r}_k = 0. \tag{5.21}$$

Finally, we reach a computable expression of the update equation (5.21) if the ansatz (5.3) is inserted there. This yields the normal derivative of w_k at Γ_k in accordance with

$$\frac{\partial \mathrm{w}_k}{\partial \mathbf{n}} = \frac{\partial w_k}{\partial \mathbf{n}} + \frac{\partial N_f}{\partial \mathbf{n}}. \tag{5.22}$$

Moreover, the term (5.17) can be rewritten as

$$\begin{aligned} \frac{\partial}{\partial s}\Big(\frac{\partial \mathrm{w}_k}{\partial \mathbf{n}} \circ \boldsymbol{\gamma}_k\Big) &= \frac{\partial}{\partial s}\Big(\frac{\partial w_k}{\partial \mathbf{n}} \circ \boldsymbol{\gamma}_k + \frac{\partial N_f}{\partial \mathbf{n}} \circ \boldsymbol{\gamma}_k\Big) \\ &= \frac{\partial}{\partial s}\Big(\frac{\partial w_k}{\partial \mathbf{n}} \circ \boldsymbol{\gamma}_k\Big) + \|\boldsymbol{\gamma}_k'\|\Big(\frac{\partial^2 N_f}{\partial \mathbf{n}\partial \mathbf{t}} \circ \boldsymbol{\gamma}_k\Big) + \kappa\|\boldsymbol{\gamma}_k'\|\Big(\frac{\partial N_f}{\partial \mathbf{t}} \circ \boldsymbol{\gamma}_k\Big). \end{aligned}$$

From this the term $\partial^2 \mathrm{w}_k/(\partial \mathbf{n}\partial \mathbf{t})$ results in the form

$$\frac{\partial^2 \mathrm{w}_k}{\partial \mathbf{n}\partial \mathbf{t}} \circ \boldsymbol{\gamma}_k = \frac{1}{\|\boldsymbol{\gamma}_k'\|}\frac{\partial}{\partial s}\Big(\frac{\partial w_k}{\partial \mathbf{n}} \circ \boldsymbol{\gamma}_k\Big) + \kappa\Big(\frac{\partial N_f}{\partial \mathbf{t}} \circ \boldsymbol{\gamma}_k\Big) + \frac{\partial^2 N_f}{\partial \mathbf{n}\partial \mathbf{t}} \circ \boldsymbol{\gamma}_k. \tag{5.23}$$

The normal derivative $\partial w_k/\partial \mathbf{n}$ at Γ_k, which is contained in equation (5.21), is found by the Dirichlet-to-Neumann map (5.5). Additionally, since the approximate Neumann data $\partial w_k/\partial \mathbf{n}$ have a trigonometric representation, their derivative with respect to s can analytically be computed.

Remark 5.4. The derivation of a second order update equation, as done in Section 3.2.2, would require the analytical computation of the second order derivative of the Neumann data of w_k in the direction $\delta \mathrm{r}_k \mathbf{e}_r$. For the determination of this term more smoothness on the boundary is necessary, at least C^3-smoothness,

which forms a very artificial space in the present context. Additionally, we remind that the theoretical and numerical results from Chapters 2 and 3 reveal that, even if the second order update equation yields a more robust trial method compared to the (standard) first order update equation, it is still not better than the trial method with improved first order update when an appropriate function $\beta(r_k)$ is imposed as damping parameter. Therefore, we confine our investigation to the first order update equation to derive later the improved first order update rule.

5.2.2 Solution of the update equation

For the numerical solution of the linearized update equation (5.21), we apply the same numerical techniques as they were described in Section 3.3. Namely, we formulate the linear update equation as a minimization problem in the discrete or in the continuous least-squares sense. The linear residual function in case of the discrete least-squares method reads

$$\begin{aligned}\big(\mathrm{F}(\delta \mathrm{r}_k^\nu)\big)(s_i) =& \Big(\frac{\partial \mathrm{w}_k}{\partial \mathbf{n}}(s_i) - h(s_i)\Big) - \Bigg[\bigg(\kappa(s_i)\frac{\partial \mathrm{w}_k}{\partial \mathbf{n}}(s_i) + f(s_i) + \frac{\partial h}{\partial \mathbf{n}}(s_i)\bigg)\langle \mathbf{e}_r, \mathbf{n}\rangle \\ &- \bigg(\frac{1}{\|\boldsymbol{\gamma}_k'\|}\frac{\partial}{\partial s}\Big(\frac{\partial \mathrm{w}_k}{\partial \mathbf{n}}(s_i)\Big) - \frac{\partial h}{\partial \mathbf{t}}(s_i)\bigg)\langle \mathbf{e}_r, \mathbf{t}\rangle\Bigg]\delta \mathrm{r}_k^\nu(s_i),\end{aligned}$$

where $\delta \mathrm{r}_k^\nu(s_i)$ is the update function discretized similarly to (3.26). Likewise, we define the function $\big(F(\delta \mathrm{r}_k)\big)(s)$ for the variational formulation in the space V_ν (for more details consult the theory presented in Section 3.3.2).

5.2.3 Numerical examples

We close this section by executing some numerical tests of the trial method when the standard update rule (5.2) with constant damping parameter β is performed.

Example 5.5. In the first example, we have chosen an ellipse as the initial guess of the free boundary Γ_0 and an x-shaped interior boundary Σ. The respective parametrizations are

$$\boldsymbol{\gamma}_0 : [0, 2\pi] \to \Gamma_0, \quad s \mapsto \boldsymbol{\gamma}_0(s) = \sqrt{0.1\cos^2(2s) + 0.12\sin^2(2s)}\begin{bmatrix}\cos(s)\\ \sin(s)\end{bmatrix}$$

and

$$\boldsymbol{\gamma}_\Sigma : [0, 2\pi] \to \Sigma, \quad s \mapsto \boldsymbol{\gamma}_\Sigma(s) = \sqrt{0.01\cos^2(2s) + 0.05\sin^2(2s)}\begin{bmatrix}\cos(s)\\ \sin(s)\end{bmatrix}.$$

We consider the overdetermined boundary value problem for Poisson's equation with $f(x, y) = 80$ and boundary data

$$g(x, y) = x^2 + y^2 + 1, \quad h(x, y) = -\lambda.$$

An appropriate Newton potential is analytically given by $N_f(x, y) = -20(x^2+y^2)$. The free boundary is represented by 16 degrees of freedom and the boundary element method is performed with 600 boundary elements per boundary. Note that this numerical setting, particularly the number of the unknowns in the discretization of the free boundary Γ, are adjusted to the difficulties that were observed during the tests. The stopping criterion remains the same as in previous chapters, namely $\|\delta \mathrm{r}\| < 10^{-8}$. The solutions which are computed by the trial method for the chosen values of the parameter λ are displayed in Figure 5.2.

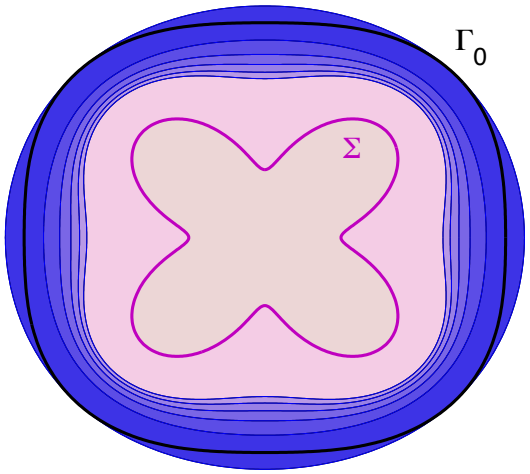

Figure 5.2: Solutions of the free boundary problem in case of an x-shaped interior boundary.

	parameter λ	11	12	13	14	15	16
pointwise updates	standard update	188	–	–	–	–	–
	update with damping ($\beta = 0.8$)	239	65	–	–	–	–
	update with damping ($\beta = 0.5$)	386	76	47	34	26	43
variational updates	standard update	188	–	–	–	–	–
	update with damping ($\beta = 0.8$)	239	78	–	–	–	–
	update with damping ($\beta = 0.5$)	386	76	47	34	214	–

Table 5.1: Number of boundary updates of the trial method in case of an x-shaped interior boundary.

It can be seen in Table 5.1 that, likewise to the trial method with first order update for the Dirichlet data (cf. Section 3.4), the trial method with first order

update for the Neumann data does not converge without damping (row entitled "standard update"). We stress that the damping parameters $\beta = 0.5$ and $\beta = 0.8$ were found by trial and error, i.e., without following any systematic rule (row entitled "update with damping"). Again, the approach "discretize-then-optimize" shows better performance than the approach "optimize-then-discretize". Furthermore, it is remarkable that in this example the trial method requires considerably more iterations to detect the solution of the free boundary problem than in the examples presented in Section 3.4. As regards the convergence order of the trial method, there is no doubt that this is only linear. Thus, we attach no importance to graphically display the convergence history of the trial method. △

Example 5.6. For the same domain and numerical setting as described in Example 5.5 we consider now the Laplace equation instead of the Poisson equation, i.e., $f = 0$, and thus $N_f = 0$. The resulting optimal boundary $\Gamma^\star$ for the values of the parameter λ under consideration are graphically illustrated in Figure 5.3.

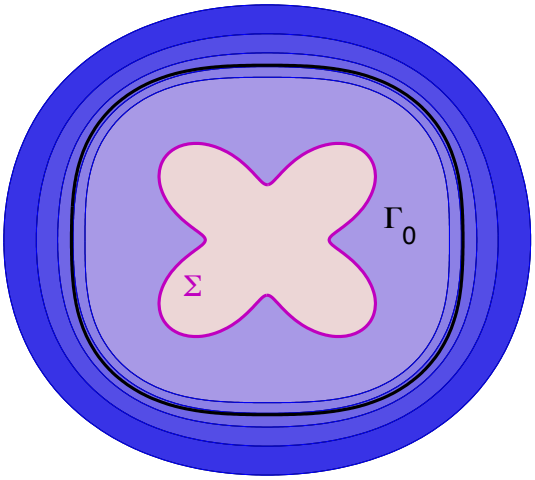

Figure 5.3: Solutions of the free boundary problem in case of an x-shaped interior boundary.

The associated numbers of updates needed by the trial method to converge are tabulated in Table 5.2. This table suggests convergence of the trial method only in case of a damping parameter β which is smaller than in Example 5.5. The damping parameter contributes to the convergence of the trial method by avoiding oscillations of the free boundary during the iterative procedure. The standard update without damping does not converge for any of the parameters λ under consideration. The approach "optimize-then-discretize" for minimizing the defect in equation (5.21), as we have noticed also in Section 3.4, causes more oscillations than the approach "discretize-then-optimize". Therefore, from now on we consider only the first approach. △

	parameter λ	3	4	5	6	7	8
pointwise updates	standard update	–	–	–	–	–	–
	update with damping ($\beta = 0.1$)	74	65	57	51	53	–
variational updates	standard update	–	–	–	–	–	–
	update with damping ($\beta = 0.1$)	–	–	–	51	–	–

Table 5.2: Number of boundary updates of the trial method in case of an x-shaped interior boundary.

Example 5.7. In the third example the interior boundary Σ is peanut-shaped with parametrization

$$\boldsymbol{\gamma}_\Sigma : [0, 2\pi] \to \Sigma, \quad s \mapsto \boldsymbol{\gamma}_\Sigma(s) = \begin{bmatrix} -0.025\cos(s) \\ 0.03\sin(s)\big(1.25 + \cos(2s)\big) \end{bmatrix}.$$

The numerical setting of this problem involves the Poisson equation with $f(x, y) = 10$, the boundary data $g(x, y) = 1$ and $h(x, y) = -\lambda(x^2 + y^2 + 1)$, the Newton potential $N_f(x, y) = -\frac{5}{2}(x^2 + y^2)$, 26 degrees of freedom for the representation of the free boundary and 400 boundary elements on each boundary. The trial method starts with the boundary Γ_0 being a circle of radius 0.08.

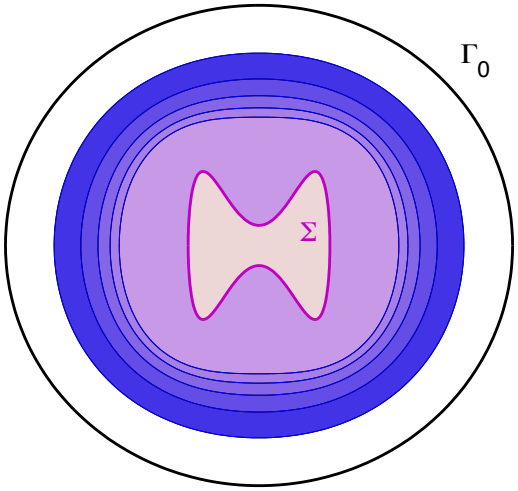

Figure 5.4: Solutions of the free boundary problem in case of a peanut-shaped interior boundary.

In Figure 5.4 are displayed the domain under consideration and the solutions of the free boundary problem for the chosen values of the parameter λ. The number of iterations of the trial method for each value of the parameter λ, as they are tabulated in Table 5.3, show again a poor convergence of the trial method unless a damping parameter is introduced. △

parameter λ	15	20	25	30	35
standard update	–	–	–	–	–
update with damping ($\beta = 0.1$)	74	69	64	60	58

Table 5.3: Number of boundary updates of the trial method in case of a peanut-shaped interior boundary.

In contrast to the trial method which is based on boundary updates according to the Dirichlet data, the trial method which is based on boundary updates according to the Neumann data shows a weak performance with respect to the convergence. This is caused by the fact that the Neumann data seems to be more sensitive with respect to oscillations which are generated by the update procedure for the free boundary. Algorithm's 5.1 peculiar behavior is explained in the subsequent section where the convergence analysis of the trial method is elucidated.

5.3 Convergence of the trial method

The update of the free boundary in the radial direction is equivalent to a perturbation of the domain Ω in the same direction, i.e., $\mathbf{V} = q\mathbf{e}_r$. In this regard, results from shape sensitivity analysis apply.

5.3.1 Shape derivative of the state

The function w satisfies the boundary value problem (5.1). In Lemma 5.8, we determine the boundary value problem that the associated local shape derivative dw satisfies.

Lemma 5.8. *The local shape derivative* dw *under the perturbation* $\mathbf{V}$ *is given as the solution of the boundary value problem*

$$\Delta \mathrm{dw}[\mathbf{V}] = 0 \qquad \text{in} \quad \Omega \tag{5.24a}$$

$$\mathrm{dw}[\mathbf{V}] = 0 \qquad \text{on} \quad \Sigma \tag{5.24b}$$

$$\mathrm{dw}[\mathbf{V}] = -\frac{\partial \mathrm{w}}{\partial \mathbf{n}} \langle \mathbf{V}, \mathbf{n} \rangle \qquad \text{on} \quad \Gamma\,. \tag{5.24c}$$

Proof. The results from the proof of Lemma 4.10 about the differential equation in Ω and the boundary condition at Σ apply also here. To determine the Dirichlet

data at Γ we compute the material derivative of the function w under the perturbation $\mathbf{V}$ with the help of the Definition 4.2. The Dirichlet data of function w_ε at the boundary Γ_ε are equal to zero and the same holds for the Dirichlet data of the function w at the boundary Γ. Hence, we obtain

$$\dot{\mathrm{w}}[\mathbf{V}](\mathbf{x}) = \lim_{\varepsilon \to 0} \frac{\mathrm{w}_\varepsilon(\mathbf{x}_\varepsilon) - \mathrm{w}(\mathbf{x})}{\varepsilon} = 0, \qquad \mathbf{x} \text{ on } \Gamma.$$

From Remark 4.4, the orthogonality argument and the boundary condition $\mathrm{w} = 0$ on Γ we finally get

$$\mathrm{dw}[\mathbf{V}] = -\langle \nabla \mathrm{w}, \mathbf{V} \rangle = -\langle \nabla \mathrm{w}, \mathbf{n} \rangle \langle \mathbf{V}, \mathbf{n} \rangle = -\frac{\partial \mathrm{w}}{\partial \mathbf{n}} \langle \mathbf{V}, \mathbf{n} \rangle.$$

□

The unknown Neumann data of the local shape derivative dw at the boundary Γ can be found by applying the boundary element method to the Dirichlet-to-Neumann map (5.5) associated with the boundary value problem (5.24).

5.3.2 Convergence rate of the trial method

The technique of determining the convergence order of the trial method follows the procedure described in Section 4.3 in a very similar way. To that end, the self-mapping $\Phi_N : C^2_{\mathrm{per}}\big([0, 2\pi]\big) \to C^2_{\mathrm{per}}\big([0, 2\pi]\big)$ is defined by

$$\Phi_N(r) := r + \delta \mathrm{r}(r),$$

where $\delta \mathrm{r}$ is the update function resulting from the first order Taylor expansion of the Neumann data with respect to $\delta \mathrm{r}$ at the boundary Γ. Namely, it holds that

$$\delta \mathrm{r}(r) = \frac{\dfrac{\partial \mathrm{w}}{\partial \mathbf{n}} \circ \boldsymbol{\gamma} - h \circ \boldsymbol{\gamma}}{\left(\left(\kappa \dfrac{\partial \mathrm{w}}{\partial \mathbf{n}} + f + \dfrac{\partial h}{\partial \mathbf{n}} \right) \circ \boldsymbol{\gamma} \right) \langle \mathbf{e}_r, \mathbf{n} \rangle - \left(\dfrac{1}{\|\boldsymbol{\gamma}'\|} \left(\dfrac{\partial \mathrm{w}}{\partial \mathbf{n}} \circ \boldsymbol{\gamma} \right)' - \dfrac{\partial h}{\partial \mathbf{t}} \circ \boldsymbol{\gamma} \right) \langle \mathbf{e}_r, \mathbf{t} \rangle}, \tag{5.25}$$

provided that the denominator of (5.25) is pointwisely nonzero on $[0, 2\pi]$. In view of relation (4.35), we examine the convergence of the trial method by estimating the directional derivative $\mathrm{d}\Phi_N[q]$ at $\Gamma^\star$. The following theorem provides the necessary calculations.

Theorem 5.9. *Consider the trial method based on the update function* (5.25). *Then, for a given perturbation* $\mathbf{V} = q\mathbf{e}_r$, *it holds*

$$\mathrm{d}\Phi_N[q](r^\star) = \frac{\dfrac{\partial \mathrm{dw}^\star[q\mathbf{e}_r]}{\partial \mathbf{n}} \circ \boldsymbol{\gamma}^\star}{\left(\left(\kappa h + f + \dfrac{\partial h}{\partial \mathbf{n}}\right) \circ \boldsymbol{\gamma}^\star\right)\langle \mathbf{e}_r, \mathbf{n}\rangle}, \tag{5.26}$$

where $\boldsymbol{\gamma}^\star = r^\star \mathbf{e}_r$ *and* $\partial \mathrm{dw}^\star[q\mathbf{e}_r]/\partial \mathbf{n}$ *denotes the Neumann data of the local shape derivative of* $\mathrm{w}^\star$ *into the direction* $q\mathbf{e}_r$, *which satisfies the boundary value problem*

$$\begin{aligned} \Delta \mathrm{dw}^\star[q\mathbf{e}_r] &= 0 && \text{in} \quad \Omega^\star \\ \mathrm{dw}^\star[q\mathbf{e}_r] &= 0 && \text{on} \quad \Sigma \\ \mathrm{dw}^\star[q\mathbf{e}_r] &= -h\langle q\mathbf{e}_r, \mathbf{n}\rangle && \text{on} \quad \Gamma^\star. \end{aligned} \tag{5.27}$$

Proof. The operator Φ_N at the optimal boundary $\Gamma^\star$ with parametrization $\boldsymbol{\gamma}^\star$ and at the boundary $\Gamma^\star_\varepsilon$ with parametrization $\boldsymbol{\gamma}^\star_\varepsilon = r^\star_\varepsilon \mathbf{e}_r = (r^\star + \varepsilon q)\mathbf{e}_r$ is given as

$$\Phi_N(r^\star) = r^\star + \delta \mathrm{r}(r^\star) \quad \text{and} \quad \Phi_N(r^\star + \varepsilon q) = r^\star + \varepsilon q + \delta \mathrm{r}(r^\star_\varepsilon),$$

respectively. We compute the derivative of Φ_N at $r^\star$ in the direction q as follows:

$$\begin{aligned} \mathrm{d}\Phi_N[q](r^\star) &= \lim_{\varepsilon \to 0} \frac{\Phi_N(r^\star + \varepsilon q) - \Phi_N(r^\star)}{\varepsilon} \\ &= \lim_{\varepsilon \to 0} \frac{r^\star + \varepsilon q + \delta \mathrm{r}(r^\star + \varepsilon q) - r^\star - \delta \mathrm{r}(r^\star)}{\varepsilon} \\ &= q + \lim_{\varepsilon \to 0} \frac{\delta \mathrm{r}(r^\star + \varepsilon q) - \delta \mathrm{r}(r^\star)}{\varepsilon}, \end{aligned} \tag{5.28}$$

where

$$\delta \mathrm{r}(r^\star_\varepsilon) = \frac{\dfrac{\partial \mathrm{w}^\star_\varepsilon}{\partial \mathbf{n}_\varepsilon} \circ \boldsymbol{\gamma}^\star_\varepsilon - h \circ \boldsymbol{\gamma}^\star_\varepsilon}{\left(\left(\kappa \dfrac{\partial \mathrm{w}^\star_\varepsilon}{\partial \mathbf{n}_\varepsilon} + f + \dfrac{\partial h}{\partial \mathbf{n}_\varepsilon}\right) \circ \boldsymbol{\gamma}^\star_\varepsilon\right)\langle \mathbf{e}_r, \mathbf{n}_\varepsilon\rangle - \left(\dfrac{\partial}{\partial \mathbf{t}_\varepsilon}\left(\dfrac{\partial \mathrm{w}^\star_\varepsilon}{\partial \mathbf{n}_\varepsilon} \circ \boldsymbol{\gamma}^\star_\varepsilon\right) - \dfrac{\partial h}{\partial \mathbf{t}_\varepsilon} \circ \boldsymbol{\gamma}^\star_\varepsilon\right)\langle \mathbf{e}_r, \mathbf{t}_\varepsilon\rangle}$$

and $\delta \mathrm{r}(r^\star) = 0$ by construction. The functions $\mathrm{w}^\star_\varepsilon$ and $\mathrm{w}^\star$ satisfy the boundary value problems

$$\begin{aligned} -\Delta \mathrm{w}^\star &= f && \text{in} \quad \Omega^\star, \\ \mathrm{w}^\star &= g && \text{on} \quad \Sigma, \\ \mathrm{w}^\star &= 0 && \text{on} \quad \Gamma^\star, \end{aligned} \qquad \begin{aligned} -\Delta \mathrm{w}^\star_\varepsilon &= f && \text{in} \quad \Omega^\star_\varepsilon \\ \mathrm{w}^\star_\varepsilon &= g && \text{on} \quad \Sigma \\ \mathrm{w}^\star_\varepsilon &= 0 && \text{on} \quad \Gamma^\star_\varepsilon. \end{aligned}$$

On the optimal boundary it holds $(\partial \mathrm{w}^\star/\partial \mathbf{n}) \circ \boldsymbol{\gamma}^\star = h \circ \boldsymbol{\gamma}^\star$. Applying this relation to (5.28), the first term of the enumerator of (5.28) becomes

$$\begin{aligned}\frac{\partial \mathrm{w}_\varepsilon^\star}{\partial \mathbf{n}_\varepsilon} \circ \boldsymbol{\gamma}_\varepsilon^\star - \frac{\partial \mathrm{w}^\star}{\partial \mathbf{n}} \circ \boldsymbol{\gamma}^\star &= \langle \nabla \mathrm{w}_\varepsilon^\star \circ \boldsymbol{\gamma}^\star, \mathbf{n} \rangle - \langle \nabla \mathrm{w}^\star \circ \boldsymbol{\gamma}^\star, \mathbf{n} \rangle + \langle \nabla \mathrm{w}_\varepsilon^\star \circ \boldsymbol{\gamma}_\varepsilon^\star, \mathbf{n}_\varepsilon \rangle \\ &\quad - \langle \nabla \mathrm{w}_\varepsilon^\star \circ \boldsymbol{\gamma}^\star, \mathbf{n}_\varepsilon \rangle + \langle \nabla \mathrm{w}_\varepsilon^\star \circ \boldsymbol{\gamma}^\star, \mathbf{n}_\varepsilon \rangle - \langle \nabla \mathrm{w}_\varepsilon^\star \circ \boldsymbol{\gamma}^\star, \mathbf{n} \rangle\end{aligned}$$

while the second term of the enumerator is equivalent to

$$\lim_{\varepsilon \to 0} \frac{h \circ \boldsymbol{\gamma}_\varepsilon^\star - h \circ \boldsymbol{\gamma}^\star}{\varepsilon} = \frac{\partial h}{\partial (q\mathbf{e}_r)} \circ \boldsymbol{\gamma}^\star. \tag{5.29}$$

Hence, in view of

$$\begin{aligned}&\lim_{\varepsilon \to 0} \frac{1}{\varepsilon} \Big(\frac{\partial \mathrm{w}_\varepsilon^\star}{\partial \mathbf{n}_\varepsilon} \circ \boldsymbol{\gamma}_\varepsilon^\star - \frac{\partial \mathrm{w}^\star}{\partial \mathbf{n}} \circ \boldsymbol{\gamma}^\star \Big) \\ &\qquad = \frac{\partial \mathrm{dw}^\star[q\mathbf{e}_r]}{\partial \mathbf{n}} \circ \boldsymbol{\gamma}^\star + \frac{\partial}{\partial (q\mathbf{e}_r)} \Big(\frac{\partial \mathrm{w}^\star}{\partial \mathbf{n}} \circ \boldsymbol{\gamma}^\star \Big) + \Big\langle \nabla \mathrm{w}^\star \circ \boldsymbol{\gamma}^\star, \frac{\partial \mathbf{n}}{\partial (q\mathbf{e}_r)} \Big\rangle.\end{aligned}$$

and (5.29), we obtain

$$\begin{aligned}&\lim_{\varepsilon \to 0} \frac{1}{\varepsilon} \Big(\frac{\partial \mathrm{w}_\varepsilon^\star}{\partial \mathbf{n}_\varepsilon} \circ \boldsymbol{\gamma}_\varepsilon^\star - h \circ \boldsymbol{\gamma}_\varepsilon^\star \Big) \\ &\qquad = \frac{\partial \mathrm{dw}^\star[q\mathbf{e}_r]}{\partial \mathbf{n}} \circ \boldsymbol{\gamma}^\star + \frac{\partial}{\partial (q\mathbf{e}_r)} \Big(\frac{\partial \mathrm{w}^\star}{\partial \mathbf{n}} \circ \boldsymbol{\gamma}^\star \Big) + \langle \nabla \mathrm{w}^\star \circ \boldsymbol{\gamma}^\star, \frac{\partial \mathbf{n}}{\partial (q\mathbf{e}_r)} \rangle - \frac{\partial h}{\partial (q\mathbf{e}_r)} \circ \boldsymbol{\gamma}^\star.\end{aligned} \tag{5.30}$$

In (5.30), the Neumann data of the local shape derivative $\mathrm{dw}^\star[q\mathbf{e}_r]$ at the boundary $\Gamma^\star$ are contained. In accordance with equation (5.9), the derivative of the Neumann data of $\mathrm{w}^\star$ in the direction $\mathbf{V} = q\mathbf{e}_r$ is given by

$$\begin{aligned}\frac{\partial}{\partial (q\mathbf{e}_r)} \Big(\frac{\partial \mathrm{w}^\star}{\partial \mathbf{n}} \circ \boldsymbol{\gamma}^\star \Big) = \Bigg[&\Big(\frac{\partial^2 \mathrm{w}^\star}{\partial \mathbf{n}^2} \circ \boldsymbol{\gamma}^\star \Big) \langle \mathbf{e}_r, \mathbf{n} \rangle + \Big(\frac{\partial^2 \mathrm{w}^\star}{\partial \mathbf{n} \partial \mathbf{t}} \circ \boldsymbol{\gamma}^\star \Big) \langle \mathbf{e}_r, \mathbf{t} \rangle \\ &+ \Big(\frac{\partial \mathrm{w}^\star}{\partial \mathbf{t}} \circ \boldsymbol{\gamma}^\star \Big) \frac{\langle \mathbf{e}_r, \mathbf{t} \rangle}{\|\boldsymbol{\gamma}^{\star\prime}\|} \Bigg] q - \Big(\frac{\partial \mathrm{w}^\star}{\partial \mathbf{t}} \circ \boldsymbol{\gamma}^\star \Big) \frac{\langle \mathbf{e}_r, \mathbf{n} \rangle}{\|\boldsymbol{\gamma}^{\star\prime}\|} q'.\end{aligned} \tag{5.31}$$

Due to the Dirichlet boundary condition $\mathrm{w}^\star = 0$ at $\Gamma^\star$, equation (5.31) simplifies according to

$$\frac{\partial}{\partial (q\mathbf{e}_r)} \Big(\frac{\partial \mathrm{w}^\star}{\partial \mathbf{n}} \circ \boldsymbol{\gamma}^\star \Big) = \Bigg[\Big(\frac{\partial^2 \mathrm{w}^\star}{\partial \mathbf{n}^2} \circ \boldsymbol{\gamma}^\star \Big) \langle \mathbf{e}_r, \mathbf{n} \rangle + \Big(\frac{\partial^2 \mathrm{w}^\star}{\partial \mathbf{n} \partial \mathbf{t}} \circ \boldsymbol{\gamma}^\star \Big) \langle \mathbf{e}_r, \mathbf{t} \rangle \Bigg] q.$$

The derivative of the normal vector at the boundary Γ in the direction $\mathbf{V} = q\mathbf{e}_r$ is expressed by

$$\frac{\partial \mathbf{n}}{\partial (q\mathbf{e}_r)} = q \frac{\langle \mathbf{e}_r, \mathbf{t} \rangle}{\|\boldsymbol{\gamma}'\|} \mathbf{t} - q' \frac{\langle \mathbf{e}_r, \mathbf{n} \rangle}{\|\boldsymbol{\gamma}'\|} \mathbf{t} \tag{5.32}$$

(details about (5.32) are reported in Section 4.1.3). Since the derivative of the normal vector (5.32) is pointing only to the tangential direction and since it holds $\mathrm{w}^\star = 0$ at the boundary $\Gamma^\star$, the third term on the right hand side of (5.30) vanishes. For the subsequent step, we bear in mind the preceding results about the terms included in (5.30) and recall the relations (5.18) and (5.19). This in combination with the decomposition of the derivative $\partial h/\partial(q\mathbf{e}_r)$ into its normal and tangential components changes (5.30) to

$$\lim_{\varepsilon\to 0}\frac{\dfrac{\partial \mathrm{w}^\star_\varepsilon}{\partial \mathbf{n}_\varepsilon}\circ\boldsymbol{\gamma}^\star_\varepsilon - h\circ\boldsymbol{\gamma}^\star_\varepsilon}{\varepsilon} = \frac{\partial \mathrm{dw}^\star[q\mathbf{e}_r]}{\partial\mathbf{n}}\circ\boldsymbol{\gamma}^\star - \left(\left(\kappa\frac{\partial \mathrm{w}^\star}{\partial\mathbf{n}} + f + \frac{\partial h}{\partial\mathbf{n}}\right)\circ\boldsymbol{\gamma}^\star\right)\langle q\mathbf{e}_r,\mathbf{n}\rangle + \left(\frac{\partial}{\partial\mathbf{t}}\left(\frac{\partial \mathrm{w}^\star}{\partial\mathbf{n}}\circ\boldsymbol{\gamma}^\star\right) - \frac{\partial h}{\partial\mathbf{t}}\circ\boldsymbol{\gamma}^\star\right)\langle q\mathbf{e}_r,\mathbf{t}\rangle. \tag{5.33}$$

Inserting (5.33) into (5.28) and taking into account that $(\partial \mathrm{w}^\star/\partial\mathbf{n})\circ\boldsymbol{\gamma}^\star = h\circ\boldsymbol{\gamma}^\star$, it follows that

$$\begin{aligned}\mathrm{d}\Phi_N[q](r^\star) &= \frac{\dfrac{\partial \mathrm{dw}^\star[q\mathbf{e}_r]}{\partial\mathbf{n}}\circ\boldsymbol{\gamma}^\star}{\left(\left(\kappa\dfrac{\partial \mathrm{w}^\star}{\partial\mathbf{n}} + f + \dfrac{\partial h}{\partial\mathbf{n}}\right)\circ\boldsymbol{\gamma}^\star\right)\langle\mathbf{e}_r,\mathbf{n}\rangle - \left(\dfrac{\partial}{\partial\mathbf{t}}\left(\dfrac{\partial \mathrm{w}^\star}{\partial\mathbf{n}}\circ\boldsymbol{\gamma}^\star\right) - \dfrac{\partial h}{\partial\mathbf{t}}\circ\boldsymbol{\gamma}^\star\right)\langle\mathbf{e}_r,\mathbf{t}\rangle} \\ &= \frac{\dfrac{\partial \mathrm{dw}^\star[q\mathbf{e}_r]}{\partial\mathbf{n}}\circ\boldsymbol{\gamma}^\star}{\left(\left(\kappa h + f + \dfrac{\partial h}{\partial\mathbf{n}}\right)\circ\boldsymbol{\gamma}^\star\right)\langle\mathbf{e}_r,\mathbf{n}\rangle},\end{aligned}$$

which completes finally the proof. □

The convergence of the trial method is ensured when the mapping Φ_N is contractive. This holds if the norm of (5.26) at $\Gamma^\star$ is smaller than 1, that is,

$$\left\|\mathrm{d}\Phi_N[q](r^\star)\right\|_X = \left\|\frac{\dfrac{\partial \mathrm{dw}^\star[\mathbf{V}]}{\partial\mathbf{n}}\circ\boldsymbol{\gamma}^\star}{\left(\left(\kappa h + f + \dfrac{\partial h}{\partial\mathbf{n}}\right)\circ\boldsymbol{\gamma}^\star\right)\langle\mathbf{e}_r,\mathbf{n}\rangle}\right\|_X \overset{!}{<} 1.$$

Since $h < 0$ and $\langle\mathbf{V},\mathbf{n}\rangle \neq 0$ for all nontangential fields $\mathbf{V}$, the solution $\mathrm{dw}^\star$ of the boundary value problem (5.24) is not zero and thus $\partial \mathrm{dw}^\star[\mathbf{V}]/\partial\mathbf{n}$, too. Therefore one can expect only linear convergence of the trial method. What is more, in contrast to the directional derivative $\mathrm{d}\Phi_D[q]$ (4.43) where the denominator is always strictly negative near the optimal boundary, the denominator in (5.26) may have zeros. Consequently, the possibility of a non-defined directional derivative cannot be excluded. A practicable and efficient way to avoid such a problem and

the risk of divergence of the trial method is to choose a sufficiently large value for the inhomogenity f such that the denominator does not change the sign.

Note that, for the particular case of a free boundary problem with the Laplace equation and constant Neumann data $h(x, y) = const.$ at Γ, the method converges only when the optimal boundary $\Gamma^\star$ is convex. In any other case, as the denominator contains the curvature κ, the directional derivative of Φ_N, i.e.,

$$\mathrm{d}\Phi_N[q](r^\star) = \frac{1}{\kappa h \langle \mathbf{e}_r, \mathbf{n} \rangle} \left(\frac{\partial \mathrm{dw}^\star[\mathbf{V}]}{\partial \mathbf{n}} \circ \boldsymbol{\gamma}^\star \right) \tag{5.34}$$

is not well defined. This result provides a satisfactory explanation for the oscillations of the free boundary and the divergence of the method which were many times observed during the numerical tests.

Looking back to Example 5.5 we can deduce that the large value of the inhomogenity of the Poisson equation, i.e., $f(x, y) = 80$, constitutes the reason for the convergence of the trial method for larger values of the parameter λ compared to Example 5.6 where the Laplace equation is considered. The conclusions from equation (5.34) can also explain the observation in Example 5.6 that the trial method always converges even though only the Laplace equation is considered; the optimal boundaries are all convex.

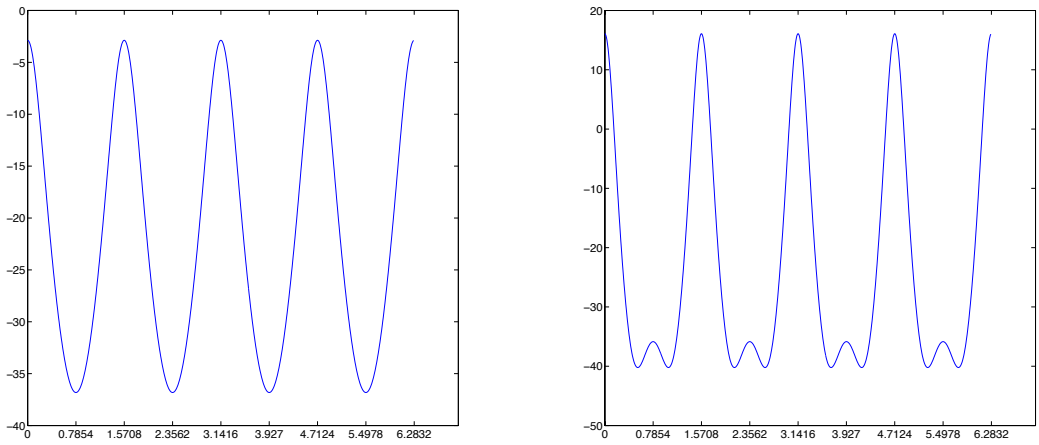

Figure 5.5: Denominator of the update function (5.25) in case of the Laplace equation and Neumann data $h = -7$ (left) and $h = -8$ (right).

In Figures 5.5 and 5.6 we plot the denominator of the update function δr from (5.25) and the denominator of the derivative of Φ_N from (5.34) when using the same domain and numerical setting as in Example 5.6. In particular, the value of the denominators are displayed for $\lambda = 7$ (left plot) and for $\lambda = 8$ (right

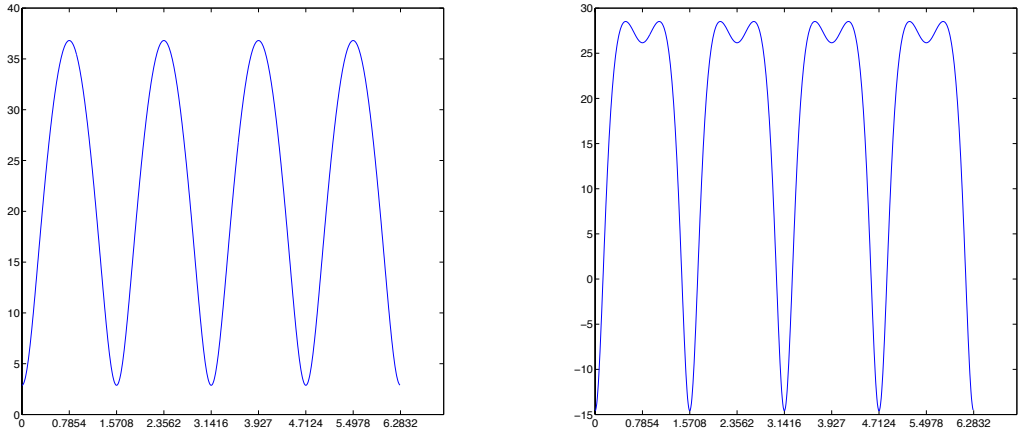

Figure 5.6: Denominator of the derivative (5.34) in case of the Laplace equation and Neumann data $h = -7$ (left) and $h = -8$ (right).

plot). In the first case the trial method is converging, while in the second case no convergence is achieved. However, both outcomes can be explained by studying the graphics in more detail. There, for $\lambda = 7$ it is seen that, the denominator of the update function $\delta\mathrm{r}$ remains always negative while the denominator of the derivative of Φ_N remains always positive. Hence, the update is well defined for $\lambda = 7$. This is though not the case for $\lambda = 8$ as we observe that the denominator in both functions is changing the sign.

5.3.3 Modified update rule

Our suggestion to overcome this difficulty, which occurs always in case of the Laplace equation and $h = const.$, is to modify the update rule. Namely, instead of the update function (5.25) we propose to use

$$\Delta\mathrm{r}(r) := \kappa\delta\mathrm{r}(r) = \frac{\dfrac{\partial \mathrm{w}}{\partial \mathbf{n}} \circ \boldsymbol{\gamma} - h}{\Big(\dfrac{\partial \mathrm{w}}{\partial \mathbf{n}} \circ \boldsymbol{\gamma}\Big)\langle \mathbf{e}_r, \mathbf{n}\rangle - \dfrac{\langle \mathbf{e}_r, \mathbf{t}\rangle}{\kappa\|\boldsymbol{\gamma}'\|}\dfrac{\partial}{\partial s}\Big(\dfrac{\partial \mathrm{w}}{\partial \mathbf{n}} \circ \boldsymbol{\gamma}\Big)}. \tag{5.35}$$

The self-mapping is thus accordingly modified to

$$\Phi_m(r) = r + \Delta\mathrm{r}(r). \tag{5.36}$$

Following the proof of Theorem 5.9, we compute the derivative of Φ_m in the direction q as follows:

$$\begin{aligned}
\mathrm{d}\Phi_m[q](r^\star) &= \lim_{\varepsilon\to 0} \frac{\Phi_m(r^\star+\varepsilon q)-\Phi_m(r^\star)}{\varepsilon} \\
&= q + \lim_{\varepsilon\to 0} \frac{\Delta \mathrm{r}(r^\star+\varepsilon q)-\Delta \mathrm{r}(r^\star)}{\varepsilon} \\
&= q + \lim_{\varepsilon\to 0} \frac{\Delta \mathrm{r}(r^\star+\varepsilon q)}{\varepsilon} \\
&= q + \frac{1}{h\langle \mathbf{e}_r,\mathbf{n}\rangle} \lim_{\varepsilon\to 0} \frac{1}{\varepsilon} \frac{\dfrac{\partial \mathrm{w}_\varepsilon^\star}{\partial \mathbf{n}_\varepsilon}\circ \boldsymbol{\gamma}_\varepsilon^\star - h}{\varepsilon}
\end{aligned} \tag{5.37}$$

By using that $\partial \mathrm{w}^\star/\partial \mathbf{n} = h$ at the optimal boundary $\Gamma^\star$, the limit in (5.37) corresponds to

$$\lim_{\varepsilon\to 0} \frac{\dfrac{\partial \mathrm{w}_\varepsilon^\star}{\partial \mathbf{n}_\varepsilon}\circ \boldsymbol{\gamma}_\varepsilon^\star - h}{\varepsilon} = \frac{\partial \mathrm{dw}^\star[q\mathbf{e}_r]}{\partial \mathbf{n}}\circ\boldsymbol{\gamma}^\star + \frac{\partial}{\partial(q\mathbf{e}_r)}\Big(\frac{\partial \mathrm{w}^\star}{\partial \mathbf{n}}\circ\boldsymbol{\gamma}^\star\Big) + \langle \nabla \mathrm{w}^\star\circ\boldsymbol{\gamma}^\star, \frac{\partial \mathbf{n}}{\partial(q\mathbf{e}_r)}\rangle. \tag{5.38}$$

We can compute the derivative of Φ_m by using the given Dirichlet boundary condition at the boundary $\Gamma^\star$ and inserting (5.38) into (5.37). This leads to

$$\begin{aligned}
\mathrm{d}\Phi_m[q](r^\star) &= q + \frac{\dfrac{\partial \mathrm{dw}^\star[q\mathbf{e}_r]}{\partial \mathbf{n}}\circ\boldsymbol{\gamma}^\star - \kappa h q\langle \mathbf{e}_r,\mathbf{n}\rangle}{h\langle \mathbf{e}_r,\mathbf{n}\rangle} \\
&= (1-\kappa)q + \frac{1}{h\langle \mathbf{e}_r,\mathbf{n}\rangle}\left(\frac{\partial \mathrm{dw}^\star[q\mathbf{e}_r]}{\partial \mathbf{n}}\circ\boldsymbol{\gamma}^\star\right).
\end{aligned} \tag{5.39}$$

The mapping Φ_m is contractive if

$$\big\|\mathrm{d}\Phi_m[q](r^\star)\big\|_X = \left\|(1-\kappa)q + \frac{1}{h\langle \mathbf{e}_r,\mathbf{n}\rangle}\left(\frac{\partial \mathrm{dw}^\star[q\mathbf{e}_r]}{\partial \mathbf{n}}\circ\boldsymbol{\gamma}^\star\right)\right\|_X < 1.$$

In particular, for the new modified self-mapping Φ_m we obtain a denominator which is always negative near the optimal boundary, as $h<0$ and $\langle \mathbf{e}_r,\mathbf{n}\rangle > 0$ in case of starlike domains.

5.3.4 Improved trial method

For the modified update rule from Section 5.3.3 we derive an improved trial method in a similar way as in Section 4.3.2. We introduce a function $\beta(r)$ which

transforms the self-mapping Φ_m to

$$\Phi_m(r) = r + \beta(r)\Delta\mathrm{r}(r). \tag{5.40}$$

The directional derivative of the self-mapping (5.40) at the optimal boundary is given by

$$\mathrm{d}\Phi_m[q](r^\star) = q + \beta(r^\star) \lim_{\varepsilon\to 0} \frac{\Delta\mathrm{r}(r_\varepsilon^\star)}{\varepsilon},$$

which in view of (5.39) reads as

$$\mathrm{d}\Phi_m[q](r^\star) = q + \beta(r^\star) \left(\frac{\dfrac{\partial \mathrm{dw}^\star[q\mathbf{e}_r]}{\partial \mathbf{n}} \circ \boldsymbol{\gamma}^\star}{\Big(\dfrac{\partial \mathrm{w}^\star}{\partial \mathbf{n}} \circ \boldsymbol{\gamma}^\star\Big)\langle \mathbf{e}_r, \mathbf{n}\rangle - \dfrac{\langle \mathbf{e}_r, \mathbf{t}\rangle}{\kappa \|\boldsymbol{\gamma}^{\star\prime}\|}\Big(\dfrac{\partial}{\partial s}\Big(\dfrac{\partial \mathrm{w}^\star}{\partial \mathbf{n}} \circ \boldsymbol{\gamma}^\star\Big)\Big)} - \kappa q \right). \tag{5.41}$$

The function $\beta(r) : [0, 2\pi] \to \mathbb{R}$ should improve the trial method in two regards. Firstly, it should avoid the necessity to conduct endless tests of the trial method until an appropriate damping parameter is found. Secondly, the function $\beta(r)$ should be chosen such that the speed of convergence is increased. These goals are achieved if we define the function $\beta(r)$ such that the derivative from (5.41) vanishes for the direction

$$q := \lim_{k\to\infty} \frac{r_k - r^\star}{\|r_k - r^\star\|_X},$$

provided that this limit exists. Unfortunately, $r^\star$ is not known beforehand. Nevertheless, the choice $q_k = r_k - r_{k-1}$ with $q_0 = 1$ is proven by numerical results to be a direction for which the function β could enforce the convergence. Hence, we perform updates of the free boundary by using the update rule

$$\boldsymbol{\gamma}_{k+1} = \boldsymbol{\gamma}_k + \beta(r_k)\Delta\mathrm{r}(r_k)\mathbf{e}_r$$

for the update function (5.35) and the function β given by

$$\beta(r_k) = \left[\frac{1}{h\langle \mathbf{e}_r, \mathbf{n}\rangle} \left(\frac{\partial \mathrm{dw}_k[q_k\mathbf{e}_r]}{\partial \mathbf{n}} \circ \boldsymbol{\gamma}_k \right) - \kappa q_k \right]^{-1} q_k. \tag{5.42}$$

The Neumann data of the shape derivative contained in (5.42) are found by applying the boundary element method to the boundary value problem (5.24).

Before we close this section, we would like to comment on the choice of the function $\beta(r_k)$. Numerical tests have shown that it can be chosen as in (5.42)

but also as

$$\beta(r_k) = \left[\frac{\frac{\partial \mathrm{dw}_k[q_k \mathbf{e}_r]}{\partial \mathbf{n}} \circ \boldsymbol{\gamma}_k}{\Big(\frac{\partial \mathrm{w}_k}{\partial \mathbf{n}} \circ \boldsymbol{\gamma}_k\Big)\langle \mathbf{e}_r, \mathbf{n}\rangle - \frac{\langle \mathbf{e}_r, \mathbf{t}\rangle}{\kappa \|\boldsymbol{\gamma}_k'\|} \frac{\partial}{\partial s}\Big(\frac{\partial \mathrm{w}_k}{\partial \mathbf{n}} \circ \boldsymbol{\gamma}_k\Big)} - \kappa q_k \right]^{-1} q_k. \tag{5.43}$$

Likewise, for the boundary value problem (5.24) there is the possibility to consider in the Dirichlet boundary condition (5.24c) either the Neumann data of w_k at the actual boundary Γ_k or the desired Neumann data at the optimal boundary. For the numerical results in Section 5.4 the second alternative in combination with (5.42) has been employed. However, numerical tests do not clearly show the superiority of one of these choices. In fact, all above mentioned alternatives could be applied.

The results about the convergence of the trial method are illustrated and validated in the following section in case of circular boundaries.

5.3.5 Trial method for circular boundaries

For concentric circular boundaries Σ and Γ_k, the corresponding Dirichlet boundary value problem is given as

$$\begin{aligned} -\frac{\partial^2 \mathrm{w}_k}{\partial r^2} - \frac{1}{r}\frac{\partial \mathrm{w}_k}{\partial r} &= 0 \qquad \text{in} \quad \Omega_k \\ \mathrm{w}_k &= 1 \qquad \text{on} \quad \Sigma \\ \mathrm{w}_k &= 0 \qquad \text{on} \quad \Gamma_k\,. \end{aligned} \tag{5.44}$$

The solution of the boundary value problem (5.44) is analytically computable. On the new boundary Γ_{k+1} the Neumann boundary condition with constant data should be satisfied. The unknown Neumann data at the actual boundary Γ_k are given by

$$\frac{\partial \mathrm{w}_k}{\partial r}(r_k) = \frac{1}{r_k \log \dfrac{r_\Sigma}{r_k}}.$$

Since the curvature of a circle is constant and given by $\kappa = 1/r_k$, the update function (5.25) becomes in view of the identities $\langle \mathbf{e}_r, \mathbf{n}\rangle = 1$ and $\langle \mathbf{e}_r, \mathbf{t}\rangle = 0$

$$\delta \mathrm{r}(r_k) = \frac{\frac{\partial \mathrm{w}_k}{\partial r}(r_k) - h}{\kappa \frac{\partial \mathrm{w}_k}{\partial r}(r_k)} = -\frac{h}{r_k \frac{\partial \mathrm{w}_k}{\partial r}(r_k)} + r_k.$$

The standard update rule used in the trial method is thus

$$r_{k+1} = r_k + \delta \mathrm{r}(r_k) = 2r_k - hr_k^2 \log \frac{r_\Sigma}{r_k}.$$

Hence, the associated self-mapping is defined as

$$\Phi_N(r_k) = 2r_k - hr_k^2 \log \frac{r_\Sigma}{r_k}.$$

Its derivative at the optimal boundary reads as

$$\frac{\partial \Phi_N}{\partial r}(r^\star) = \frac{1}{\log \frac{r_\Sigma}{r^\star}}. \tag{5.45}$$

We can check the validity of (5.26) by computing $\partial \Phi_N(r^\star)/\partial r$ directly from this formula, i.e., by using

$$\frac{\partial \Phi_N}{\partial r}(r^\star) = \frac{1}{\kappa h} \frac{\partial \mathrm{dw}^\star[\mathbf{e}_r]}{\partial r}(r^\star). \tag{5.46}$$

The Neumann data of the shape derivative $\mathrm{dw}^\star[\mathbf{e}_r]$ are given as the Neumann data of the solution to the boundary value problem

$$\begin{aligned} -\frac{\partial^2 \mathrm{dw}^\star[\mathbf{e}_r]}{\partial r^2} - \frac{1}{r}\frac{\partial \mathrm{dw}^\star[\mathbf{e}_r]}{\partial r} &= 0 && \text{in} \quad \Omega^\star \\ \mathrm{dw}^\star[\mathbf{e}_r] &= 0 && \text{on} \quad \Sigma \\ \mathrm{dw}^\star[\mathbf{e}_r] &= -h && \text{on} \quad \Gamma^\star. \end{aligned}$$

The solution $\mathrm{dw}^\star$ can analytically be computed on circular domains and its Neumann data are

$$\frac{\partial \mathrm{dw}^\star[\mathbf{e}_r]}{\partial r}(r^\star) = \frac{h}{r^\star \log \frac{r_\Sigma}{r^\star}} = h^2. \tag{5.47}$$

Substituting the enumerator of (5.46) by (5.47) leads to

$$\frac{\partial \Phi_N}{\partial r}(r^\star) = \frac{1}{\log \frac{r_\Sigma}{r^\star}},$$

which coincides indeed with (5.45).

We distinguish three aspects related to the convergence of the trial method.

Convergence: The fixed-point iteration method converges locally and has a fixed-point whenever

$$\frac{1}{\left|\log \frac{r_\Sigma}{r^\star}\right|} < 1.$$

Damped fixed-point iteration: Nevertheless, we can always get linear convergence by introducing a suitable constant β such that

$$\left\| \frac{\partial \Phi_N}{\partial r}(r^\star) \right\|_X = \left| 1 - \beta \left(1 + \frac{1}{\log \dfrac{r^\star}{r_\Sigma}} \right) \right| < 1.$$

Hence, the parameter β should lie in the interval

$$0 < \beta < 2 \left(1 + \frac{1}{\log \dfrac{r^\star}{r_\Sigma}} \right)^{-1}.$$

Superlinear convergence rate: For a superlinear convergence, the damping parameter

$$\beta = \left(1 + \frac{1}{\log \dfrac{r^\star}{r_\Sigma}} \right)^{-1}$$

should be used in the update rule for the free boundary. Then, the derivative $\partial \Phi_N / \partial r$ vanishes and yields the desired superlinear convergence.

Example 5.10. A numerical example is always helpful for the validation of the theoretical findings. To that end, we consider the boundaries Γ_0 and Σ as they are displayed in Figure 4.2 of Example 4.17 and the Neumann data $h = -20$. In this case, the optimal free boundary has radius $r^\star = 0.1$. The trial method with the standard update (i.e. $\beta = 1$) is not converging. We discover that

$$\frac{1}{\left| \log \dfrac{r_\Sigma}{r^\star} \right|} = 1.04 > 1,$$

which explains the divergence of the respective trial method. However, if we will choose a damping parameter β such that the following inequality is satisfied

$$0 < \beta < 2 \left(1 + \frac{1}{\log \dfrac{r^\star}{r_\Sigma}} \right)^{-1} = 0.96,$$

then the method is converging linearly (see the red graph in Figure 5.7). When using the function $\beta(r_k)$ given by

$$\beta(r_k) = \left(1 + \frac{1}{\log \dfrac{r_k}{r_\Sigma}} \right)^{-1},$$

we gain quadratic convergence (see the blue graph in Figure 5.7). △

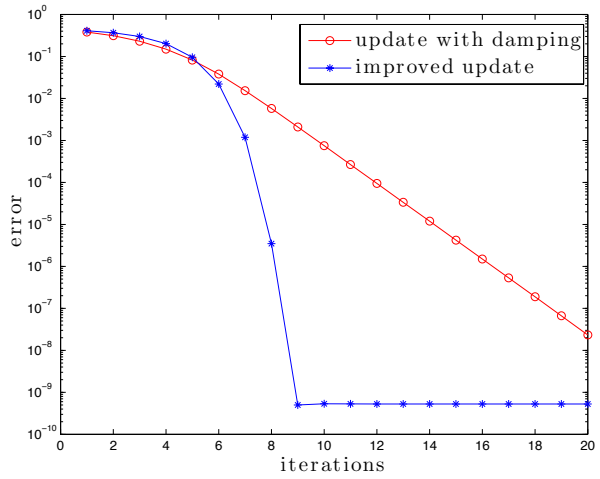

Figure 5.7: Convergence history of the trial methods in case of a circular domain.

5.4 Numerical examples

In the last section we present some tests which show in practice the improvement in the convergence of the trial method by applying the new update rules.

Example 5.11. In the first example we consider the original Bernoulli free boundary problem. This means that we search for the boundary Γ such that the Laplace equation is satisfied in domain Ω with Dirichlet boundary condition $g(x, y) = 1$ on Σ, homogeneous Dirichlet boundary condition on Γ and constant Neumann boundary condition $h(x, y) = -\lambda$ on Γ. We prescribe a peanut-shaped fixed boundary Σ with parametrization

$$\boldsymbol{\gamma}_\Sigma : [0, 2\pi] \to \Sigma, \quad s \mapsto \boldsymbol{\gamma}_\Sigma(s) = \begin{bmatrix} 0.06 \sin(s)\big(1.25 + \cos(2s)\big) \\ 0.085 \cos(s) \end{bmatrix}.$$

The initial guess to the trial free boundary is chosen to be the ellipse parametrized by

$$\boldsymbol{\gamma}_0 : [0, 2\pi] \to \Gamma_0, \quad s \mapsto \boldsymbol{\gamma}_0(s) = \sqrt{0.01 \cos^2(2s) + 0.012 \sin^2(2s)} \begin{bmatrix} \cos(s) \\ \sin(s) \end{bmatrix}.$$

The free boundary problem is solved with 30 degrees of freedom for the representation of the free boundary and 600 boundary elements per boundary. In

Figure 5.8, the solutions of Bernoulli's free boundary problem are displayed for the values of the parameter λ under consideration, where the outermost boundary corresponds to $\lambda = 10$ and the innermost boundary to $\lambda = 18$.

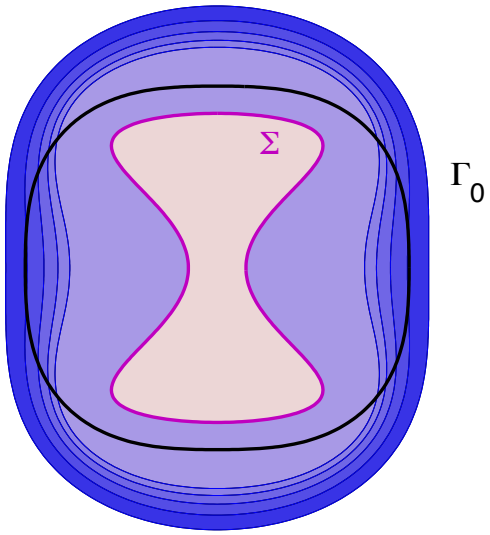

Figure 5.8: Solutions of the free boundary problem in case of a peanut-shaped interior boundary.

It is seen from Figure 5.8 that for the smallest value $\lambda = 10$ the optimal boundary $\Gamma^\star$ is approximately an ellipse and hence convex. Therefore, as we figure out of Table 5.4, the trial method is converging for an appropriate damping parameter not only for the modified update rule (row entitled "modified update with damping ($\beta = 0.01$)") but also for the standard update rule (row entitled "update with damping ($\beta = 0.005$)"). Note that, the stopping criterion of the trial method is $\|\Delta \mathrm{r}\| < 10^{-8}$ and $\|\delta \mathrm{r}\| < 10^{-8}$, respectively. For the rest of the values of λ for which, as in Figure 5.8 is shown, the optimal boundary is nonconvex, the trial method is not converging any more in case of the standard update function (5.25). In both cases however, we notice that a damping parameter is essential.

The determination of an appropriate damping parameter is an expensive procedure. An unnecessarily small damping parameter can increase the number of iterations drastically, while an inappropriate bigger one can lead to divergence. This time and effort can be saved thanks to the improved modified update rule. The efficiency of this rule is shown in Table 5.4 (row entitled "improved modified update") where we observe that the trial method is converging for all values of λ under consideration. The convergence order of the trial methods is always only linear and thus we again omit to graphically represent the convergence history of the trial methods. △

prameter λ	10	12	14	16	18
update with damping ($\beta = 0.005$)	230	–	–	–	–
modified update with damping ($\beta = 0.01$)	93	81	65	114	77
improved modified update	101	84	89	132	131

Table 5.4: Number of boundary updates of the trial method in case of a peanut-shaped interior boundary.

Example 5.12. In the second example we solve the Bernoulli free boundary problem for the Laplace equation with constant Neumann data $h = -\lambda$ on Γ and Dirichlet data $g = 1$ on Σ. The interior boundary Σ is randomly generated, cf. Figure 5.9. The initial guess Γ_0 is an ellipse which is parametrized by

$$\boldsymbol{\gamma}_0 : [0, 2\pi] \to \Gamma_0, \quad s \mapsto \boldsymbol{\gamma}_0(s) = \sqrt{0.1\cos^2(2s) + 0.11\sin^2(2s)} \begin{bmatrix} \cos(s) \\ \sin(s) \end{bmatrix}.$$

The solutions of the free boundary problem are shown for the chosen values of λ in Figure 5.9. The implementation uses 50 degrees of freedom, i.e., $\nu = 25$, to represent the free boundary and 500 boundary elements per boundary.

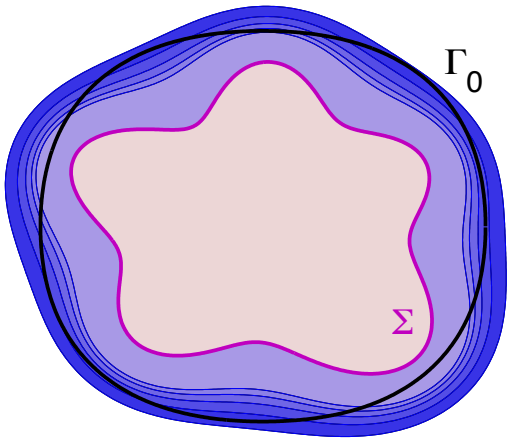

Figure 5.9: Solutions of the free boundary problem in case of a random interior boundary.

In Table 5.4 the numbers of iterations needed by the trial method to converge are shown. There are no results with respect to the standard update rule as in this case (like in the examples in Section 5.2.3) the optimal boundary is nonconvex for all chosen values of the parameter λ. Thus, the trial method based on the standard update rule is not converging in this case. The improvement of the trial method based on the modified update rule and based on the function $\beta(r)$ is also demonstrated by this example. △

prameter λ	8	10	12	14	16
modified update with damping ($\beta = 0.01$)	179	146	130	122	125
improved modified update	114	94	92	101	92

Table 5.5: Number of boundary updates of the trial method in case of a random interior boundary.

Example 5.13. The last example refers to a domain Ω which consists of several interior boundaries. We solve the associated original Bernoulli free boundary problem, where its solutions are depicted in Figure 5.10 for different values of the Neumann data $h = -\lambda$.

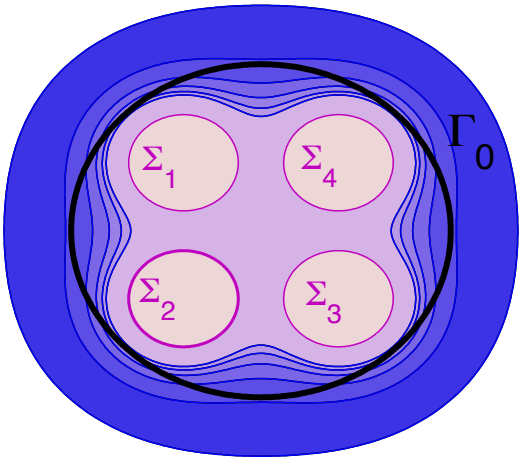

Figure 5.10: Solutions of the free boundary problem in case of several interior boundaries.

For the implementation there have been used 400 boundary elements per boundary, i.e., 2000 in all, and 30 degrees of freedom for the representation of the free boundary. As it is shown in Table 5.6, we achieve convergence for the trial method and for all the chosen values of the parameter λ when the modified update rule (5.35) with damping parameter $\beta = 0.05$ is applied. The standard update rule converges for the same damping parameter only for $\lambda = 2$, as for this value the optimal boundary is convex. The improved modified update rule shows a slight improvement in the number of the iterations for some values of the parameter λ. The convergence rate of the trial methods remains linear in this case too. △

parameter λ	2	4	6	8	10	12
update with damping ($\beta = 0.05$)	125	–	–	–	–	–
modified update with damping ($\beta = 0.05$)	117	65	49	45	46	51
improved modified update	118	79	68	48	51	–

Table 5.6: Number of boundary updates of the trial method in case of several interior boundaries.

Chapter 6

Conclusion

This thesis is a significant contribution to the current literature on trial methods for the solution of free boundary problems. The research started with the choice of the violated boundary condition and consequently with the choice of the boundary value problem which defines the state equation.

Firstly, the boundary value problem with Neumann boundary condition at the free boundary has been considered. On this boundary value problem, there are many works published concerning its numerical solution. However, this is the first time in the context of trial methods that the collocation method has been employed as boundary element method to solve the state equation instead of the usual Galerkin method. The collocation method based on trigonometric polynomials, in particular, combines an exponential approximation power with the ability of computing higher order derivatives of the functions which are necessary for the update rules. Besides Poisson's equation, our method applies also for the Stokes or the Helmholtz equation, due to the fact that they are all partial differential equations for which the fundamental solution is explicitly known. Therefore, we can formulate the state problem as a boundary integral equation and solve it numerically by a boundary element method.

Secondly, the effect of a second order update on the convergence of the trial method has been investigated. We discovered that the trial method based on the second order update equation is more robust compared to the trial method based on the first order update equation. However, there is always the possibility of inserting some damping parameter to eliminate the oscillations during the iterative process and hence to enforce the convergence also in case of the first order update equation. This can be a costly procedure as long as there exists no systematic rule for the determination of such a damping parameter. Additionally,

it does not necessarily ensure the convergence of the trial method.

This finding enhanced our understanding of the trial method but a thorough examination of the convergence analysis of the trial method was still necessary. So we explained the linear convergence of the trial method and obtained some indication about the construction of a higher order convergent scheme. By means of shape sensitivity analysis the matter of always getting linear convergence was elucidated and an improved and robust trial method was derived. Next, one of the most significant findings to emerge from this thesis was proposed, namely a Newton-type update. It yields a powerful trial method as regards the following three aspects; it converges quadratically, it is applicable also for nonconvex boundaries and it does not require the change of the state equation.

In contrast to the trial method with violated Dirichlet boundary data, very little is found in the literature about the trial method for violated Neumann data. In the last part of the thesis, we shed light on the theoretical aspects about the convergence analysis of the related trial method. Furthermore, to the best of our knowledge, we were the first that numerically implemented the trial method for this problem without considering only concentric circular domains. For these reasons, this thesis contains valuable results on this class of trial methods, with the most important one being the stabilized update equation so that the trial method converges also for nonconvex free boundaries.

The derived trial methods for the solution of a free boundary problem can be used in various applications. One thus has to bear in mind that the main issue of the trial method is that the update function should be carefully defined. A future perspective of the results of this thesis is their extension to the three-dimensional case. Then, the described collocation method is not applicable anymore but can be substituted by the Galerkin method, whereas the derivation of the update equations and update rules follows in a very similar way the presented technique.

Bibliography

[1] A. Acker, *A free boundary optimization problem*, SIAM J. Math. Anal., 9 (1978), pp. 1179–1191.

[2] ——, *How to approximate the solutions of certain free-boundary problems for the Laplace equation using the contraction principle*, J. Appl. Match. Phys. (ZAMP), 32 (1981), pp. 22–33.

[3] ——, *Convergence results for an analytical trial free-boundary method*, IMA J. Numer. Anal., 8 (1988), pp. 357–364.

[4] ——, *On the geometric form of Bernoulli configurations*, Math. Methods Appl. Sci., 10 (1988), pp. 1–14.

[5] ——, *On the qualitative theory of parameterized families of free boundaries,*, J. reine. angew. Math., 393 (1989), pp. 134–167.

[6] I. Akduman and R. Kress, *Electrostatic imaging via conformal mapping*, Inverse Problems, 18 (2002), pp. 1659–1672.

[7] G. Alessandrini, V. Isakov, and J. Powell, *Local uniqueness in the inverse conductivity problem with one measurement*, Trans. Amer. Math. Soc., 347 (1995), pp. 3031–3041.

[8] H. W. Alt and L. A. Caffarelli, *Existence and regularity for a minimum problem with free boundary*, J. Reine Angew. Math., 325 (1981), pp. 105–144.

[9] K. Atkinson and G. Chandler, *Boundary integral equation methods for solving Laplace's equation with nonlinear boundary conditions: the smooth boundary case*, Math. Comp., 55 (1990), pp. 451–472.

[10] K. Atkinson and W. Han, *Theoretical numerical analysis: A functional analysis framework*, vol. 39 of Texts in Applied Mathematics, Springer, 3rd ed., 2009.

[11] A. Beurling, *On free-boundary problems for the Laplace equation*, Sem. on analytic functions, Inst. Adv. Stud. Princeton, (1957), pp. 248–263.

[12] J. F. Bonnans, J. C. Gilbert, C. Lemaréchal, and C. A. Sagastizábal, *Numerical optimization: Theoretical and practical aspects*, Universitext, Springer, Berlin, 2nd ed., 2006.

[13] F. Bouchon, S. Clain, and R. Touzani, *Numerical solution of the free boundary Bernoulli problem using a level set formulation*, Comput. Methods Appl. Mech. Engrg., 194 (2005), pp. 3934–3948.

[14] ——, *A perturbation method for the numerical solution of the Bernoulli problem*, J. Comput. Math., 26 (2008), pp. 23–36.

[15] M. Brühl, *Explicit characterization of inclusions in electrical impedance tomography*, SIAM J. Math. Anal., 32 (2001), pp. 1327–1341.

[16] M. Brühl and M. Hanke, *Numerical implementation of two noniterative methods for locating inclusions by impedance tomography*, Inverse Problems, 16 (2000), pp. 1029–1042.

[17] R. Chapko and R. Kress, *A hybrid method for inverse boundary value problems in potential theory*, J. Inverse Ill-Posed Probl., 13 (2005), pp. 27–40.

[18] O. Coulaud and A. Henrot, *Numerical approximation of a free boundary problem arising in electromagnetic shaping*, SIAM J. Numer. Anal., 31 (1994), pp. 1109–1127.

[19] M. Crouzeix, *Variational approach of a magnetic shaping problem*, European J. Mech. B Fluids, 10 (1991), pp. 527–536.

[20] M. Crouzeix, P. Féat, and F.-J. Sayas, *Theoretical and numerical study of a free boundary problem by boundary integral methods*, M2AN Math. Model. Numer. Anal., 35 (2001), pp. 1137–1158.

[21] C. W. Cryer, *A survey of trial-boundary methods for the numerical solution of free boundary problems*, MRC Techn. Summary Rep., 1693, (1976).

[22] M. C. Delfour and J.-P. Zolésio, *Shapes and geometries: Metrics, analysis, differential calculus, and optimization*, vol. 22 of Advances in Design and Control, Society for Industrial and Applied Mathematics (SIAM), Philadelphia, 2nd ed., 2011.

[23] J. E. Dennis, Jr. and R. B. Schnabel, *Numerical methods for unconstrained optimization and nonlinear equations*, vol. 16 of Classics in Applied Mathematics, Society for Industrial and Applied Mathematics (SIAM), Philadelphia, 1996.

[24] J. Descloux, *Stability of the solutions of the bidimensional magnetic shaping problem in absence of surface tension*, European J. Mech. B Fluids, 10 (1991), pp. 513–526.

[25] K. Eppler, *Optimal shape design for elliptic equations via BIE-methods*, Int. J. Appl. Math. Comput. Sci., 10 (2000), pp. 487–516.

[26] K. Eppler and H. Harbrecht, *Numerical solution of elliptic shape optimization problems using wavelet-based BEM*, Optim. Methods Softw., 18 (2003), pp. 105–123.

[27] ——, *Exterior electromagnetic shaping using wavelet BEM*, Math. Methods Appl. Sci., 28 (2005), pp. 387–405.

[28] ——, *Fast wavelet BEM for 3d electromagnetic shaping*, Appl. Numer. Math., 54 (2005), pp. 537–554.

[29] ——, *A regularized Newton method in electrical impedance tomography using shape Hessian information*, Control Cybernet., 34 (2005), pp. 203–225.

[30] ——, *Efficient treatment of stationary free boundary problems*, Appl. Numer. Math., 56 (2006), pp. 1326–1339.

[31] ——, *Tracking Neumann data for stationary free boundary problems*, SIAM J. Control Optim., 48 (2009/10), pp. 2901–2916.

[32] ——, *Tracking Dirichlet data in L^2 is an ill-posed problem*, J. Optim. Theory Appl., 145 (2010), pp. 17–35.

[33] A. Fasano, *Some free boundary problems with industrial applications*, in Shape optimization and free boundaries, vol. 380 of NATO Adv. Sci. Inst. Ser. C Math. Phys. Sci., pp. 113–142.

[34] C. A. J. Fletcher, *Computational Galerkin methods*, Springer Series in Computational Physics, Springer, New York, 1984.

[35] R. Fletcher, *Practical methods of optimization*, John Wiley & Sons, New York, 2nd ed., 2001.

[36] M. Flucher and M. Rumpf, *Bernoulli's free-boundary problem, qualitative theory and numerical approximation*, J. Reine Angew. Math., 486 (1997), pp. 165–204.

[37] A. Friedman, *Free boundary problems in fluid dynamics*, in Equadiff 6 (Brno, 1985), vol. 1192 of Lecture Notes in Math., Springer, Berlin, 1986, pp. 17–22.

[38] A. Friedman and V. Isakov, *On the uniqueness in the inverse conductivity problem with one measurement*, Indiana Uni. Math. J., 38 (1989), pp. 563–579.

[39] P. R. Garabedian, *The mathematical theory of three-dimensional cavities and jets*, Bull. Amer. Math. Soc., 62 (1956), pp. 219–235.

[40] R. González and R. Kress, *On the treatment of a Dirichlet-Neumann mixed boundary value problem for harmonic functions by an integral equation method*, SIAM J. Math. Anal., 8 (1977), pp. 504–517.

[41] W. Hackbusch, *Integral equations*, vol. 120 of International Series of Numerical Mathematics, Birkhäuser, Basel, 1995.

[42] H. Harbrecht, *A Newton method for Bernoulli's free boundary problem in three dimensions*, Computing, 82 (2008), pp. 11–30.

[43] H. Harbrecht and G. Mitrou, *Improved trial methods for a class of generalized Bernoulli problems*, Preprint 2013-22, Mathematisches Institut, Universität Basel, Switzerland, (2013).

[44] ——, *Stabilization of the trial method for the Bernoulli problem in case of prescribed Dirichlet data*, Preprint 2013-29, Mathematisches Institut, Universität Basel, Switzerland, (2013).

[45] J. Haslinger, T. Kozubek, K. Kunisch, and G. Peichl, *Shape optimization and fictitious domain approach for solving free boundary problems of Bernoulli type*, Comput. Optim. Appl., 26 (2003), pp. 231–251.

[46] J. Haslinger and R. A. E. Mäkinen, *Introduction to shape optimization: Theory, approximation, and computation*, vol. 7 of Advances in Design and Control, Society for Industrial and Applied Mathematics (SIAM), Philadelphia, 2003.

[47] M. Hinze, R. Pinnau, M. Ulbrich, and S. Ulbrich, *Optimization with PDE constraints*, vol. 23 of Mathematical Modelling: Theory and Applications, Springer, New York, 2009.

[48] G. Hsiao and R. C. MacCamy, *Solution of boundary value problems by integral equations of the first kind*, SIAM Rev., 15 (1973), pp. 687–705.

[49] G. C. Hsiao and W. L. Wendland, *A finite element method for some integral equations of the first kind*, J. Math. Anal. Appl., 58 (1977), pp. 449–481.

[50] K. Ito, K. Kunisch and G. Peichl, *Variational approach to shape derivatives for a class of Bernoulli problems*, J. Math. Anal. Appl., 314 (2006), pp. 126–149.

[51] K. Kärkkäinen, *Shape sensitivity analysis for numerical solution of free boundary problems*, PhD thesis, University of Jyväskylä, 2005.

[52] K. Kärkkäinen and T. Tiihonen, *Free surfaces: shape sensitivity analysis and numerical methods*, Internat. J. Numer. Methods Engrg., 44 (1999), pp. 1079–1098.

[53] R. Kress, *Ein ableitungsfreies Restglied für die trigonometrische Interpolation periodischer analytischer Funktionen*, Numer. Math., 16 (1970/1971), pp. 389–396.

[54] ——, *Linear integral equations*, vol. 82 of Applied Mathematical Sciences, Springer, New York, 2nd ed., 1999.

[55] R. Kress and P. Serranho, *A hybrid method for sound-hard obstacle reconstruction*, J. Comput. Appl. Math., 204 (2007), pp. 418–427.

[56] C. M. Kuster, P. A. Gremaud, and R. Touzani, *Fast numerical methods for Bernoulli free boundary problems*, SIAM J. Sci. Comput., 29 (2007), pp. 622–634.

[57] F. Murat and J. Simon, *Etude de probléme d'optimal design*, in Proceedings of the 7th IFIP Conference on Optimization Techniques: Modeling and Optimization in the Service of Man, Part 2, London, UK, 1976, Springer, pp. 54–62.

[58] J. Nocedal and S. J. Wright, *Numerical optimization*, Springer Series in Operations Research and Financial Engineering, Springer, New York, 2nd ed., 2006.

[59] M. Pierre and J.-R. Roche, *Computation of free surfaces in the electromagnetic shaping of liquid metals by optimization algorithms*, European J. Mech. B Fluids, 10 (1991), pp. 489–500.

[60] A. Quarteroni, R. Sacco, and F.Saleri, *Numerical mathematics*, vol. 37 of Texts in Applied Mathematics, Springer, Berlin, 2nd ed., 2007.

[61] J. R. Roche and J. Sokołowski, *Numerical methods for shape identification problems*, Control Cybernet., 25 (1996), pp. 867–894.

[62] J. Saranen and G. Vainikko, *Trigonometric collocation methods with product integration for boundary integral equations on closed curves*, SIAM J. Numer. Anal., 33 (1996), pp. 1577–1596.

[63] P. Serranho, *A hybrid method for inverse scattering for shape and impedance*, Inverse Problems, 22 (2006), pp. 663–680.

[64] ——, *A hybrid method for inverse obstacle scattering problems*, PhD thesis, Georg-August-Universität Göttingen, 2007.

[65] J. Simon, *Differentiation with respect to the domain in boundary value problems*, Numer. Funct. Anal. Optim., 2 (1980), pp. 649–687.

[66] I. H. Sloan and A. Spence, *The Galerkin method for integral equations of the first kind with logarithmic kernel: applications*, IMA J. Numer. Anal., 8 (1988), pp. 123–140.

[67] ——, *The Galerkin method for integral equations of the first kind with logarithmic kernel: theory*, IMA J. Numer. Anal., 8 (1988), pp. 105–122.

[68] J. Sokolowski and J.-P. Zolésio, *Introduction to shape optimization: Shape sensitivity analysis*, vol. 16 of Springer Series in Computational Mathematics, Springer, Berlin, 1992.

[69] R. V. Southwell and G. Vaisey, *Relaxation methods applied to engineering problems. XII. Fluid motions characterized by 'free' stream-lines*, Philos. Trans. Roy. Soc. London. Ser. A., 240 (1946), pp. 117–161.

[70] O. Steinbach, *Numerical approximation methods for elliptic boundary value problems: Finite and boundary elements*, Springer, New York, 2008.

[71] J. Stoer and R. Bulirsch, *Introduction to numerical analysis*, vol. 12 of Texts in Applied Mathematics, Springer, New York, 3rd ed., 2002. Translated from the German by R. Bartels, W. Gautschi and C. Witzgall.

[72] D. E. Tepper, *Free boundary problem*, SIAM J. Math. Anal., 5 (1974), pp. 841–846.

[73] T. Tiihonen, *Shape optimization and trial methods for free boundary problems*, RAIRO Modél. Math. Anal. Numér., 31 (1997), pp. 805–825.

[74] ——, *Fixed point methods for internal free boundary problems*, Numer. Funct. Anal. Optim., 19 (1998), pp. 399–413.

[75] T. Tiihonen and J. Järvinen, *On fixed point (trial) methods for free boundary problems*, in Free boundary problems in continuum mechanics (Novosibirsk, 1991), vol. 106 of Internat. Ser. Numer. Math., Birkhäuser, Basel, 1992, pp. 339–350.

[76] J. I. Toivanen, J. Haslinger, and R. A. E. Mäkinen, *Shape optimization of systems governed by Bernoulli free boundary problems*, Comput. Methods Appl. Mech. Engrg., 197 (2008), pp. 3803–3815.

[77] K. G. van der Zee, E. H. van Brummelen, and R. de Borst, *Goal-oriented error estimation and adaptivity for free-boundary problems: the domain-map linearization approach*, SIAM J. Sci. Comput., 32 (2010), pp. 1064–1092.

[78] ——, *Goal-oriented error estimation and adaptivity for free-boundary problems: the shape-linearization approach*, SIAM J. Sci. Comput., 32 (2010), pp. 1093–1118.

[79] J. Wloka, *Partial differential equations*, Cambridge University Press, Cambridge, 1987. Translated from the German by C. B. Thomas and M. J. Thomas.

[80] Y. Yan and I. H. Sloan, *On integral equations of the first kind with logarithmic kernels*, J. Integral Equations Appl., 1 (1988), pp. 549–579.